Electron Spin Resonance in Frustrated Two- and Three-Dimensional Chromium Magnets

Dissertation zur Erlangung des Grades eines

Doktors der Naturwissenschaften

(Dr.rer.nat)

genehmigt vom

Fachbereich Physik der

Universität Augsburg

von

Mamoun Hemmida

aus Khartoum (Sudan)

Augsburg 2011

Referent:	Prof. Dr. Alois Loidl
Korreferent:	Prof. Dr. Armin Reller

Tag der Einreichung:	25. Februar 2011
Tag der Prüfung:	13. April 2011

Contents

1 Introduction

The goal of the present work is the experimental investigation of spin correlations and corresponding magnetic properties in two- and three-dimensional Cr^{3+} based oxides, and chalcogenides by means of electron spin resonance spectroscopy. Due to only partially filled electronic $3d^3$ shells, the Cr^{3+} ions exhibit an electron spin $S = 3/2$ and the physics of these compounds is characterized by the exchange interaction between the chromium spins dependent on lattice geometry and dimensionality. Especially in the case of magnetic frustration exotic ground- and excited states may arise. Starting from the problem of the dimensionality, theoretical work on low-dimensional magnets such as magnetic chains and layers started as early as in the twenties with the Ising [Ising 1925] spin chain, and was followed by studies of two-dimensional Ising magnets in the thirties and forties. About forty years ago systematic experimental studies on quasi low-dimensional magnets were started in several research groups. The maximum effort was attained in the seventies, the level having remained about constant since then. In most cases the systems studied are magnetic compounds consisting of weakly coupled chains or layers. Thereby, the physics community became interested in defect-mediated phase transitions. These defects have been introduced in terms of non-linear excitations. Berezinskii [Berezinskii 1972] suggested that in two-dimensions vortices can be a kind of such excitations. Shortly after, Kosterlitz and Thouless [Kosterlitz 1973] formulated a theory based on a vortex-mediated phase transition in the two-dimensional XY model. This theory has been successfully applied to describe the superfluid transition of ^{4}He films by Nelson and Kosterlitz [Nelson1977]. Shortly after, Halperin and Nelson [Halperin 1978] and independently Young [Young 1979] have extended this model to treat the successive phase transitions in two-dimensional crystals. Experimentally, the Berezinskii-Kosterlitz-Thouless (BKT) theory has been often applied to superconductors but is only rarely reported in two-dimensional magnets.

Electron spin resonance (ESR) spectroscopy is certainly one of the most powerful tools to investigate the magnetic properties of three- as well as low-dimensional spin systems, because it directly measures the spin responsible for the magnetic properties. ESR is a major probe not only to investigate the paramagnetic state of these materials at low temperatures. This thesis presents a study of the magnetic properties of seven two-dimensional chromium ordered rock salt and delafossite compounds as well as nine chromium three-dimensional spinel compounds. Besides the dimensionality in these

compounds, magnetic frustration plays a major role.

In some lattices it is not possible to satisfy all the interactions in the system to find the ground state. Often this does not lead to a single unique ground state but a variety of degenerate low energy states of the system in which non-minimized energy is equally distributed. In this case the system is said to show frustration. A good example of frustration in magnetic systems is a triangular lattice with antiferromagnetic exchange (Fig. 1.1). In this lattice, if two adjacent spins are placed antiparallel, one is faced with a dilemma for the third spin. Whichever choice is made, one of the two neighbors will not have its energy minimized. This means that in such systems the geometry of the lattice can frustrate the ordering of the spins. In two dimensions, Heisenberg spins on triangular and corner sharing kagome lattices, kagome is a japanese word and means a woven bamboo pattern, show this effect (Fig. 1.1). In three dimensions the most intensively studied systems have a pyrochlore structure, in which the magnetic ions occupy a lattice of corner sharing tetrahedra (Fig. 1.1). These systems display a classical ground state with macroscopic degeneracy, the so-called cooperative paramagnetism, in which only short-range correlations between spins are found for all temperatures. However, in real systems anisotropies and long-range interactions can lift the frustration and produce long-range order. Other manifestations of frustration in condensed matter are, for example, glass formation, the blue phase of cholesteric liquid crystals, and incommensurate states in general [Ramirez 2001].

After a short introduction to the basic principles of theory and experimental technique of ESR and to the method of the data analysis with help of the spin-Hamiltonian in Chapter 2, the third Chapter will give a brief picture of the physics of vortices in two-dimensional and higher-dimensional spaces in the frame of the symmetry context. The overview about theoretical calculations and experimental investigation of two-dimensional magnets and vortices will be given following the review article of Benner and Boucher [Benner 1990] and the Ph.D. thesis of Becker [Becker 1996], respectively.

Chapter 4 is devoted to the two-dimensional frustrated systems, ordered rock salts and delafossites where the conventional BKT scenario fails to give a clear answer about the observed unexpected spin behavior in compounds like $NaCrO_2$ [Olariu 2006]. This is because the magnetic properties of these systems are strongly influenced by the geometry. The deviations of the temperature dependence of the paramagnetic resonance linewidths from the the expected BKT behavior indicate a new kind of universality class in triangular frustrated antiferromagnets.

Based on these fundamental findings Chapter 5 will discuss the spin relaxation in the spinel chromium oxides, in which a BKT-like scenario has been applied for the first time to describe the spin-spin relaxation rate in the paramagnetic regime. This will be related to the fact that the (111) planes in the pyrochlore structure correspond to

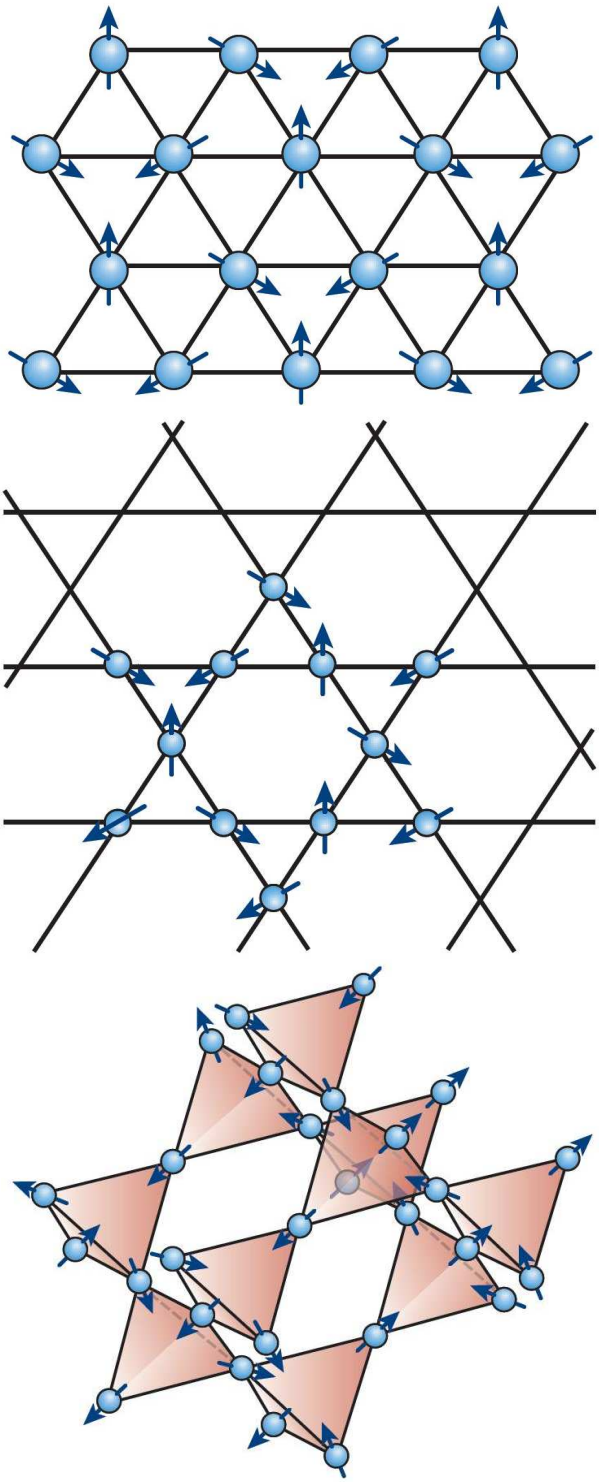

Figure 1.1: Examples of some lattices composed of triangular units where all exchange interactions cannot be simultaneously satisfied. This picture is taken from [Balents 2010].

kagome lattices. Comparative studies in related sulfide and selenide compounds do not reveal the characteristics of vortex dynamics in the spin-spin relaxation. Finally, the summary and conclusion of the thesis outlines the main results and gives perspectives for future investigations.

2 Fundamentals of Electron Spin Resonance Spectroscopy

2.1 Introduction

The following chapter is devoted to the fundamentals of electron spin resonance (ESR) spectroscopy, also termed electron paramagnetic resonance (EPR) spectroscopy. In this work, the first term will be used. ESR is a very sensitive and informative technique which investigates different kinds of paramagnetic species including ions of transition metals, free radicals, and F-centres in alkali halides.

Nearly seven decades are elapsed since the first observation of ESR by Zavoisky in 1944 [Zavoisky 1945]. During this time, several textbooks, many monographs, a few handbooks and a large number of reviews were written including the great deal of achievements in theory, instrumentation and application to an enormous number of materials. The following short survey of ESR is based on the comprehensive treatises written by Abragam and Bleaney [Abragam 1970], Altshuler and Kozyrev [Altshuler 1974], Pake and Estle [Pake 1973], and Poole [Poole 1997]. Note that CGS-units are used in this thesis to be compatible with those used in the main references.

2.2 Basic ESR Concept

ESR is based on the fact that the electron interacts with the external static magnetic field **H** via its magnetic moment

$$\overrightarrow{\mu} = -g\mu_{\mathrm{B}}\mathbf{S} \tag{2.1}$$

Here μ_{B} denotes the Bohr magneton equal to $e\hbar/2mc = 9.2741 \times 10^{-21}$ erg/Oe where e and m are charge and mass of the electron, respectively, $\hbar$ is the reduced Planck constant and c is the speed of light in vacuum. g is a dimensionless constant called the electron g-factor, which is equal to 2.0023 for the free electron and **S** is the electron spin (all bold terms used here refer to vector quantities). In general for a paramagnetic atom or ion the total spin **J=L+S** and corresponding magnetic moment is built up from the sum of the spin **S** and orbital **L** combination of the unpaired electrons of the valence shell following Hund's rules. However, here the orbital moment **L** was neglected, because for

$3d$ ions built in a solid **L** is quenched by the crystal field. Then the g-value corresponds approximately to the free-electron spin value with correction of the order of λ/Δ where λ denotes the spin-orbit coupling and Δ the crystal field splitting ($\lambda \ll \Delta$). Choosing the static magnetic field in the z-direction, the spin Hamiltonian reads:

$$\mathcal{H}_{\mathrm{Zee}} = -\mu \cdot \mathbf{H} = g\mu_{\mathrm{B}} S_{\mathrm{z}} H \tag{2.2}$$

This leads to an equidistant splitting of the $2S + 1$ electron spin energy levels $E = g\mu_{\mathrm{B}} H m_{\mathrm{s}}$ ($-S \leq m_{\mathrm{s}} \leq +S$), the so-called Zeeman effect. Taking $S = 1/2$ results in the eigen energies $E = \pm 1/2 g\mu_{\mathrm{B}} H$ for spin up and spin down, respectively. The energy difference between these two states is $\Delta E = g\mu_{\mathrm{B}} H$ and corresponds to the energy of a photon required to cause a magnetic dipolar transition by flipping the spin population. This transition can take place by applying an oscillating magnetic field $\mathbf{H}_1$ of microwave frequency ω perpendicular to **H** where the resonance condition, $\hbar\omega = g\mu_{\mathrm{B}} H_{\mathrm{res}}$, is fulfilled.

In real samples, which contain a large number of spins, the absorbed radiation $\hbar\omega$ induces the electrons in the lower energy level to jump into the higher energy state. However, the inverse process also occurs, i.e. the electrons in the higher energy level jump to the lower level. In thermal equilibrium, the relative population of these two levels is described by the Boltzmann distribution:

$$N_+/N_- = \exp[\Delta E/k_{\mathrm{B}} T] \tag{2.3}$$

where k_{B} is the Boltzmann constant and T is the temperature of the sample. Provided that the relaxation is fast enough to maintain thermal equilibrium, the population of lower energy level is larger than that of the upper one and as a consequence one can detect a signal. In the case of X-band spectrometer ($f \approx 9.4$ GHz) and resonance field $H_{\mathrm{res}} = 3400$ Oe at room temperature, the ratio N_+/N_- is 0.999. To enhance this ratio and resulting signal one can increase the field or lower the temperature.

In principle, one can understand the ESR experiment simply by introducing the macroscopic magnetization vector (the magnetic moment per unit volume). In a constant field $\mathbf{H}_0$, a population of electron spins exhibits a magnetization $\mathbf{M}_0$, which is parallel to $\mathbf{H}_0$ under thermal equilibrium conditions. Applying $\mathbf{H}_1$ perpendicular to the z-axis, the microwave frequency excitations will progressively disturb this magnetization. After switching off the microwave one expects:

$$\frac{dM_{\mathrm{z}}}{dt} = -\frac{M_{\mathrm{z}} - M_0}{T_1} \tag{2.4}$$

where T_1 is the time to return to the equilibrium distribution of the magnetization, the so-called relaxation time. The relaxation time along the direction of H is called the lon-

gitudinal relaxation time or the spin-lattice relaxation time. It measures the interaction between the spin system and its surroundings, mostly the lattice vibrations (phonons), because by returning into in the equilibrium state, energy has to be transferred from the spin system to the lattice. It is important to note that only phonons which have fluctuations with frequencies that match the ESR frequency are capable to induce transitions. Additionally, other spin-lattice interactions like direct Raman and Orbach processes can take place in the solid state materials.

In the plane perpendicular to $\mathbf{H}$, the M_x and M_y components should be zero in thermal equilibrium. After microwave irradiation they will relax back to zero in a time T_2 such that

$$\frac{dM_\mathrm{x}}{dt} = -\frac{M_\mathrm{x}}{T_2}, \qquad \frac{dM_\mathrm{y}}{dt} = -\frac{M_\mathrm{y}}{T_2} \tag{2.5}$$

where T_2 is the transverse relaxation time. Unlike T_1, T_2 occurs without the exchange of energy with the lattice but within the ensemble of spins in the sample and, thus, it is often called spin-spin relaxation time. In general T_2 is essentially smaller than T_1. According to Larmor [Larmor 1896], the behavior of a system with a mechanical moment $\mathbf{L}$ (here spin moment S) and magnetic moment $\mathbf{M}$ in the field $\mathbf{H}$ directed along the z-axis is equivalent to the behavior at $H = 0$ in the coordinate system which revolves uniformly about the z-axis with an angular frequency (Larmor) $\omega_0 = \gamma H$, where $\gamma = M/L$ (here $M/S = g\mu_B/\hbar$) is the gyromagnetic ratio. Including the so-called gyromagnetic effect, Bloch [Bloch 1946] formulated the set of equations written above in a general form as:

$$\frac{d\mathbf{M}}{dt} = -\gamma[\mathbf{M} \times \mathbf{H}] - \frac{M_z - M_0}{T_1}\mathbf{e}_z - \frac{M_y}{T_2}\mathbf{e}_y - \frac{M_x}{T_2}\mathbf{e}_x \tag{2.6}$$

where $\mathbf{e}_\mathrm{x}, \mathbf{e}_\mathrm{y}$, and $\mathbf{e}_\mathrm{z}$ denote the unit vectors in x, y, and z directions, respectively. These equations are known as the Bloch equations. They can be solved for a number of cases of interest, very often by using a rotating reference frame method in which the coordinates are changed to ones which rotate in the xy-plane at the resonance frequency. In the case of continuous wave (CW) ESR with $\gamma^2 H_1^2 T_1 T_2 \ll 1$, i.e. strong damping, one obtains a Lorentz-peak centered at $\omega = \gamma H_\mathrm{res}$ with a half width at half maximum (HWHM) linewidth $\Delta H = 1/\gamma T_2$ for the transverse magnetization (Eq. 2.13).

2.3 The CW-ESR Instrument

Generally, a standard CW-ESR spectrometer consists of a microwave source, a resonant cavity (the resonator), an electromagnet, power supply with field control (and field sweep) a field modulator and a detector diode and a lock-in-amplifier. The main part of the source is a vacuum tube with electron emitting cathode, resonator anode and reflector

cathode, producing microwave oscillations in a small range of frequencies (klystron). In modern spectrometers, alternatively a Gunn diode is usually used. A wave-guide transmits the microwaves to the resonator cavity in which the sample is placed. Coupling the wave-guide, which is a rectangular pipe used to carry microwaves, to the resonator can be achieved by means of a tunable coupling hole or iris. The size of the iris controls the amount of microwaves which will be reflected back from the cavity and how much will enter the cavity. The iris accomplishes this by carefully matching the impedances (the resistance to the waves) of the cavity and the waveguide. Automatic frequency control (AFC) locks the source at the resonator frequency. The microwave power is directed from the source to the resonator through a circulator, which simultaneously redirects the reflected power to the detector.

The source and detector are parts of the so-called microwave bridge. Another, important element of the microwave bridge is the reference arm, which supplies the detector with additional power controlled by a power input regulator (attenuator) to keep the detector diode in its working point. There is a phase shifter to insure that the reference arm transmitted in the microwaves are in phase with the microwaves reflected from the cavity when the two signals meet at the detector. The detector produces an inherent noise inversely proportional to the frequency of the detected signal. Using a pure amplifier, enhances the registered signal and keeps the signal-to-noise ratio without a significant change. To improve the signal-to-noise ratio, a small amplitude with field modulation is introduced, usually at 100 KHz and the resulting signal is rectified by lock-In technique. The field modulator consists of small Helmholtz coils which are usually built in the resonator wall along the direction of the field. At the resonance condition, the modulation field is swept back and forth through a part of the ESR signal leading to transforming the signal into a sine wave with an amplitude proportional to the slope of the resonance line. If the field modulation is small compared to the linewidth, the modulated signal appears as the first derivative of the ESR intensity vs. magnetic field strength (cf. Fig. 2.1).

The resonator concentrates the microwaves at the sample to optimize the weak signal. A resonator is a metal box with a rectangular or cylindrical shape which resonates with microwaves, i.e. it stores the microwave energy. In case of critical coupling of the resonator to the microwave bridge, at the resonance frequency, no microwaves will be reflected back, but will remain inside the resonator. Resonators are characterized by their quality factor (Q), which indicates how efficiently microwave energy can be stored. As Q increases, the sensitivity of the spectrometer increases. The Q factor is defined as:

$$Q = \frac{2\pi(\textit{power stored in the resonator})}{(\textit{power dissipated per cycle})} \tag{2.7}$$

Dissipation of the energy is due to the generated electric field and resulting electrical

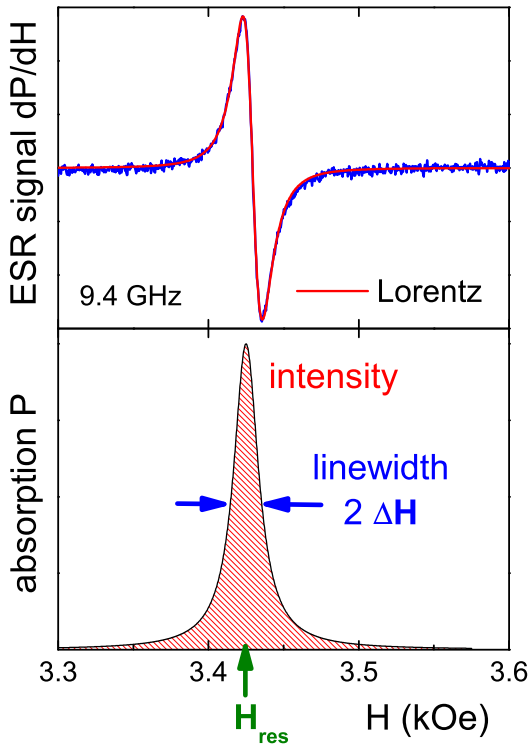

Figure 2.1: Upper frame: detected ESR signal as the first derivative. Lower frame: the corresponding absorbed microwave power.

current in the side walls which in turn generates heat. In an ESR experiment, the magnetic field component is the important part of the microwave field. Therefore, the sample should be placed in the electric field minimum and the magnetic field maximum to obtain the largest signal.

In this work, ESR measurements have been done using a commercial CW X-band spectrometer (Bruker Elexsys 500). The microwave source is a Gunn diode operating at a frequency of 9.4 GHz and a maximum power output of 200 mW. Figure 2.2 shows the general layout of the used ESR spectrometer. A water cooled electromagnet allows for field sweeps up to 18 kOe. Resonance for materials with $g \approx 2$ occurs at an external magnetic field ≈ 3.4 kOe.

For low temperature measurements from 4 K to 300 K we used a continuous helium flow cryostat in which the liquid helium is supplied from a Dewar through an insulated transfer tube. The helium flows through a heat exchanger where it is evaporated and heated up to the required temperature and supplied to the sample space. The temperature is measured by a thermocouple with liquid nitrogen as reference temperature. Higher temperatures up to 550 K can be approached using liquid nitrogen.

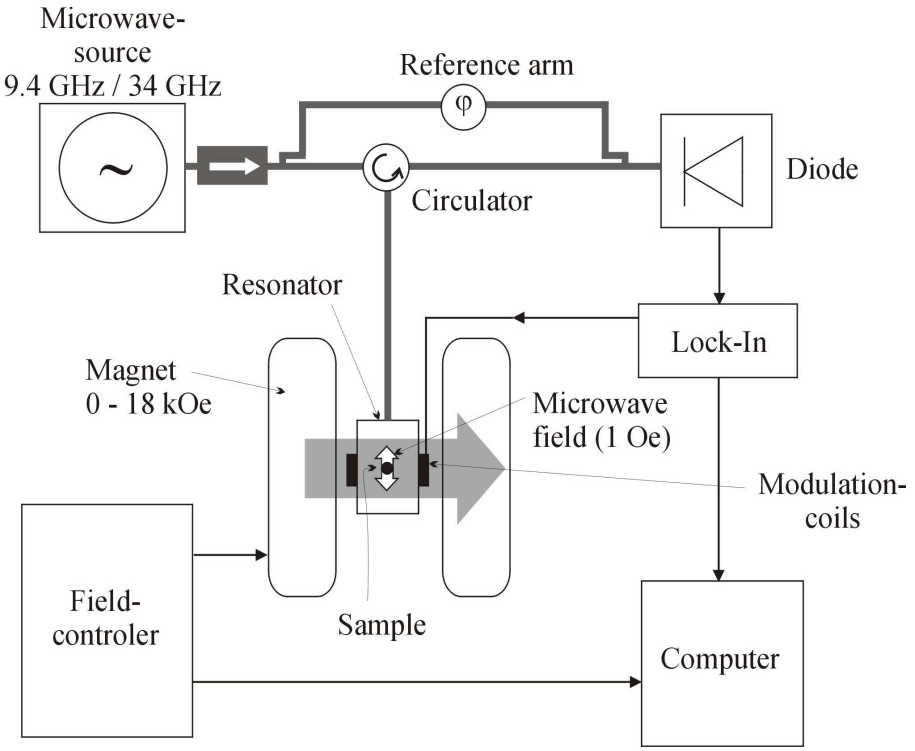

Figure 2.2: Block diagram of the ESR (Bruker ElexSys 500) spectrometer.

2.4 ESR Characteristics

By means of ESR experiments, a great deal of information is obtained from several characteristics. The three main quantities of them will be discussed in some details in the following sections.

2.4.1 Spin Susceptibility and Linewidth

When a paramagnetic sample in the resonator is tuned through the resonance condition $\hbar\omega = g\mu_{\mathrm{B}}H_{\mathrm{res}}$, the unpaired spins interact with the rf field $\mathbf{H}_1$ at the sample. This interaction manifests itself as a frequency change (dispersion) or a Q change (absorption) in the resonator. In terms of spin susceptibility ($M(\omega) = \chi(\omega) \cdot H(\omega)$), dispersion χ' and absorption χ'' can be expressed together in a complex quantity as:

$$\chi(\omega) = \chi'(\omega) - i\chi''(\omega) \tag{2.8}$$

Most ESR spectrometers detect only absorbtion, i.e. $\chi''(\omega)$. Therefore, the average power absorbed per unit volume can be given by:

$$P_{abs} = \frac{\omega}{2}\chi''(\omega)H_1^2 \tag{2.9}$$

However, Kramers and Kronig have shown that $\chi'(\omega)$ and $\chi''(\omega)$ are not independent of each other and related by the equations:

$$\chi'(\omega) = \frac{2}{\pi}\int_0^\infty \frac{\omega'\chi''(\omega')d\omega'}{\omega'^2-\omega^2} + \chi'(\infty), \quad \chi''(\omega) = -\frac{2\omega}{\pi}\int_0^\infty \frac{\chi'(\omega')-\chi'(\infty)d\omega'}{\omega'^2-\omega^2} \tag{2.10}$$

where $\chi'(\infty)$ is usually zero. In the case of the static susceptibility, $\chi'(0) = \chi_0$, the first relation connects the dispersion at $\omega = 0$ to the total intensity of the absorption over the full frequency range, in which the spin-spin relaxation phenomena taking place, as:

$$\chi'(0) = \frac{2}{\pi}\int_0^\infty \frac{\chi''(\omega)d\omega}{\omega} \tag{2.11}$$

In most cases, the experiment entails varying the magnetic field at a fixed frequency. This leads to:

$$\chi_0 = \frac{2g\mu_B}{\pi\hbar\omega}\int_0^\infty \chi''(H)dH \propto \int_0^\infty P_{abs}(H)dH \propto I_{ESR} \tag{2.12}$$

where I_{ESR} is the intensity of the absorbed line. Therefore the static susceptibility is simply given by the area under the magnetic resonance.

In general case, for a Lorentzian absorption line, the spectrum as function of the magnetic field reads:

$$P_{abs}(H) \propto \chi''(H) + \alpha\chi'(H) = \frac{\Delta H + \alpha\cdot(H-H_{res})}{(H-H_{res})^2+(\Delta H)^2} \tag{2.13}$$

in which the dispersion to absorption ratio, α, describes the asymmetry of the line. α has the values 0 and 1 for ideal insulators and metals, respectively. $\Delta H = \frac{\hbar}{g\mu_B T_2}$ is the HWHM. Note that in the case of broad lines where the linewidth is of the same order of magnitude as the resonance field, one has to take into account the resonance at the reversed field $-H_{res}$ as well. The double integrated intensity of the ESR spectrum, I_{ESR}, can be obtained as:

$$I_{ESR} \propto y'_{max}(\Delta H)^2 \tag{2.14}$$

where y'_{max} is the maximum amplitude of the derivative of dP_{abs}/dH. The measurement of ΔH will give information on the interactions between the paramagnetic ions and the surroundings. The most important sources of broadening are: dipolar interaction between the spins, anisotropic exchange interactions, crystal fields, and hyperfine interaction.

2.4.2 Resonance Field and g-Factor

Recalling the resonance condition, one has take into account that local magnetic fields H_{loc} will be present at the spin's site in addition to the external magnetic field H_{ext}. The total resonance field is $H_{\mathrm{res}} = H_{\mathrm{loc}} + H_{\mathrm{ext}}$ and the resulting effective g-factor is:

$$g_{\mathrm{eff}} = \frac{\hbar\omega}{\mu_{\mathrm{B}} H_{\mathrm{res}}} \tag{2.15}$$

g_{eff} may shift considerably from the value of the free electron $g_{\mathrm{e}} = 2.0023$ as $\Delta g = g_{\mathrm{eff}} - g_{\mathrm{e}}$ residual influence of spin-orbit coupling effects of covalent bonding as well as the local susceptibility. In anisotropic crystals, the g-value is considered as a symmetrical tensor with six different components $g_{\mathrm{ij}} = g_{\mathrm{ji}}$.

2.5 The Spin Hamiltonian

One of the most useful concepts that has been introduced into the basic theory of ESR is that of the "Spin Hamiltonian". This idea was introduced by Pryce [Pryce 1950], and extended shortly after by Abragam and Pryce [Abragam 1951]. The success of this method is due to the fact that the energy changes (orbital levels splitting) which are usually treated in the frame of perturbation theory, are precisely the same, if the effect of angular momentum is ignored and is replaced by an anisotropic coupling between the electron spin and the magnetic field. In this thesis, the matter of interest is to consider the following Hamiltonian:

$$\mathcal{H} = \mathcal{H}_{\mathrm{Zee}} + \mathcal{H}_{\mathrm{int}} = \mathcal{H}_{\mathrm{Zee}} + \mathcal{H}_{\mathrm{DD}} + \mathcal{H}_{\mathrm{CF}} + \mathcal{H}_{\mathrm{HF}} + \mathcal{H}_{\mathrm{ex}} \tag{2.16}$$

The term $\mathcal{H}_{\mathrm{int}}$ includes all other interactions like dipole-dipole interaction, crystal-electric field, hyperfine interaction, and the Heisenberg exchange interactions. Then the equation of motion for the magnetization $\mathbf{M} = -g\mu_{\mathrm{B}} \sum_i \mathbf{S}_{\mathrm{i}}$ reads

$$\frac{d\mathbf{M}}{dt} = \frac{i}{\hbar}[\mathcal{H}, \mathbf{M}] = \frac{i}{\hbar}([\mathcal{H}_{\mathrm{Zee}}, \mathbf{M}] + [\mathcal{H}_{\mathrm{int}}, \mathbf{M}]) \tag{2.17}$$

Note that the Heisenberg exchange interaction does not contribute to the equation of motion, because due to its isotropy it commutes with the magnetization $[\mathcal{H}_{\mathrm{ex}}, \mathbf{M}] = 0$. The first commutator in Eq. (2.17) again describes the Larmor precession due to the torque of the magnetic field. The second commutator contains stochastic torques, which every spin feels from spatially fluctuating local anisotropic interactions, and, thus, results in a Gaussian distribution of resonance fields.

Before dipolar and crystal field will be considered, the Heisenberg exchange will be shortly introduced. When magnetic cations in a crystal are located within a few atomic

distances of each other they begin to interact strongly compared with simple dipolar interactions. Such a kind of interaction is called exchange interaction and can be described by the effective Hamiltonian:

$$\mathcal{H}_{\mathrm{ex}} = -2\sum_{i<j} J_{ij}\mathbf{S}_{\mathrm{i}} \cdot \mathbf{S}_{\mathrm{j}} \tag{2.18}$$

This concept of the exchange interaction was introduced into solid state physics by Heisenberg [Heisenberg 1926, Heisenberg 1928]. It soon became clear that the simple direct exchange model was not often applicable. One of the main difficulties that was recognized was that in insulating crystals, magnetic cations were usually isolated from each other by non-magnetic anions, and were so far apart that the small overlap between them would predict small exchange constants J_{ij} and so would result in very low magnetic transition temperatures. But in many insulating crystals which have much higher transition temperatures, this simple model does not work. Additionally, the existence of complex spin structures like ferrimagnets [Néel 1932] or spiral configurations indicate the competition between ferromagnetic and antiferromagnetic interactions of nearest neighbor and next nearest-neighbor spins [Kaplan 1959]. These considerations suggest the importance of indirect exchange mechanisms. To overcome these difficulties, Kramers [Kramers 1934] introduced the concept of "super-exchange". He showed that super-exchange could be produced by the admixture of excited states in which electrons were transferred from anion orbitals to cation orbitals. Anderson [Anderson 1959] considered molecular orbitals formed of the admixture of the localized $3d$ orbitals and p orbitals of the intervening negative ion (O^{2-}, S^{2-}, Se^{2-}, etc.). The wavefunction of localized d spins extends over the neighboring negative ion. There is a probability of electron transfer from one $3d$ orbital of the magnetic ion to the neighboring $3d$ orbitals. The repulsive Coulomb interaction tends to prevent such a transition. In other words, when one d electron of the magnetic ion jumps into the unoccupied site of the neighboring magnetic ion, there is an energy increase by U, where U is the repulsive Coulomb interaction. In this picture, the antiferromagnetic super-exchange interaction is expressed by:

$$\mathcal{H}_{\mathrm{ex}} = 4\frac{t^2}{U}\mathbf{S}_{\mathrm{i}} \cdot \mathbf{S}_{\mathrm{j}} \tag{2.19}$$

where t is the transfer matrix element of the electron transfer from one atom to the other and U is the Coulomb interaction between two electrons with different spin direction. This corresponds to the Hubbard Hamiltonian in the limit of $U \gg t$, where the electrons are localized in the lattice points, forming an insulator.

The main features of the super-exchange interactions are usually explained in terms of the so-called Goodenough-Kanamori-Anderson rules [Goodenough 1955, Kanamori 1959, Anderson 1963]. The development of these rules came about through a long-term inter-

play between empirical observations and the development of theoretical models (semi-empirical rules). According to these rules, a 180°-super-exchange (the magnetic ion-cation(ligand)-magnetic ion angle is 180°) of two magnetic ions with partially filled d shells is strongly antiferromagnetic, whereas a 90°-super-exchange interaction is ferromagnetic and much weaker. For a more complete discussion of the empirical application of these rules, one is referred to the book of Goodenough [Goodenough 1963]. Furthermore, application to systems in this work will be discussed in chapter five.

Considering the Cr^{3+} spins, further discussions about the second and the third Hamiltonian terms (Eq. 2.21) will be done in the following two subsections.

2.5.1 Dipole-Dipole Interaction

The theory of dipolar broadening has been developed by Van Vleck [Van Vleck 1948]. He has treated in detail the particular case of free spins. The Hamiltonian of the magnetic dipole-dipole interaction between the spins is given by:

$$\mathcal{H}_{\mathrm{DD}} = g^2\mu_{\mathrm{B}}^2 \sum_{ij} [\frac{\mathbf{S}_{\mathrm{i}} \cdot \mathbf{S}_{\mathrm{j}}}{R_{\mathrm{ij}}^3} - \frac{3(\mathbf{S}_{\mathrm{i}} \cdot \mathbf{R}_{\mathrm{ij}})(\mathbf{S}_{\mathrm{j}} \cdot \mathbf{R}_{\mathrm{ij}})}{R_{\mathrm{ij}}^5}] \tag{2.20}$$

where the vector $\mathbf{R}_{\mathrm{ij}}$ connects the sites i and j. At high-temperature limit ($J/k_{\mathrm{B}}T \to 0$), the total mean square width or the second moment of the field distribution M_2 is obtained from the calculation of dipolar broadening as follows:

$$M_2^{DD} = \frac{\hbar^2}{g^2\mu_{\mathrm{B}}^2}\langle\omega^2\rangle = \frac{3S(S+1)}{4} \sum_{ij} \frac{g^2\mu_{\mathrm{B}}^2(3\cos^2\theta_{\mathrm{ij}} - 1)^2}{R_{\mathrm{ij}}^6} \tag{2.21}$$

If all orientations are present in a polycrystalline sample, $\langle(3\cos^2\theta_{\mathrm{ij}} - 1)^2\rangle = 4/5$. For the exchange magnetic field, H_{ex}, Anderson and Weiss [Anderson 1953] derived the following relation:

$$H_{\mathrm{ex}} = \frac{1.68|J|\sqrt{S(S+1)}}{g\mu_{\mathrm{B}}} \tag{2.22}$$

Since the exchange energy is large compared to both the dipolar and electric field energies, exchange narrowing effects must be considered. Kubo and Tomita [Kubo 1954], Anderson [Anderson 1954], and Yokota [Yokota 1955] have derived a general expression of the dipolar contribution to the ESR linewidth as:

$$\Delta H_{\mathrm{DD}} = \frac{M_2^{DD}}{H_{\mathrm{ex}}}[1 + \frac{2}{3}e^{-\frac{1}{2}(\frac{H_{\mathrm{res}}}{H_{\mathrm{ex}}})^2} + \frac{5}{3}e^{-2(\frac{H_{\mathrm{res}}}{H_{\mathrm{ex}}})^2}] \tag{2.23}$$

If $H_{\mathrm{res}} \gg H_{\mathrm{ex}}$, then the ESR linewidth is:

$$\Delta H_{\mathrm{DD}} = \frac{M_2^{DD}}{H_{\mathrm{ex}}} \tag{2.24}$$

However, if $H_{\mathrm{res}} \ll H_{\mathrm{ex}}$, one obtains for the extremely narrowed Lorentzian linewidth:

$$\Delta H_{\mathrm{DD}} = \frac{10}{3}\frac{M_2^{DD}}{H_{\mathrm{ex}}} \tag{2.25}$$

It is important to note that in the case of single crystal, and $H_{\mathrm{ex}} \gg H_{\mathrm{res}}$ Eq. 2.21 should be adapted in the following expression which was given by Yamada and Ikebe [Yamada 1972]:

$$M_2^{DD} = \frac{\hbar^2}{g^2\mu_{\mathrm{B}}^2} < \omega^2 >= \frac{3S(S+1)}{2}\sum_{ij}\frac{g^2\mu_{\mathrm{B}}^2(1+\cos^2\theta_{\mathrm{ij}})}{R_{\mathrm{ij}}^6} \tag{2.26}$$

where θ_{ij} is the angle between the direction of R_{ij} and the applied field. Furthermore, Eq. 2.24 can be used to calculate the dipolar contribution to the ESR linewidth in this case.

If one has a moment at every site in a simple cubic lattice, then the lattice sum $\sum_{\mathrm{ij}}\frac{1}{R_{\mathrm{ij}}^6} = \frac{8.5}{d^6}$. Therefore the dipolar contribution to the second moment can be determined as:

$$M_2^{DD} = g^2\mu_{\mathrm{B}}^2 S(S+1)\frac{5.1}{d^6} \tag{2.27}$$

where d denotes the distance between the nearest neighbor spins. For body centered cubic (BCC) and face centered cubic (FCC) lattices, the lattice sums are $\frac{29.03}{d^6}$ and $\frac{115.6}{d^6}$, respectively [Gutowsky 1952]. In the high temperature range $T \gg J/k_{\mathrm{B}}$, the Curie-Weiss law $\chi = C/(T-\Theta_{\mathrm{CW}})$ is valid. The Curie-Weiss temperature Θ_{CW} is related to the exchange integral J by the Weiss molecular-field equation:

$$\Theta_{\mathrm{CW}} = \frac{2z|J|S(S+1)}{3k_{\mathrm{B}}} \tag{2.28}$$

where z is the number of nearest neighbors (coordination number). H_{ex} is related to Θ_{CW} in the following way:

$$H_{\mathrm{ex}} = \frac{(2.52)k_{\mathrm{B}}\Theta_{\mathrm{CW}}}{g\mu_{\mathrm{B}}z\sqrt{S(S+1)}} \tag{2.29}$$

By considering chromium spinels: $z = 6$, $S = 3/2$, $g = 2$, $d = a\sqrt{2}/4$, where a is the lattice constant in $\mathring{A} = 10^{-8}$ cm, one obtains in (CGS) unit system:

$$\Delta H_{\mathrm{DD}} = \frac{3437037730}{a^6\Theta_{\mathrm{CW}}} \tag{2.30}$$

$$H_{\mathrm{ex}} = (1614)\Theta_{\mathrm{CW}} \tag{2.31}$$

2.5.2 Zero-Field Splitting

Zero-field splitting is one of the most prominent properties of transition metal complexes possessing spin quantum numbers S greater than $\frac{1}{2}$. As magnetic susceptibilities and ESR spectra are delicately influenced by zero-field splitting, it is important to reveal the origin of the zero-field splitting and, if possible, its relation to the coordination geometry around the metal ion. Mainly, there are two types of interactions between a paramagnetic ion in a solid and its surroundings; (a) interaction between the magnetic dipoles, and (b) interactions between the paramagnetic ion and the diamagnetic neighbors (ligands: e.g. O^{2-} or F^{-}). The first point has been discussed in the previous section, while the second one should be the matter of interest in this section. These ligands consist of charged ions which set up strong internal electric fields. As a good approximation, these fields can be considered to be static. The symmetry of the electric fields depends on the local arrangement of the ligands. For example considering an iron group's ion, six surrounding negative ligands (sixfold) form an octahedron, while eight surrounding negative ligands (eightfold) forming a cube. In both cases, the rotational symmetry is the same. But for cubic coordination, the splitting of e_g- and t_{2g}-orbitals is reversed from that for octahedral coordination. Similarly, in tetrahedral coordination, the d-levels split into e- and t_2-orbitals, but the level scheme is opposite to that for octahedral coordination. The reversal in the splitting of the levels on going from a less than half full to a more than half full d-shell, i.e. from n electrons to $10 - n$ holes is a general rule. Thus Cr^{3+} ($3d^3$) has the opposite splitting to Co^{2+} ($3d^7$) and V^{3+} ($3d^2$) is opposite to Ni^{2+} ($3d^8$) etc. For further examples see also [Zeiger 1973].

In general, the crystal field in the $3d$ group (of the order of 10^4 K) is larger than the spin-orbit coupling λLS, with $J = L \pm S$ (~ 100 K) but smaller than the Coulomb interaction between the electrons within the shell. The main reason is that the $3d$ shell is outermost in the ions so that it interacts directly with the ligands. Therefore the coupling of L and S is broken up so that the atomic states (terms) are no longer specified by their J values. This led to the $(2L+1)(2S+1)$ degeneracy. In the $4d$ and $5d$ (palladium and platinum groups, respectively), the crystal field is very strong and is of the same order as the Coulomb interaction ($\sim 10^5$ K). Contrary, in the $4f$ and $5f$ (rare earth and actinide groups, respectively), the effect of the crystal field is considerably weaker than the spin-orbit coupling. This is due to the fact that the partially filled $4f$ and $5f$ shells are shielded or screened by external s and p shells. Thus J is a good quantum number and the ground state is $2J + 1$ times degenerate.

Now focusing on the Cr^{3+} ion in an octahedral crystal field, the ground state is $^4F_{3/2}$

Bethe	Γ_1	Γ_2	Γ_3	Γ_4	Γ_5	Γ_6	Γ_7	Γ_8
Mulliken	A_1	A_2	E	T_1	T_2	$E_{\frac{1}{2}}$	$E_{\frac{5}{2}}$	G
Degeneracy	1	1	2	3	3	2	2	4

Table 2.1: Two different kinds of notations are listed here. The old one was suggested by Bethe [Bethe 1929] and used widely in several old literatures but rarely in the present time, while the other notations were used by Mulliken [Mulliken 1935] a few years later. Nowadays these are mostly in use. In this work Mulliken's notations will be used.

(without crystal field, only spin-orbit coupling). As was mentioned above, an important source of line broadening for magnetic systems with spin $S > 1/2$ is the zero-field splitting of the Zeeman levels due to the crystal field. The crystal field splitting of the orbital levels removes the sevenfold orbital degeneracy ($2L + 1 = 7$) and the levels are split into a lower singlet and two higher lying triplets (see Table 2.1). The orbital singlet state is a spin quartet state $^4A_2$. This fourfold degeneracy is not removed even by the combined action of the cubic field and spin-orbit coupling. But, the combination of a trigonal distortion and the spin-orbit interaction splits this quartet into two Kramers doublets with quantum numbers $M_\mathrm{s} = \pm 3/2$ and $M_\mathrm{s} = \pm 1/2$ and also causes the g-factor to be anisotropic; (Kramers theorem states that there always will be at least a twofold degenerate state in the presence of electric fields having any kind of symmetry, provided that the number of electrons is odd [Kramers 1930]). It is removed only by application of an external magnetic field (Fig. 2.3). If a small axial field is present, the fourfold spin degeneracy is removed as well. The two doublets split up again in an external magnetic field and diverge linearly (the left hand side in Fig. 2.3). In the case of the axial symmetric system with an external field applied along the c-axis, including the Zeeman effect, the effective Hamiltonian is expressed by

$$\mathcal{H}_\mathrm{eff} = \mathcal{H}_\mathrm{Zee} + \mathcal{H}_\mathrm{CF} = g_\parallel \mu_\mathrm{B} H_\mathrm{z} S_\mathrm{z} + D[S_\mathrm{z}^2 - \frac{1}{3}S(S+1)] \tag{2.32}$$

where D is the zero-field splitting parameter. In his calculation of D, Van Vleck [Van Vleck 1939] considered excited states which are only arising from the free ionic term ^4F. As mentioned above, under an octahedral field this term splits into a ground orbital singlet state $^4A_2$ and two orbital triplet excited states $^4T_1$ and $^4T_2$ (see Fig. 2.3). In his second order perturbation treatment approach, Van Vleck discards the $^4T_1$ state, because there is no matrix element of the spin-orbit interaction between it and the ground state. The resultant calculation of D led to a clear discrepancy from the experimental data, see for example [Mehran 1975]. Sugano and Tanabe [Sugano 1958] have pointed

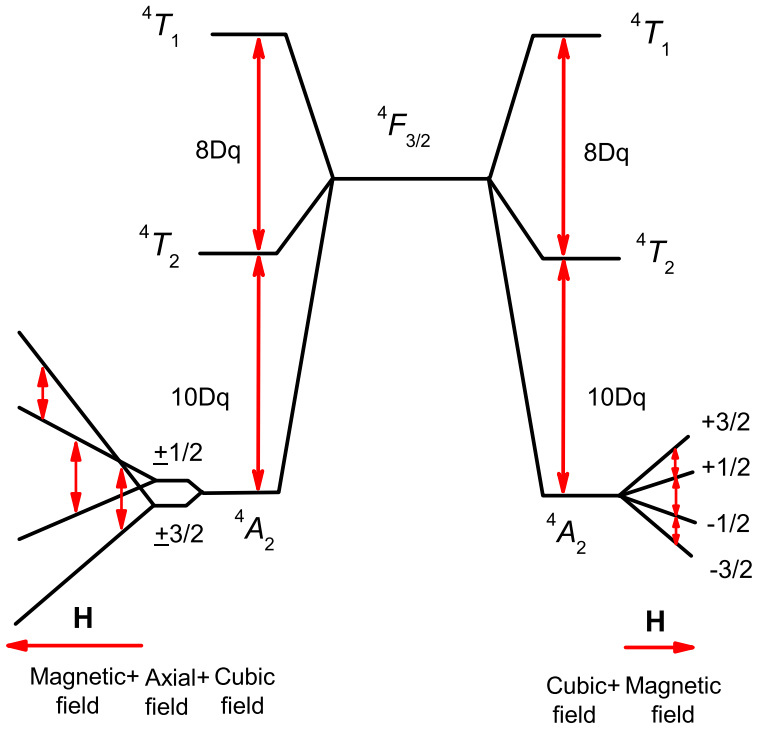

Figure 2.3: Energy level diagram of Cr^{3+} in an octahedral cubic and in an axial field. The right-hand side of the figure shows the electronic splittings of the ground state ^4F into the lowest lying singlet $^4A_2$ and two higher lying triplets $^4T_2$ and $^4T_1$. The relative separation of these triplets is $10Dq$ and $18Dq$, respectively. The ground state is not split by spin-orbit coupling. The left-hand side shows the effect of the addition of a small axial field to the cubic field: the fourfold spin degeneracy is split into two Kramers doublets [Low 1960].

out that the Van Vleck theory is actually a third order perturbation one since the $^4T_2$ excited state is split by the trigonal field and another third order term which is almost equal but of opposite sign. This "ignored" term arises from the fact that the state $^4T_1$ is connected to $^4A_2$ by the trigonal interaction and to $^4T_2$ by the spin-orbit interaction. The only way to avoid this cancelation of both terms is to assume an anisotropic spin-orbit parameter ξ which can be produced by configuration mixing and covalency effects. Using the third-order perturbation approach based on the strong-field coupling scheme, and considering other excited states arising from the free ionic term ^2G, Macfarlane [Macfarlane 1967, Macfarlane 1970] has derived analytical formulae for calculating D and $g_{\|}$ in terms of the spectroscopic parameters $10Dq$ (measures the strength of the interaction between the metal d electrons and their ligand environment), B and C (both describe the effect of the $d-d$ inter-electron repulsion) and trigonal crystal field parameters ν, ν' (which define actual symmetry lowering from the octahedral to trigonal symmetry around a $3d$ ion). Explicitly, this derivation accounts also for the covalency

effect (*the Nephelauxetic effect*: the name comes from the Greek for *cloud-expanding*), denoted as N parameter, expresses the fact that the repulsion between the d electrons in a compound is larger than the average for the corresponding free ion. For a free Cr^{3+} ion, the spin-orbit parameter ξ_0 and the average radial values $\langle r_0^2\rangle$ and $\langle r_0^4\rangle$, B_0 and C_0 parameters or Racah parameters are related to those in the compound via N as [Zhou 1983]:

$$\langle r^2\rangle = \langle r_0^2\rangle N^2 (a.u.)^2, \quad \langle r^4\rangle = \langle r_0^4\rangle N^4 (a.u.)^4, \quad \xi = \xi_0 N^2 cm^{-1} \tag{2.33}$$

$$B = B_0 N^4 cm^{-1}, \quad C = C_0 N^4 cm^{-1} \tag{2.34}$$

Knowing the values in the case of the free ion Cr^{3+} given in [Abragam 1970] or [Zhou 1983], one can use the Macfarlane formulae to determine D, $g_\parallel$ and Δg parameters in the following way:

$$D = \frac{2}{9}\xi^2\nu\left(\frac{1}{D_1^2} - \frac{1}{D_3^2}\right) - \sqrt{2}\xi^2\nu'\left(\frac{2}{3D_1D_4} + \frac{1}{D_2D_3} + \frac{1}{3D_3D_4} + \frac{1}{D_2D_4}\right) \tag{2.35}$$

$$\begin{aligned} g_\parallel =& g_e - \frac{8\xi}{3D_1}N^2 - \frac{2\xi^2}{3D_2^2}(N^2 + g_e) \\ &+ \frac{4\xi^2}{9D_3^2}(N^2 - 2g_e) + \frac{8\xi^2}{9D_1^2}(N^2 - 2g_e) \\ &- \frac{4\xi^2}{3D_1D_2}N^2 + \frac{4\xi^2}{9D_1D_3}N^2 + \frac{4\xi^2}{3D_2D_3}N^2 \\ &+ \frac{8\xi}{9D_1^2}N^2\nu - \frac{8\sqrt{2}\xi}{3D_1D_4}N^2\nu' \end{aligned} \tag{2.36}$$

$$\Delta g = g_\parallel - g_\perp = \frac{4\xi N^2}{3D_1^2}\nu - \frac{4\sqrt{2}\xi N^2}{D_1D_4}\nu' \tag{2.37}$$

where g_e is the g-value of the free electron, D_i ($i = 1 - 4$) are the zeroth-order energy denominators which are defined as:

$$D_1 = \Delta = 10Dq, \quad D_2 = 15B + 5C, \quad D_3 = \Delta + 9B + 3C, \quad D_4 = \Delta + 12B \tag{2.38}$$

The cubic field parameter Dq and Racah parameters B and C can be obtained from the optical absorbtion spectra of the studied system. Using the point-charge-dipole model, Dq as well as the trigonal field parameters ν and ν' can be defined as:

$$Dq = -eq\left(1 + \frac{5p}{eR}\right)\frac{\langle r^4\rangle}{6R^5} \tag{2.39}$$

$$\begin{aligned}\nu =& \frac{9}{7}(3\cos^2\alpha - 1)eq(1+\frac{3p}{eR})\frac{\langle r^2\rangle}{R^3} \\ &+ \frac{5}{21}(35\cos^4\alpha - 30\cos^2\alpha + 3)eq(1+\frac{5p}{eR})\frac{\langle r^4\rangle}{R^5} \\ &+ \frac{5\sqrt{2}}{3}\cos\alpha\sin^3\alpha \times eq(1+\frac{5p}{eR})\frac{\langle r^4\rangle}{R^5}\end{aligned} \tag{2.40}$$

$$\begin{aligned}\nu' =& -\frac{3\sqrt{2}}{7}(3\cos^2\alpha - 1)eq(1+\frac{3p}{eR})\frac{\langle r^2\rangle}{R^3} \\ &+ \frac{5\sqrt{2}}{84}(35\cos^4\alpha - 30\cos^2\alpha + 3)eq(1+\frac{5p}{eR})\frac{\langle r^4\rangle}{R^5} \\ &+ \frac{5}{6}\cos\alpha\sin^3\alpha \times eq(1+\frac{5p}{eR})\frac{\langle r^4\rangle}{R^5}\end{aligned} \tag{2.41}$$

where q is the charge of the ligand, p is the electric dipole moment of the ligand, R is the bonding length and α is the bonding angle. For the spinel structure, when the octahedra undergo a distortion in the direction [111], both R and α can be calculated via the lattice constant a and the ligand distorted position x as:

$$R = \sqrt{3x^2 - 2x + 0.375}a, \qquad \alpha = \arcsin[\frac{\sqrt{\frac{2}{3}}(0.75 - 2x)}{\sqrt{3x^2 - 2x + 0.375}}] \tag{2.42}$$

For an ideal octahedron, $\alpha \approx 54.7°$. In a real crystal this angle differs from that value due to the distortion.

According to Bersohn [Bersohn 1952], the second moment due to the crystal field splitting contribution M_2^{CF} can be expressed as:

$$M_2^{CF} = \frac{D^2}{5}[4S(S+1) - 3] \tag{2.43}$$

Therefore the contribution of the crystal field splitting to ΔH can be estimated as:

$$\Delta H_{\mathrm{CF}} = \frac{M_2^{CF}}{H_{\mathrm{ex}}} \tag{2.44}$$

For the angular dependence measurements, the uniaxial term of the crystal field contribution to the second moment can be given in the following way [Huber 1999]:

$$M_2^{CF} = \frac{D^2}{10}[4S(S+1) - 3](1 + \cos^2\phi) \tag{2.45}$$

where the polar angle ϕ is measured between external field and crystallographic c-axis.

Finally, in the extreme narrowing case, the dipolar and crystal field contributions to

$\Delta H_{\mathrm{Total}}$ can be given in the following way:

$$\Delta H_{\mathrm{Total}} = \frac{10/3 M_2^{DD} + M_2^{CF}}{H_{\mathrm{ex}}} \tag{2.46}$$

However, neglecting the 10/3-effect one can rewrite Eq. 2.46 in the following way as:

$$\Delta H_{\mathrm{Total}} H_{\mathrm{ex}} = M_2^{DD} + M_2^{CF} \tag{2.47}$$

In the case of layered triangular lattices, considering a single crystal sample, one can take the summation $\sum_{ij}(1+\cos^2\theta_{\mathrm{ij}})$, Eq. 2.26, over a hexagon into two different directions in which the magnetic field is applied on them. As the magnetic field is applied parallel to the *ab*-plane, the summation gives 9, while for the orientation along the *c* crystal axis one obtains 6. The crystal field contributions to the second moment lead to $M_{2ab}^{CF} = \frac{6D^2}{5}$ and $M_{2c}^{CF} = \frac{12D^2}{5}$ in the same respective order mentioned above. One can relate both expressions as $M_{2\mathrm{c}}^{CF} = 2M_{2\mathrm{ab}}^{CF}$. Therefore, the crystal field contribution to the second moment in the *ab*-plane can be given as follows:

$$M_{2\mathrm{ab}}^{CF} = \frac{\frac{\Delta H_{obs.}^{ab}}{\Delta H_{obs.}^{c}} M_{2\mathrm{c}}^{DD} - M_{2\mathrm{ab}}^{DD}}{[1 - 2\frac{\Delta H_{obs.}^{ab}}{\Delta H_{obs.}^{c}}]} \tag{2.48}$$

where $M_{2\mathrm{ab}}^{DD}$ and $M_{2\mathrm{c}}^{DD}$ are the dipolar second moments, and $\Delta H_{\mathrm{obs.}}^{ab}$ and $\Delta H_{\mathrm{obs.}}^{c}$ are the observed ESR linewidths at room temperature in *ab*-plane and *c*-axis, respectively. In a two-dimensional polycrystalline sample, dipolar second moment and crystal field contributions to the ESR linewidth are given as:

$$M_{2,\mathrm{poly}}^{DD} = \frac{1}{3} M_{2\mathrm{c}}^{DD} + \frac{2}{3} M_{2\mathrm{ab}}^{DD} = \frac{45 g^2 \mu_{\mathrm{B}}^2}{r^6} \tag{2.49}$$

$$M_{2,\mathrm{poly}}^{CF} = \frac{1}{3} M_{2\mathrm{c}}^{CF} + \frac{2}{3} M_{2\mathrm{ab}}^{CF} = \frac{8}{5} D^2 \tag{2.50}$$

2.5.3 Hyperfine Interaction

Like the *g*-factor, the hyperfine structure constant A is determined by a tensor and, therefore, one can detect the effects of anisotropy. This coupling between electron spin and nuclear spin can be represented by a term $\mathbf{S} \cdot A \cdot \mathbf{I}$ in the spin Hamiltonian given by Eq. 2.21. The hyperfine structure is found to be smaller than the fine structure splitting, and smaller than the Zeeman splitting at microwave frequencies. In the case of a strong-field spectrum for nuclear spin I, each electron level splits into $2I+1$ equally spaced levels. Magnetic dipolar transitions are allowed for $\Delta M_{\mathrm{s}} = \pm 1$ and $\Delta M_{\mathrm{I}} = 0$ in which M_{I} is the nuclear magnetic quantum number. The physical reason of this selection rule is that the nucleus may undergo $2I+1$ orientations in the magnetic field produced by

the surrounding electrons. This field is $10^5 - 10^6$ Oe and, therefore, is much larger than the external field. The radio frequency magnetic field causing transitions between the electronic levels does not affect the nuclear magnetic moment very much. Since each electronic level sets up different magnetic fields, the transition between two electronic levels differs for each of the $2I + 1$ nuclear orientations. Thus each electron's transition spectrum consists of $2I + 1$ lines. As the spectrum is observed at fixed frequency and variable magnetic field, one finds $2I + 1$ equally spaced lines associated with the cases in which the fixed microwave quantum equals the difference in energy between the levels. In the case of a cubic field acting on Cr^{3+}, at the usual temperatures the population of all the $2I + 1$ levels is approximately equal and, therefore, the $2I + 1$ lines are equally intense and equidistant. This makes it easy to discriminate the hyperfine structure from the fine structure [Low 1960].

Like the coupling between the electron and the applied magnetic field, this coupling can be factorized into two components $A_\parallel$ and $A_\perp$ parallel and perpendicular to the local symmetry axis, respectively. The isotropic contribution is characterized by the core polarization κ. κ is related to the quantity $\langle r^{-3} \rangle$ as:

$$\kappa \approx -2\chi/(3\langle r^{-3} \rangle) \tag{2.51}$$

where χ is characteristic of the density of unpaired spins of s-electrons at the nucleus of the central Cr^{3+} ion. In some 3d ions such as V^{2+}, Mn^{2+}, and Cu^{2+}, χ has been found to attain the nearly constant value -3; more precisely -2.8, -3.1, and -2.9 in the same respective order. Abragam and coworkers [Abragam 1955], assumed that for Cr^{3+} ions χ should also have the same value, i.e. -3. On the other hand, the electron-nuclear dipole-dipole interaction contribution to the hyperfine constants $A_\parallel$ and $A_\perp$ is characterized by the orbital coefficients a and b of a $3d$ orbital $ad_{\mp 2} \mp bd_{\pm 1}$. These coefficients describe the admixtures between the $d_{\mp 2}$ and $d_{\pm 1}$ orbitals due to the crystal field interaction. In terms of a and b, one can write $A_\parallel$ and $A_\perp$ in the following two expressions [McGarvey 1964]:

$$\begin{aligned} A_\parallel &= P[\frac{4}{21}(1 - 2a^2 + b^2) - \kappa] \\ A_\perp &= P[-\frac{2}{21}(1 - 2a^2 + b^2) - \kappa] \end{aligned} \tag{2.52}$$

here $P = N^2 P_0$ is the dipolar structure parameter and N^2 is the covalence parameter. $P_0 = -40 \times 10^{-4}$ cm^{-1} for the free Cr^{3+} ion [Manoogian 1974]. For ideally octahedrally coordinated ligands (cubic symmetry), one has $b/a = 1/\sqrt{2}$, $a^2 = 2/3$, $b^2 = 1/3$ and then $(1 - 2a^2 + b^2) = 0$. In this case, the hyperfine constant is isotropic and is given by $-P\kappa$. If $a^2 < \frac{2}{3}$ and $b^2 > \frac{1}{3}$ then $(1 - 2a^2 + b^2)$ is positive and $A_\parallel < A_\perp$. This means that the

d electrons in chromium are concentrated more along the molecular trigonal axes than in the isotropic case. Such a polarization of electronic charge would occur when the six ligand ions surrounding the chromium are distorted from an octahedral configuration by compression along the trigonal axes. This leads to a negative D parameter which is not the case in compounds which are considered here. If $a^2 > \frac{2}{3}$ and $b^2 < \frac{1}{3}$ then $(1 - 2a^2 + b^2)$ is negative and $A_{\parallel} > A_{\perp}$. This case corresponds to a positive D and a trigonal extension of the octahedron. According to McGarvey [McGarvey 1964], it is possible to observe anisotropy in the hyperfine spectra when the angle between the trigonal axis and Cr-O bond is 55.3°. For an ideal octahedron the angle would be 54.7° (Eq. 2.42). In order to estimate $A_{\parallel}$ and $A_{\perp}$, one needs to determine a and b coefficients. Wu and Dong [Wu 2005], gave an expression of a and b based on the energy matrix for the d orbitals under trigonal distortions for Cr^{3+} in guanidinium aluminum sulfate hexahydrate ($C(NH_2)_3Al(SO_4)_2{\cdot}6H_2O$) as:

$$\begin{aligned} \frac{b}{a} =& \frac{-(1400Dq - 315\sqrt{2}\nu' - 3DQ}{20(140\sqrt{2}Dq - 18\sqrt{2}\nu + 9\nu'}) \\ DQ^2 =& (1960000(Dq)^2 - 448000Dq\nu + 28800\nu^2 \\ & + 14000\sqrt{2}Dq\nu' - 14400\sqrt{2}\nu\nu' + 25650\nu'^2) \end{aligned} \tag{2.53}$$

3 Vortices in Two-Dimensional Magnets

The physical properties of two-dimensional systems such as bulk layered compounds but also surfaces, thin films and multilayers are in the focus of basic solid state research. Many of those properties are not observed in three dimensional systems, but are exclusive of the reduced dimensionality of those structures. The study of the way in which cooperative phenomena are influenced by the dimensionality of the lattice, symmetry properties of the lattice, and the quantum mechanical nature of the spin has led to a revolution in our concepts of phase transitions and critical phenomena, see for example [de Jongh 1990].

3.1 The Berezinskii-Kosterlitz-Thouless Phase Transition

For the classical XY model, the Hamiltonian consists of a simple exchange interaction between the nearest neighbors:

$$\mathcal{H} = -J \sum_{<ij>} (S_{\mathrm{ix}} S_{\mathrm{jx}} + S_{\mathrm{iy}} S_{\mathrm{jy}}) = -JS^2 \sum_{<ij>} \cos(\theta_{\mathrm{i}} - \theta_{\mathrm{j}}) \tag{3.1}$$

where the spins S_{i} are classical vectors of magnitude S constrained to lie in the xy-plane. These spins can, therefore, be specified by their orientation θ_{i} ($0 \leq \theta_{\mathrm{i}} < 2\pi$) with respect to the S_{x} axis. The XY model possesses the so-called circular symmetry or $U(1)$. Due to the theorem of Mermin and Wagner [Mermin 1966], there is no spontaneous moment in a two-dimensional system with only nearest-neighbor interaction and having continuous symmetry. This leads to the absence of long-range ordering in the system, but to a characteristic change in the behavior of the correlation length.

If one considers the correlation function for two spins located at sites 0 and n in the range of $J/k_{\mathrm{B}}T \ll 1$ [Izyumov 1988]:

$$\langle S_0 S_{\mathrm{n}} \rangle \sim \exp(-|n| \ln \frac{k_{\mathrm{B}}T}{J}) = (\frac{J}{k_{\mathrm{B}}T})^{|n|} \tag{3.2}$$

the correlation function falls off exponentially with the distance between the two spins for sufficiently high temperatures. At low temperatures in the region $J/k_{\mathrm{B}}T \gg 1$, we have a power behavior of the correlation function:

$$\langle S_0 S_\mathrm{n} \rangle \sim \exp(-\frac{k_\mathrm{B} T \ln |n|}{2\pi J}) = (\frac{1}{|n|})^{\frac{k_\mathrm{B} T}{2\pi J}} \tag{3.3}$$

The temperature at which the exponential behavior of the correlation function (Eq. 3.2) is replaced by the power behavior (Eq. 3.3) corresponds to a certain topological phase transition, the so-called Berezinskii-Kosterlitz-Thouless (BKT) transition. The corresponding temperature T_KT, (Kosterlitz-Thouless temperature), is estimated as:

$$T_\mathrm{KT} = \frac{\pi J}{2 k_\mathrm{B}} \tag{3.4}$$

Berezinskii [Berezinskii 1972], and later Kosterlitz and Thouless [Kosterlitz 1973], showed that below this temperature a pairing of non-linear excitations (vortices) begins in which a bound vortex-antivortex state forms. Above T_KT all such pairs dissociate in a free vortex gas. However, Eq. 3.4 usually does not give the exact value of T_KT because of the mixed contribution of vortices and spin-waves. A rigorous treatment via a normalization method, which has been developed by Kosterlitz [Kosterlitz 1974] and subsequently José et al. [José 1977], led to a corrected estimation of T_KT:

$$\frac{\pi J}{k_\mathrm{B} T_\mathrm{KT}} - 2 = \exp(-\frac{\pi^2 J}{2 k_\mathrm{B} T_\mathrm{KT}}) \tag{3.5}$$

Additionally, the temperature dependence of the vortex correlation length was derived as:

$$\begin{aligned} \xi &= \xi_0 \exp[\frac{b}{(T/T_\mathrm{KT} - 1)^\nu}], \quad T > T_\mathrm{KT} \\ \xi &= \infty, \quad T < T_\mathrm{KT} \end{aligned} \tag{3.6}$$

where $\nu = 0.5$ and $b = \pi/2$ is found for a square lattice.

A few years later, Halperin and Nelson [Halperin 1978] and independently Young [Young 1979] developed the BKT theory to be applicable to two-dimensional crystals. This development has been done in such a way that vortices can be replaced by dislocations (position defects) as well as disclinations (angle defects). This led to a reduction of the exponent ν in Eq. 3.6, i.e.:

$$\xi = \xi_0 \exp[\frac{b}{(T/T_\mathrm{m} - 1)^{0.37}}] \tag{3.7}$$

where b takes any arbitrary value. Here T_m substitutes T_KT in Eq. 3.6 and denotes the melting temperature. This model describes the two-dimensional melting process from the solid phase to an intermediate liquid crystal phase. The intermediate phase melts

further to an isotropic liquid phase. It is known as Kosterlitz-Thouless-Halperin-Nelson-Young (KTHNY) model.

In real two-dimensional magnets a residual interaction between neighboring magnetic layers always exists. This interlayer interaction J', together with the anisotropy of the intralayer interaction J, can give rise to formation of three-dimensional long-range order even for $J' \ll J$. It was shown that for the XY model with interplanar coupling the ordering temperature T_{N} is expected to be somewhat larger than T_{KT} and, consequently, the BKT transition is masked by three-dimensional magnetic order [Hikami 1980]. For a square lattice, Hikami and Tsuneto [Hikami 1980] scaled the correlation length ξ to the lattice constant a, and related them to the inter- and intralayer interactions as:

$$\frac{\xi^2}{a^2} = \frac{J}{J'} = \frac{\xi_0^2}{a^2} \exp[\frac{\pi}{(T/T_{\mathrm{KT}} - 1)^{0.5}}] \tag{3.8}$$

Recently, detailed theoretical investigations revealed that the existence of vortices and the BKT transition is not confined to the pure XY model, but even a weak planar anisotropy is enough to provide for vortex excitations in a two-dimensional magnet [Cuccoli 2003].

3.2 Vortices in Frustrated Antiferromagnets

In a two-dimensional Heisenberg triangular antiferromagnet (TAF), frustration is partially released by forming a local 120° spin structure. Short-range spin correlations give rise to an additional degree of freedom called the vector chirality. Although the spins are not long-range ordered, the vector chirality can reveal some kind of long-range order at a finite temperature. One may define the vector chirality κ for each triangle as a vector product of the two neighboring spins averaged over three spin pairs:

$$\overrightarrow{\kappa} = \frac{2}{3\sqrt{3}}[\mathbf{S}_1 \times \mathbf{S}_2 + \mathbf{S}_2 \times \mathbf{S}_3 + \mathbf{S}_3 \times \mathbf{S}_1] \tag{3.9}$$

The sign of $\overrightarrow{\kappa}$ represents each of the two chiral states, i.e., either $\overrightarrow{\kappa} < 0$ (left-handed) or $\overrightarrow{\kappa} > 0$ (right-handed). In the case of a Heisenberg system, chiral vectors as defined above cannot be independent, because they can be transferred one into another by a continuous transformation and $\overrightarrow{\kappa}$ becomes a three-dimensional vector. More precisely, the right-handed chiral state can be transformed into the left-handed chiral state via a continuous spin rotation of π making use of the third dimension of the Heisenberg spin space [Hirakawa 1990].

Kawamura and Miyashita (KM) studied theoretically the ordering process in the two-dimensional Heisenberg TAF via Monte-Carlo simulations and found Z_2-vortices, formed by the chiral vectors and characterized by a two-valued topological quantum number,

only (Fig. 3.1) [Kawamura 1984]. This kind of vortex is somewhat different from that of BKT. BKT vortices are characterized by infinite topological quantum numbers. In the case of Z_2-vortices, the spin-correlation function decays exponentially in the whole temperature regime $T \geq 0$ K, i.e. even below the KM transition. The corresponding KM transition temperature is estimated as $T_{\mathrm{KM}} = 0.31|2J/k_{\mathrm{B}}|S^2$ [Kawamura 1984]. Currently, the temperature dependence of the correlation length has been found to be similar to the BKT one, but with a slightly smaller value of $\nu = 0.42$ and an improved estimation of $T_{\mathrm{KM}} = 0.285|2J/k_{\mathrm{B}}|S^2$, which substitutes T_{KT} in Eq. 3.6, whereby b is arbitrary [Kawamura 2010].

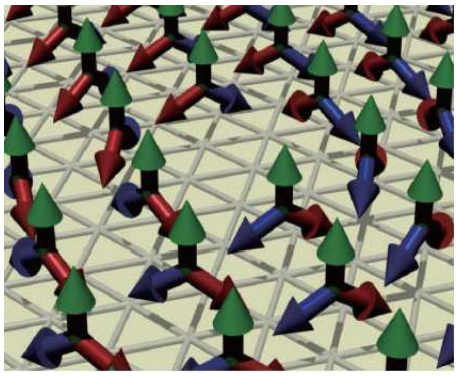

Figure 3.1: Illustration of a Z_2-vortex formed by the local 120° structure realized in the antiferromagnetic Heisenberg model on the triangular lattice [Okubo 2010].

Over two decades, a plenty of computer simulation works appeared and treated the problem in many aspects and different cases. For example, a frustrated XY TAF can reveal a combined $Z_2 \times U(1) : KM \times BKT$ symmetry: the ground state in this case possesses not only a continuous degeneracy, but also a double discrete degeneracy. So one expects an Ising-like (T_{I}) as well as an XY-like transition (T_{KT}) [Gekht 1989]. Several theoretical (analytical and numerical) studies have been done on the fully frustrated XY (FFXY) model and calculated that the two transitions occur at the same temperature, i.e. $T_{\mathrm{KT}} = T_{\mathrm{I}}$ [Choi 1985, Yosefin 1985, Berge 1986]. Monte Carlo studies on the FFXY model in a square-lattice supported the single transition with dominant Ising character [Eikmans 1989, JLee 1991]. It has been also reported that the Z_2-symmetry breaking transition may not belong to the Ising universality class and favors a single transition scenario [Ramirez-Santiago 1992, Granato 1993, Knops 1994, Ramirez-Santiago 1994, Granato 1991, Nightingale 1995]. On the other hand, other simulations are also in favor of two transitions at two different temperatures: $T_{\mathrm{KT}} \leq T_{\mathrm{I}}$ [Grest 1989, RLee 1994]. It is the general belief that the transitions at T_{KT} and at T_{I} belong to the BKT universality class and to the Ising universality class, respectively, if the transitions occur at different temperatures. It is important to note that both temperatures are found to be very close to each other T_{KT} / $T_{\mathrm{I}} = 0.9867$ and 0.9902 in [Olsson 1995, DLee 1986], respectively.

The exponent of the BKT transition has been calculated only for a square lattice by José and Ramirez-Santiago [Ramirez-Santiago 1994]. They found a non-standard exponent $\nu = 0.31$ to be compared to 0.5 in the ferromagnetic case. Further discussion about this problem can be found in [Loison 2004, Rieger 2008]. These different theoretical results mentioned above have led to a strong controversy. In this work, the analysis of the experimental data should clarify some aspects of this mysterious behavior in frustrated antiferromagnets.

3.3 Extended Berezinskii-Kosterlitz-Thouless Phase Transition

Apart from the possibility of the presence of BKT vortices ($U(1)$-symmetry) or KM vortices (Z_2-symmetry) in two-dimensional systems, the existence of further different kind of vortices is possible from the symmetry point of view.

There are several ways of introducing symmetry. In mathematics, symmetries are usually associated with operations that leave a geometrical object invariant. A sphere, for instance, remains the same under continuous rotations in space. The collection of such operations forms a mathematical group. The mathematical description of continuous symmetries (as opposed to discrete symmetries, such as those that leave a crystal lattice invariant) is codified in the notion of a Lie group, named after the Norwegian mathematician Sophus Lie. There are nine Lie groups which are classified into two families, classical and exceptional. The first one includes four different groups known as $A_\mathrm{n} = SU(n+1)$, $B_\mathrm{n} = SO(2n+1)$, $C_\mathrm{n} = SP(2n)$, $D_\mathrm{n} = SO(2n)$, of respective $n \geq 1$, $n \geq 2$, $n \geq 3$, $n \geq 4$ [Itzykson 1989, Penrose 2007]. The subscript n is called the rank of the group and measures how large the group is. There is no restriction of its maximum value. The notations SU, SO, and SP refer to special unitary, special orthogonal, and symplectic, respectively. The second family includes five groups which are known as G_2, F_4, E_6, E_7, and E_8. The words classical and exceptional are used in a sense that one knows how to describe the classical groups for every n. In contrast, in the exceptional groups, although the index value will not exceed the value 8, these groups have very high symmetries or enormous symmetry operations, which cannot be obeyed by any familiar geometrical object.

On the other hand, the objects of highest symmetry in three-dimensional space are regular polyhedra which are well-known as Platonic solids: the tetrahedron, cube (hexahedron), octahedron, dodecahedron, and icosahedron. The cube and octahedron are "dual" to each other, the same holds for the icosahedron and the dodecahedron. The word "dual" means that one can get one Platonic solid from the other when the center of each face becomes a vertex of the dual. Dual solids have the same symmetry group,

G	A_n	B_n	C_n	D_n	G_2	F_4	E_6	E_7	E_8
ν	$\frac{2}{n+3}$	$\frac{1}{n}$	$\frac{1}{2}$	$\frac{1}{n}$	$\frac{2}{5}$	$\frac{1}{4}$	$\frac{1}{7}$	$\frac{1}{10}$	$\frac{1}{16}$
h_G	$n+1$	$2n-1$	$n+1$	$2(n-1)$	4	9	12	18	30

Table 3.1: The different kinds of symetrical groups indicate all possible values of the BKT exponent [Bulgadaev 1999].

so there are three symmetry groups here: the tetrahedron, cube, and icosahedron. In the mid-19th century the Swiss mathematician Ludwig Schlaefli discovered the four-dimensional analogues of the Platonic solids, called convex regular 4-polytopes. There are exactly six of these figures; five are analogous to the Platonic solids, while the sixth one, the 24-cell, has no lower- or higher-dimensional analogue. In dimensions higher than four, there are only three convex regular polytopes: the simplex, the hypercube, and the cross-polytope. In three dimensions, these coincide with the tetrahedron, the cube, and the octahedron. Hence, to describe the three exceptional groups E_6, E_7, and E_8 in three dimensional space, one needs to fit them in the three groups of symmetry of the platonic solids mentioned above. For instance, E_8 connected to the symmetry group of icosahedron/dodecahedron. In order to fit the full symmetry operations, i.e. 696729600, one needs a geometrical object which exists in 248 dimensions! Due to the impossibility of the imagination of such objects, mathematicians use another trick by projecting them into the two-dimensional plane. In this plane, an infinite number of regular polygons can be constructed. The english geometer Coxeter derived a theory of projection of hyper-space polytopes on the plane [Coxeter 1973]. In this way, mega symmetry operations as rotations, reflections, translations etc.. are tightly packed.

In order to describe all possible symmetries in the two-dimensional systems, Bulgadaev [Bulgadaev 1999] extended the concept of the BKT phase transition to include different kinds of symmetries. Between one of these polytope characteristics, the so-called Coxeter number h_G, and the exponent ν in Eq. 3.6 he derived the following relation:

$$\nu = \frac{2}{2 + h_\mathrm{G}} \tag{3.10}$$

in which the subscript G refers to the class of the group G that describes the packed local symmetry in the lattice. The Coxeter number describes the reflection operations in the symmetry group. All symmetry groups are listed in Table 3.1.

3.4 Paramagnetic Linewidth and Vortex Dynamics above T_{KT}

To derive the influence of the vortex dynamics on the experiments, one needs to analyze the spin-spin correlation function in the critical regime. The critical regime can be theoretically described via 4-spin correlation functions. Usually, the only practical way to treat these functions is to decouple them into products of 2-spin correlation functions [Richards 1973]:

$$\langle S^{\alpha}_{\mathrm{q}}(t)S^{\beta}_{-\mathrm{q}}(t)(S^{\alpha}_{\mathrm{q}'}S^{\beta}_{-\mathrm{q}'})^{\dagger}\rangle = \delta(q-q')\langle S^{\alpha}_{\mathrm{q}}(t)(S^{\alpha}_{\mathrm{q}})^{\dagger}\rangle\langle S^{\beta}_{\mathrm{q}}(t)(S^{\beta}_{\mathrm{q}})^{\dagger}\rangle \tag{3.11}$$

Following this treatment, the general expression of the ESR linewidth reads [Benner 1990]:

$$\begin{aligned}\Delta H \sim \sum_{\mathrm{q}} \int dt e^{i\omega_0 t}[&|F^0_{\mathrm{q}}|^2\langle S^+_{\mathrm{q}}(t)S^-_{-\mathrm{q}}\rangle\langle S^z_{\mathrm{q}}(t)S^z_{-\mathrm{q}}\rangle \\ &+ |F^1_{\mathrm{q}}|^2(3|\langle S^+_{\mathrm{q}}(t)S^-_{-\mathrm{q}}\rangle|^2 + 8|\langle S^z_{\mathrm{q}}(t)S^z_{-\mathrm{q}}\rangle|^2) \\ &+ |F^2_{\mathrm{q}}|^2\langle S^-_{\mathrm{q}}(t)S^+_{-\mathrm{q}}\rangle\langle S^z_{\mathrm{q}}(t)S^z_{-\mathrm{q}}\rangle]\end{aligned} \tag{3.12}$$

where $S^{\pm} = S_{\mathrm{x}} \pm iS_{\mathrm{y}}$ and $|F^0_{\mathrm{q}}|$, $|F^1_{\mathrm{q}}|$, and $|F^2_{\mathrm{q}}|$ are geometrical coefficients resulting from a summation of dipolar contributions over all sites of a square lattice. For small q values they depend on the angle θ, which indicates the difference between the c-axis and the direction of magnetic field, as follows [Richards 1974]:

$$\begin{aligned}|F^0_{\mathrm{q}}| &\propto (3\cos^2\theta - 1) \\ |F^1_{\mathrm{q}}| &\propto \sin\theta\cos\theta \\ |F^2_{\mathrm{q}}| &\propto \sin^2\theta\end{aligned} \tag{3.13}$$

On the other hand, the space-time Fourier transformation of the spin-spin correlation functions yields the dynamic structure factors, i.e.:

$$S_{\alpha\alpha}(q,\omega) = \sum_{\mathrm{r,r'}} e^{iq\cdot(r-r')} \int_{-\infty}^{\infty} \frac{dt}{2\pi} e^{i\omega t}\langle S(r,t)S(r',t)\rangle, \quad \alpha = x,y,z \tag{3.14}$$

In a series of papers, Huber assumed that, when the vortices become free, they diffuse much like the Brownian motion of particles observed on liquid surfaces. His calculations led to a dynamical structure factor without q-dependence [Huber 1978, Huber 1980, Huber 1982]. However, Mertens and co-workers assumed that the free vortices move

ballistically [Mertens 1989, Mertens 2000]. This mechanism yields a q-dependent dynamical structure factor. It exhibits a *central peak*, i.e. a peak around $\omega = 0$, with the squared *Lorentzian* form. In the case of the in-plane correlations ($\alpha = x, y$), the vortex structure is not localized (it has no spatial Fourier transform), it follows that:

$$S_{\mathrm{xx}}(q,\omega) \sim \frac{\gamma^3 \xi^2}{(\omega^2 + \gamma^2[1 + (\xi q)^2])^2} \tag{3.15}$$

where $\gamma = \frac{\sqrt{\pi}\overline{u}}{2\xi}$, and $\overline{u}$ is the vortex average velocity. Considering an antiferromagnetic square lattice, by restricting the calculations to the first Brillouin zone, $q_0 = (\pi, \pi)$, Voelkel et al. [Voelkel 1991] derived a similar expression of the in-plane correlation function:

$$S_{\mathrm{xx}}(q,\omega) \sim \frac{\gamma^3 \xi^2}{(\omega^2 + \gamma^2[1 + (\xi q^*)^2])^2} \tag{3.16}$$

where $q^* = |q_0 - q|$. Using Fourier transformation for Eq. 3.16, one gets the time-dependent correlation function:

$$\begin{aligned} S_{\mathrm{xx}}(q,t) &\sim \int_{-\infty}^{\infty} d\omega e^{i\omega t} \frac{\gamma^3 \xi^2}{(\omega^2 + \gamma^2[1 + (\xi q^*)^2])^2} \\ &= \frac{\pi \xi^2}{2\sqrt{(1 + (\xi q^*)^2)^3}} (\gamma \sqrt{1 + (\xi q^*)^2} t + 1) e^{-\gamma \sqrt{1 + (\xi q^*)^2} t} \end{aligned} \tag{3.17}$$

Taking into account only the dominant term of Eq. 3.12 and the approximation $\omega \ll \gamma\sqrt{1 + (\xi q^*)^2}$, Becker [Becker 1996] derived a simplified expression of ΔH_{xx}:

$$\begin{aligned} \Delta H_{\mathrm{xx}} &\sim \int d^2 q |F_{\mathrm{q}}^1|^2 \int dt e^{-i\omega t} (S_{\mathrm{xx}}(q,t))^2 \\ &\sim |F_{\mathrm{q}}^1|^2 \gamma^6 \xi^4 \int \frac{d^2 q}{\gamma^7 \sqrt{[1 + (\xi q^*)^2]^7}} \\ &\sim \gamma^6 \xi^4 \int \frac{dq^* q^*}{\gamma^7 \sqrt{[1 + (\xi q^*)^2]^7}} \sim \frac{\xi^2}{\gamma} \\ &= \frac{\xi^3}{\overline{u}} \end{aligned} \tag{3.18}$$

When vortices do not completely lie within the plane, an out-of-plane component must be taken into account. According to Voelkel et al. [Voelkel 1991], the *Maxwell Velocity Distribution* of vortices relates the correlation function and the structure factor as:

$$S_{\mathrm{zz}}(q,t) = n_{\mathrm{v}}|f(q)|^2 e^{-(\frac{q\bar{u}t}{2})^2} \tag{3.19}$$

where $n_{\mathrm{v}} \approx \frac{1}{(2\xi)^2}$ and $|f(q)|$ are the vortex density and structure factor, respectively. Contrary to the in-plane structure, the non-planar vortex is static and localized (has a spatial Fourier Transform). In addition, it shows a *Gaussian Central Peak*. This peak is clearly smaller than that which appears for the in-plane vortex [Mertens 1991]. Following the same way as in Eq. 3.18, the out-of-plane linewidth ΔH_{xz} can be calculated as:

$$\Delta H_{\mathrm{xz}} \sim \int d^2q |F_{\mathrm{q}}^2|^2 \int dt e^{-i\omega t}(S_{\mathrm{xx}}(q,t))(S_{\mathrm{zz}}(q,t)) \tag{3.20}$$

The resultant calculations have shown that $\frac{\Delta H_{\mathrm{xz}}}{\Delta H_{\mathrm{xx}}} \ll 1$, which is a clear indication of the very weak contribution of the out-of-plane part [Becker 1996]. Using Eq. 3.18, finally we can write down the equation which describes spin relaxation via vortices observed in ESR measurements as a function of temperature in the following way:

$$\Delta H = \Delta H_{\infty} e^{[\frac{3b}{\sqrt{T/T_{\mathrm{KT}}-1}}]} + b \cdot T + c \tag{3.21}$$

where ΔH_{∞} is the linewidth in the high temperature limit. The residual linewidth is added to describe any increase in the linewidth as the temperature increases [Heinrich 2003]. This increase can be attributed to several effects like spin-phonon processes (see section 5.3.2). Another possibility is the influence of Jahn-Teller effect in some Jahn-Teller active ions such as Cu^{2+}.

Experimental indications of a BKT phase transition in two-dimensional magnets were found in the honeycomb layer system $BaNi_2P_2O_8$ using Nuclear Magnetic Resonance (NMR) and ESR [Gaveau 1991, Becker 1996] as well as by ESR in the isostructural compounds $BaNi_2V_2O_8$ [Heinrich 2003] and $BaNi_2As_2O_8$ [Heinrich 2004]. Inelastic Neutron Scattering (INS) successfully detected the characteristic divergence of the correlation length from the structure factor in $MnPS_3$ which also crystallizes in honeycomb structure [Rønnow 2002]. Moreover, the anisotropic field dependence of the Curie temperature T_{c} detected with ferromagnetic resonance experiments in the square lattice two-dimensional ferromagnets $(CH_3NH_3)_2CuCl_4$ and K_2CuF_4 was interpreted in terms of a BKT scenario [Demokritov 1989]. Previous ESR measurements in frustrated triangular antiferromagnets, $HCrO_2$ and $LiCrO_2$, gave a strong signature of the presence of Z_2-vortices [Ajiro 1988]. Recent high-field ESR investigations suggest also the occurrence of the Z_2-vortices in the triangular antiferromagnet $NiGa_2S_4$ [Yamaguchi 2008].

4 Traces of Magnetic Vortices in $ACrO_2$

Among many possible structures of two-dimensional magnets, the triangular lattice antiferromagnet appears as a prominent candidate for looking for exotic phenomena like vortices, solitons, and skyrmions. In the presence of frustration, one of these exotic ground states is the spin-liquid state proposed for the $S = 1/2$ triangular Heisenberg antiferromagnet by P. W. Anderson in 1973 [Anderson 1973]. He suggested that, due to geometrical frustration, the ground state, the so-called resonant valencebond state, may be described by an assembly of randomly distributed movable open singlet pairs on a two-dimensional Heisenberg triangular lattice. The discovery of superconductivity in $Na_xCoO_2{\cdot}yH_2O$ [Takada 2003] has recently motivated further research in related triangular layered alkali transition-metal oxides. In the following section, we will focus on the magnetic behavior in respective ordered rock salt compounds $HCrO_2$, $LiCrO_2$, $NaCrO_2$ and delafossite compounds $CuCrO_2$, $AgCrO_2$, $PdCrO_2$, and $CuCrS_2$.

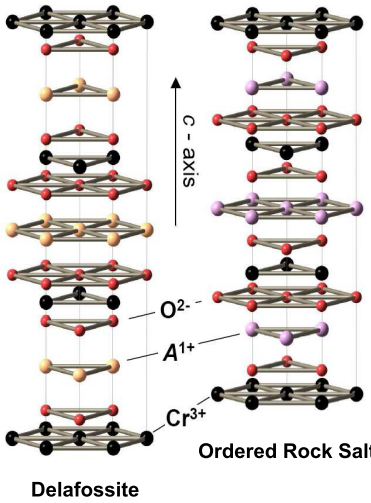

Figure 4.1: Crystal structure of ordered rock salts and delafossites. In ordered rock salts, the stacking pattern of O-A-O layers has a zigzag form, while in delafossites it has a straight form [Seki 2008].

The ordered rock-salt structure (space group $R\bar{3}m$) consists of hexagonal planes of edge-sharing CrO_6 octahedra separated by A^+ ions. Each element forms a triangular lattice and stacks along the c-axis in the sequence Cr-O-A-O-Cr. Rhombohedral stacking is realized among the Cr layers. In delafossite compounds, (space group $R\bar{3}m$), the

stacking pattern of O-A-O layers has a straight form as displayed in Fig. 4.1.

All these compounds have a significantly ionic character. The Cr^{3+} ions sit at the center of edge-sharing octahedra of O^{2-} ions, and thus the outer $3d$-orbital electron shell undergoes a crystal-field splitting to a lower energy t_{2g} triplet, and a higher energy e_g doublet. By Hund's rule, the three electrons of Cr^{3+} have aligned spins (3/2) and occupy all of the three t_{2g} states. The lack of orbital degeneracy ($\langle L \rangle = 0$) precludes the ordinary cooperative Jahn-Teller effect and ensures a very small spin anisotropy. The shape of the t_{2g} orbitals, pointing towards the neighboring Cr^{3+} ions, makes the direct exchange constant much higher than all next nearest neighbor interactions. For example, Delmas et al. [Delmas 1978] have pointed out that the superexchange interactions are ferromagnetic (except the e_g-s-e_g correlations which, however, are weak) and finally concluded that the direct t_{2g}-t_{2g} antiferromagnetic interactions overcome the superexchange interactions. Therefore, concerning their magnetic properties these compounds are a good realization of the nearest-neighbor Heisenberg model.

4.1 Magnetoelectric Phenomena in $ACrO_2$

4.1.1 Spin-Driven Ferroelectricity in $CuCrO_2$, $AgCrO_2$, $LiCrO_2$, and $NaCrO_2$

The possibility for a material to be both ferromagnetic and ferroelectric was predicted by P. Curie in 1894 [Curie 1894]. Later, the coupling term which modifies the magnetization by application of electric field (or the reverse) was predicted by an analysis of the Landau expansion of the free energy and was observed experimentally in Cr_2O_3 [Folen 1961]. In general, the transition-metal d electrons, which are essential for magnetism, reduce the tendency for off-center ferroelectric distortion. Consequently, an additional electronic or structural driving force must be present for ferromagnetism and ferroelectricity to occur simultaneously [Hill 2000]. In literature, many different mechanisms are proposed. Among them, the inverse Dzyaloshinsky-Moriya interaction appears as the most accepted mechanism to explain ferroelectricity in magnets with spiral-spin order [Katsura 2005]. For practical applications, the existence of exchange bias phenomenon allows to use antiferromagnetic materials for the storage of information.

$CuCrO_2$ and $AgCrO_2$ exhibit a 120° spin structure which is an ideal object to investigate the magnetoelectric correlation because of its simple commensurate spiral structure with the easy-axis anisotropy along the c-axis. The spin spiral propagates in the (110) plane and the spins rotate in the plane perpendicular to the wave vector. The inverse Dzyaloshinskii-Moriya model predicts that only polarization perpendicular to the spin spiral plane along the [110] direction is possible and that the net polarization vanishes due to the symmetry of the $(\mathbf{S}_\mathrm{i} \cdot \mathbf{S}_\mathrm{j})$ bonds which compensate each other in the trian-

gular antiferromagnet [Seki 2008]. This implies that the inverse Dzyaloshinskii-Moriya mechanism cannot be applicable for understanding the ferroelectric polarization in these compounds. $CuCrO_2$ reveals a sharp anomaly of the dielectric constant ε at T_N and a polarization of 25 μCm^{-2} below T_N. $AgCrO_2$ shows a smaller dielectric anomaly very close to T_N as well as less polarization of 20 μCm^{-2}. However, $LiCrO_2$ and $NaCrO_2$ do not exhibit any clear electric polarization over the whole temperature range below T_N, although ε displays a clear anomaly near T_N. This was attributed to, probably, antiferroelectric behavior due to the different rock-salt structure [Seki 2008].

Very recently, investigations in single crystalline $CuCrO_2$ revealed that ferroelectricity appears in the out-of-plane 120° spin structure where the spin chirality develops [Kimura 2008]. In addition, very recent symmetry analysis of neutron-diffraction data exhibits that two types of magnetic structures are possible, either a helicoidal, slightly modulated 120° spiral spin structure in the ground state with the spin rotation along the a-axis or a cycloidal one with the spin rotation axis parallel to the direction [120]. Regarding the ferroelectricity, both magnetic structures are compatible with the existence of an electric polarization either along the a (helicoidal magnetic order) or along the c-axis (cycloidal magnetic order) [Poienar 2009]. Shortly after, Soda et al. [Soda 2009] performed a spin-polarized-neutron study in order to clarify the origin of the ferroelectricity. The neutron-measurement results demonstrate that the spiral plane is parallel to the (100) plane. An incommensurate proper-screw magnetic structure of $CuCrO_2$ induces electric polarization. Not only the magnetic structure but also the oxygen location contributes to the ferroelectricity of $CuCrO_2$. The electric polarization of $CuCrO_2$ cannot be explained by a conventional spin-current model but by a theoretical prediction proposed by Arima [Arima 2007]. According to him, in crystals with triclinic, monoclinic, or trigonal (rhombohedral) symmetries, the proper screw type of magnetic ordering can induce ferroelectricity through the variation in the metalligand hybridization with spin-orbit coupling. The ferroelectric polarization in delafossite compounds $Cu(Fe,Al)O_2$ was successfully explained by this mechanism. In addition the spin helicities of $CuCrO_2$ can be reversed by the reversal of the electric field in the multiferroic phase. Kimura and others [Kimura 2009] demonstrate that ferroelectric polarization reversal can be tuned by using both magnetic and electric fields. The observed magnetoelectric tunability can be attributed to a small in-plane spin anisotropy and a resultant high degree of freedom for the direction of ferroelectric polarization, which is characteristic of a multiferroic triangular lattice antiferromagnet with out-of-plane 120° or more precisely 118° [Yamaguchi 2010] spin structure. This can be clarified in the following way: two characteristic magnetoelectric responses are observed: one is the magnetic-field-induced 90° flop of the spin-spiral plane accompanied by a 90° flop of the ferroelectric polarization and the other is a drastic change in polarization versus electric field hysteresis

properties by the application of a magnetic field [Kimura 2009]. Turning back to the incommensurability issue, it was pointed out that the observed lattice distortion and the incommensurate modulation of the 120° structure should cooperatively stabilize each other [Kimura 2009]. The observed in-plane lattice distortion clearly lifts the high spin degeneracy due to the strong geometrical frustration in this system. Therefore, it is natural that the in-plane lattice distortion observed in $CuCrO_2$ is driven by a spin-lattice coupling to lift the spin degeneracy. A similar but more pronounced lattice distortion has been observed in another delafossite compound, $CuFeO_2$ [Terada 2006, Ye 2006]. Otherwise, if the spin system itself favors an incommensurate ground state, a lattice distortion lowering the crystal symmetry might occur due to the exchange striction mechanism. Previous studies on the rhombohedrally stacked triangular lattice antiferromagnets [Rastelli 1986, Kadowaki 1995] suggested that a finite inter-plane interaction causes a slightly incommensurate modulation of the 120° structure. In this case, the incommensurability can be a driving force for the lattice distortion.

4.1.2 Unconventional Anomalous Hall Effect in $PdCrO_2$

In general, the transverse Hall resistivity ρ_{xy} of materials containing localized magnetic moments can be described empirically as the sum of two contributions:

$$\rho_{xy} = \rho_{OH} + \rho_{AH} = R_0 B + 4\pi R_s M \tag{4.1}$$

where ρ_{OH} is the ordinary Hall resistivity due to the Lorentz force in a perpendicular magnetic field B, ρ_{AH} is the anomalous Hall resistivity, M is the magnetization, R_0 is the ordinary Hall coefficient and depends mainly on the density of carriers, and R_s is the anomalous Hall coefficient. The word anomalous comes from the fact that the Hall effect is much stronger in ferromagnetic conductors (ten times larger) than in nonmagnetic conductors, see for example [Nagaosa 2010]. The mechanism of the anomalous Hall effect (AHE) is controversial. The key issues are whether the effect is intrinsic or extrinsic. Several theories have been formulated to clarify this point [Karplus 1954, Smit 1955, Berger 1970]. Such theories predict that ρ_{AH} depends either linearly or quadratically on the longitudinal resistivity ρ_{xx}, i.e.:

$$\rho_{xy} = a\rho_{xx} + b\rho_{xx}^2 \tag{4.2}$$

Recently, the intrinsic AHE was ascribed to the Berry phase effect in ferromagnetic semiconductors [Jungwirth 2002] and transition-metal oxides [Taguchi 2001, Fang 2003]. Currently, a similar effect has been observed in geometrically frustrated antiferromagnets, the so-called unconventional anomalous Hall effect (UAHE): in $PdCrO_2$ the measured resistivity shows a strong non-linear temperature dependence in a wide temper-

ature range above T_N. Such a dependence is markedly different from that of ordinary magnetic metals with non-frustrated localized spin moments. The estimated entropy at T_N is substantially smaller than that expected for a system with $S = 3/2$, suggesting that short-range order is still present above T_N [Takatsu 2009]. In addition, resistivity measurements in the same single crystal, exhibit a highly two-dimensional metallic behavior with an anisotropy ratio $\rho_c/\rho_{ab} > 190$ (Fig. 4.2). While the conductivity mainly originates from the Pd layers, the conduction electrons in the Pd layer are strongly affected by the localized spins on the Cr layer. By applying a magnetic field along the c-axis direction and comparing ρ_{xy} and M above T_N [Takatsu 2010], both ρ_{xy} and M exhibit a linear field dependence as expected for the conventional Hall effect. Between T_N and $T^* = 20$ K, the linear behavior still holds. The slope change of $\rho_{xy}(H,T)$ in these temperature regions can be interpreted within the conventional AHE behavior, i.e., the temperature dependence of R_S. However, once the temperature decreases below T^*, ρ_{xy} deviates from the linearity, although M still varies linearly on the magnetic fields manifesting the UAHE.

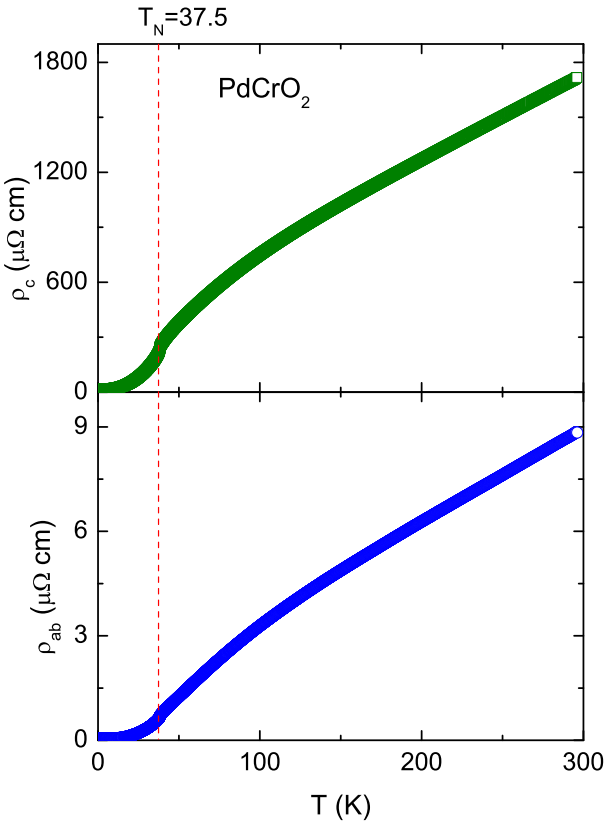

Figure 4.2: Temperature dependence of the electrical resistivity along the c-axis (ρ_c) and in the ab-plane (ρ_{ab}). Both (ρ_c) and ρ_{ab} exhibit clear anomalies at T_N, associated with the antiferromagnetic transition. Below T_N, ρ_c and ρ_{ab} behave almost in the same way. These data are taken from [Takatsu 2010].

To explain the UAHE in the frustrated magnet $PdCrO_2$, one considers the local exchange field acting on the Pd sites and the scalar spin chirality $\chi_{ijk}^{Pd} = \mathbf{s}_i \cdot (\mathbf{s}_j \times \mathbf{s}_k)$. In spin-glass systems, this chirality takes a nonzero value when the three spins span a non-coplanar configuration in spin space. It drives the local Hall current and leads to the overall Hall effect. In the weak-coupling limit it was shown that the Hall resistivity is proportional to a uniform chirality parameter with a sign that depends on the details of the band structure [Tatara 2002]. Theoretical studies of a ferromagnet with spin anisotropies on the two-dimensional kagome lattice show that a finite spin chirality, which is proportional to a solid angle subtended by spins, induces a finite Berry phase of conduction electrons. This Berry phase acts as a fictitious magnetic field, similar as in the Aharonov-Bohm effect, on the conduction electrons and leads to the anomalous Hall effect [Ohgushi 2000]. In contrast with the conventional mechanisms, this contribution appears without the spin-orbit coupling. Besides, for the spin-chirality mechanism, a ferromagnet is not necessarily ideal to induce a large Hall effect because the ferromagnetic correlation tends to align conduction electron spins parallel and decreases the chirality [Machida 2007]. In $PdCrO_2$, by applying a magnetic field along the c-axis direction, the Cr spin polarization leads to a non-vanishing net chirality and drives the UAHE [Takatsu 2010].

To summarize, the ferroelectricity as well as the unconventional anomalous Hall effect indicate the important role of the chirality inherent in the geometrically frustrated Cr spin lattice of $ACrO_2$. Further aspects of this chirality are accessible via electron spin resonance technique as will be discussed in the following sections.

4.2 Chromium Ordered Rock Salt Oxides

4.2.1 Sample Preparation and Magnetic Characterization

$HCrO_2$ powder was prepared using a hydrothermal method as follows: freshly prepared CrO_2 [Bajpai 2005] was put in a 1M LiOH solution in deionized water and heated to 200° C in a teflon-lined stainless-steel autoclave. This temperature was kept constant for a week and subsequently the sample was furnace cooled. Powder x-ray diffraction of the dark brown powder confirmed the proper formation of $HCrO_2$. Polycrystalline $LiCrO_2$ was prepared by heating a mixture of Li_2CO_3 (Aldrich, 99.99%) and Cr_2O_3 (Aldrich, 98.0%) at 1123 K in air for one day. X-ray powder diffraction reveals single phase formation and the peaks can be indexed using the trigonal space group, $R\bar{3}m$ [Alexander 2007]. Polycrystalline $NaCrO_2$ was prepared by mixing high purity $NaCO_3$ and Cr_2O_3, with 2% Na in excess of the stoichiometric amount, and grinding in an agate mortar. The mixture was pressed into pellets, wrapped in Zr foil, and heated in a dense alumina boat at $T = 750°$ C for 30 hours under flowing Ar with one intermediate

grinding. Characterization of the samples by powder x-ray diffraction showed them to be single phase with excellent crystalline quality [Olariu 2006]. The lattice parameters have been found to be $a = 2.976(1)$ Å, $c = 13.36(1)$ Å [Hamilton 1963], $a = 2.8949(12)$ Å, $c = 14.363(2)$ Å [Alexander 2007], and $a = 2.975(1)$ Å, $c = 15.968(5)$ Å [Soubeyroux 1979] for $HCrO_2$, $LiCrO_2$, and $NaCrO_2$, respectively.

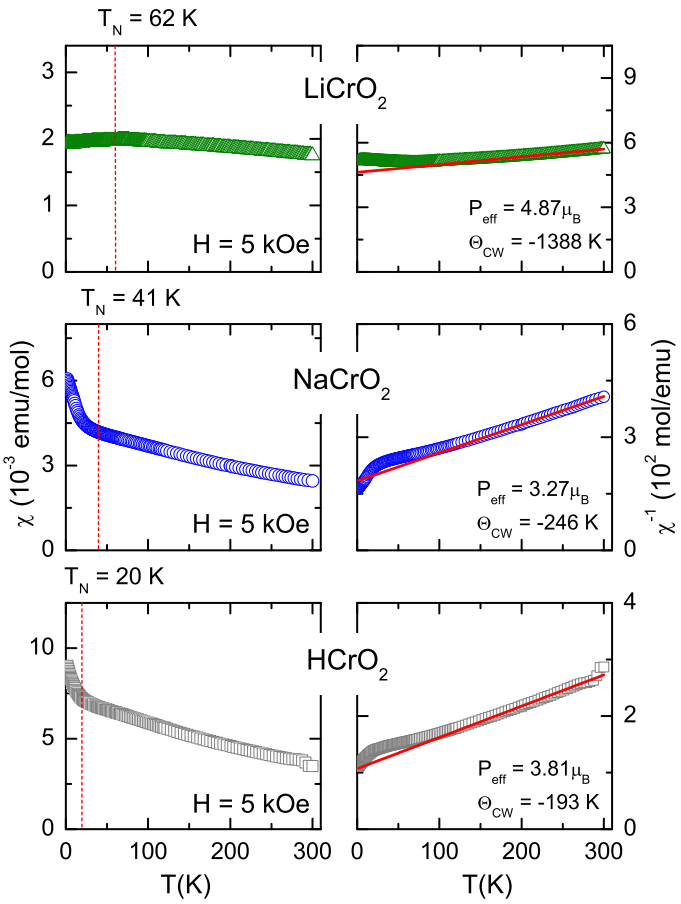

Figure 4.3: Left-hand frames: temperature dependence of the magnetic susceptibility of $HCrO_2$, $LiCrO_2$, and $NaCrO_2$. Measurements are carried out in an applied field of 5 kOe between 2 K and 300 K. The right-hand frames depict the inverse susceptibilities. In order to determine the Curie temperature Θ_{CW} and the effective magnetic moment, a linear fit of the data was performed between $200 - 300$ K.

The magnetic properties of all compounds are dominated by Cr^{3+} ions with $S = 3/2$ spin, which is surrounded by the octahedron of O^{2-} quenching the orbital moment. The magnetic susceptibility of $HCrO_2$ follows a Curie-Weiss law at high temperatures with a Curie temperature of $\Theta_{CW} = -193$ K resulting in the exchange constant, following Eq. 2.28, $J/k_B = \Theta_{CW}/15 \approx -13$ K. The resulting effective magnetic moment is obtained as $P_{eff} = 3.81\mu_B$ which is in a good agreement with the expected value of $3.87\mu_B$

for Cr^{3+}. The Néel temperature is $T_N = 20$ K (Fig. 4.3, the lower frame). The magnetic susceptibility of $LiCrO_2$, reveals a weak broad maximum at 65 K as a characteristic of a quasi-two-dimensional antiferromagnet (Fig. 4.3, the upper frame). At high temperatures, the susceptibility follows a Curie-Weiss law with a large antiferromagnetic Curie temperature $\Theta_{CW} = -1388$ K. The system undergoes a phase transition at $T_N = 62$ K. The effective paramagnetic moment $P_{eff} = 4.87\mu_B$ is larger than expected due to the fact that the asymptotic Curie-Weiss behavior is not yet reached at room temperature and the purely paramagnetic regime develops at higher temperatures only because of the large J/k_B. This means that one is still in the strongly antiferromagnetically correlated temperature range. Therefore, following the Curie-Weiss law, for the direct six neighbors the antiferromagnetic exchange constant is obtained as $J/k_B = \Theta_{CW}/15 = -93$ K which is much larger than that given by Alexander et al. as -39 K in Ref. [Alexander 2007]. For $NaCrO_2$, the magnetic susceptibility continuously increases down to $T = 49$ K (the middle frame in Fig. 4.3). The effective moment of $3.27\mu_B$ is clearly lower than the theoretical value $3.87\mu_B$. Note that $NaCrO_2$ displays a substantial Curie-like contribution at low temperatures which leads to a discrepancy in the effective moment value. Subtracting this Curie-contribution, yields a rough correction of the effective moment and Curie-Weiss temperature as $P_{eff} = 3.44\mu_B$, and $\Theta_{CW} = -300$ K, respectively. The antiferromagnetic transition is obtained from specific-heat measurements. Comparative specific heat measurements on the non-magnetic compound $NaScO_2$ were scaled and used to subtract the lattice contributions in $NaCrO_2$. The resulting magnetic specific heat exhibits a prominent peak at $T_N = 41$ K [Olariu 2006]. The corrected in-plane exchange constant $J/k_B \approx -20$ K is equal to that value given by Olariu [Olariu 2006].

4.2.2 ESR-Measurements

Typical resonance spectra obtained in the paramagnetic regime are depicted in Fig. 4.4. All compounds reveal a single exchange-narrowed resonance line, which is perfectly described by a Lorentzian curve. At elevated temperatures the resonance fields of all three compounds correspond to a g-value of about $g = 2$ indicating the quenched orbital moment of the half-filled t_{2g} state in Cr^{3+} with pure spin $S = 3/2$. The spectra broaden rapidly, shifting to higher resonance fields and becoming undetectable on approaching T_N. The temperature dependences of the intensities are illustrated in Fig. 4.5. The intensities have been scaled on the spin susceptibilities. The deviation of the ESR intensities from the static spin susceptibilities at low temperatures is probably due to short range order effects. Martinho et al. [Martinho 2001] have pointed out that the deviation of the ESR intensities from static spin susceptibilities at low temperatures can be attributed to the increasing influence of nonresonant relaxational modes with strongly increasing linewidth (see also section 5.2.2).

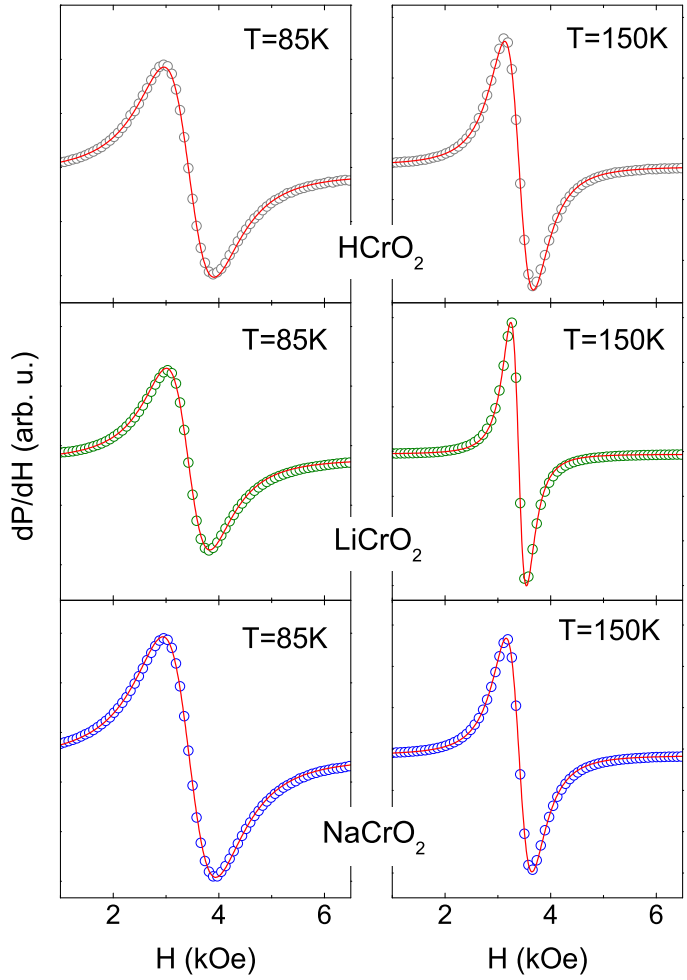

Figure 4.4: ESR spectra of $HCrO_2$, $LiCrO_2$, and $NaCrO_2$ in X-band ($\nu = 9.4$ GHz) for selected temperatures in the paramagnetic regime. The solid line indicates the fit with the field derivative of a Lorentz line.

The linewidth at room temperature amounts to 305 Oe, 158 Oe, and 287 Oe for the H-, Li- and Na-system, respectively. The corresponding resonance fields at the same temperature are 3384 Oe, 3390 Oe, and 3394 Oe. These linewidths diverge as they reach T_N. To characterize this divergence, the temperature dependence of the linewidth was analyzed in terms of critical behavior, as in [Heinrich 2003], and the BKT model (Eq. 3.21), but without any residual constant or linear contributions. Both models yield a satisfactory fitting of the linewidth data in the whole temperature range and the corresponding results are summarized in Table 4.1. Regarding the critical behavior, the parameter T_N approximates the literature values for all three compounds within an error bar of $5 - 14\%$. The critical exponent attains values of $p \approx 0.69 - 0.85$, in satisfactory agreement with [Ajiro 1988, Moreno 2004]. This value is rather small and theoretically unexpected for two dimensional magnets [Benner 1990] where such low exponents usually

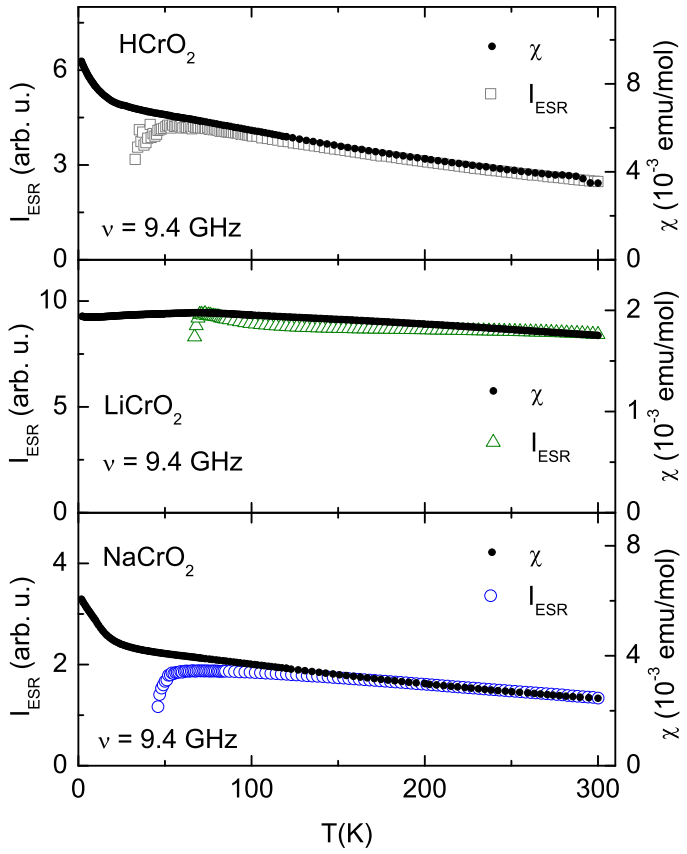

Figure 4.5: Temperature dependence of the intensity in $HCrO_2$, $LiCrO_2$, and $NaCrO_2$. The ESR intensities are scaled on the corresponding magnetic susceptibilities.

appear only near T_N due to three-dimensional antiferromagnetic fluctuations.

The BKT model is more favorable in all three compounds considering the coefficient of determination R^2. Contrary to previous applications of this model on ESR or NMR data [Gaveau 1991, Becker 1996, Heinrich 2003], where either only a narrow temperature regime near T_N was evaluated or additional relaxation contributions had to be added in order to fit a broader temperature regime, we now achieve an excellent description of the whole temperature range $T_N \leq T \leq 300$ K by the BKT scenario only, without adding any residual linewidth contribution. This establishes the dominant role of magnetic vortices for the spin relaxation in these systems.

In $LiCrO_2$ the ratio $T_{KT} \approx 0.9T_N$ is typical for a BKT transition [Gaveau 1991]. The small value of $b = 0.52$ is not in contradiction with theory, because this depends on the details of the underlying model and values lower than 1.5 were achieved in calculations as well [Mertens 1989, Heinekamp 1985]. These observations are supported by recent NMR experiments in $LiCrO_2$, which obtained a BKT transition at 55 K from the temperature dependence of the ^{7}Li nuclear spin-lattice relaxation rate [Alexander 2007]. For $NaCrO_2$ the parameter $b = 1.49$ fairly agrees with the value 1.5 derived from early calculations

	$HCrO_2$	$LiCrO_2$	$NaCrO_2$
J/k_B (K)(*Literatures*)*	-12	-39	-20
T_N (K) (*Literatures*)**	20	62	41
Critical behavior			
C (Oe)	1822(81)	318(2)	1147(15)
p	0.78(1)	0.69(1)	0.85(1)
T_N(K)	23.3(5)	65.2(1)	36.0(2)
R^2	0.99771	0.99848	0.99895
BKT model			
ΔH_∞(Oe)	94(3)	75(1)	77(1)
b	4.1(5)	0.52(1)	1.49(2)
T_{KT}(K)	2.6(6)	56.8(1)	19.2(2)
R^2	0.99863	0.99981	0.99974
KTHNY model			
ΔH_∞(Oe)	55(2)	46.5(3)	43.5(5)
b	2.0(1)	0.67(1)	1.41(1)
T_m(K)	8.4(6)	58.9(1)	23.9(1)
R^2	0.99861	0.99994	0.99977
KM model			
T_{KM} (K) [Theory]***	15.39	50.02	25.65
ΔH_∞(Oe)	66(2)	58.17(9)	56.5(8)
b	2.9(2)	0.601(2)	1.41(1)
T_{KM} (K)	4.49(9)	58.09(4)	22.11(9)
R^2	0.99824	0.99992	0.99977
BKT model with free ν			
ΔH_∞(Oe)	84(22)	44(2)	48(7)
b	3.0(1.5)	0.69(1)	1.40(1)
T_{KT}(K)	4(3)	59.1(1)	23(1)
ν	0.47(8)	0.36(1)	0.39(3)
R^2	0.99864	0.99995	0.99977

Table 4.1: Fit parameters for the temperature dependence of the ESR linewidth corresponding to critical behavior $\Delta H = C/(T/T_N - 1)^p$, BKT model $\Delta H = \Delta H_\infty \exp(3b/\tau^{0.5})$ with $\tau = T/T_{KT} - 1$, KTHNY model $\Delta H = \Delta H_\infty \exp(3b/\tau^{0.37})$ with $\tau = T/T_m - 1$, and KM model $\Delta H = \Delta H_\infty \exp(3b/\tau^{0.42})$ with $\tau = T/T_{KM} - 1$. In the last part of the table, the exponent ν was given free. The quality of the fit is characterized by the coefficient of determination $R^2 = 1 - \sum_i (y_i - f_i)^2 / \sum_i (y_i - \bar{y})^2$, where y_i, f_i, and $\bar{y}$ denote the data, the corresponding fit values, and the total average of the data, respectively. *[Ajiro 1988, Delmas 1978], **[Ajiro 1988, Alexander 2007, Soubeyroux 1979],***[Kawamura 2010].

[Kosterlitz 1974], whereas the ratio $T_{KT} \approx 0.5T_N$ is rather small. For $HCrO_2$ the ratio $T_{KT} \approx 0.13T_N$ is even smaller and the value of $b \approx 4.1$ unexpectedly large.

For further analysis of the data we recall the broad peak around 25 K found in the μSR data for $NaCrO_2$, which indicates strong magnetic fluctuations even below T_N and was interpreted as a gradual freezing into the ground state [Olariu 2006]. Such a scenario is strongly reminiscent to the refined BKT model, or KTHNY model. All linewidth data are very well described, using the modified correlation length of the KTHNY model, as illustrated in the lower panel of Fig. 4.6. The R^2 values are even improved as compared to the BKT fit for Li- and $NaCrO_2$. The logarithmic plot of ΔH vs. $\tau^{-0.37}$ shown in the inset reveals a linear dependence in the whole temperature range under consideration. For the record, using the exponent ν as free fourth fit parameter yields $\nu = 0.36(1)$, 0.39(3), and 0.47(8) for Li-, Na-, and $HCrO_2$, respectively. In this way Li- and $NaCrO_2$ are preferably described in terms of the KTHNY model. The other fit-parameter values like ΔH_∞, b, T_{KT} as well as R^2 are also comparable to those obtained in the KTHNY model (see Table 4.1). For $HCrO_2$ the exponent ν lies close to 0.5, but with a large error bar. The other fit parameters exhibit quite large uncertainties, as well. The R^2 value is, moreover, rather similar for BKT, KTHNY, and free ν fitting. Therefore, there is no clear preference for one of these approaches in $HCrO_2$. Fit parameters obtained from KM model [Kawamura 2010], have been also listed in (Table 4.1). Note that the KM scenario yields a comparable quality of the fit like the KTHNY scenario. Further discussion of the similarity of both scenarios are given in the next section.

The upper frame of Fig. 4.6 shows that the resonance fields can be simultaneously described by the melting scenario with slightly different T_m, although theoretical predictions do not exist yet. For $LiCrO_2$, T_m is close to T_N indicating only minor importance of fluctuations below T_N and in accordance with the well defined three-dimensional magnetic order established by neutron scattering [Soubeyroux 1979]. Very recently, a peak was observed in the μSR-relaxation at about $0.9T_N \approx 56$ K, which is very close to T_m indicating a narrowed fluctuation regime below T_N [Olariu 2009]. In $NaCrO_2$ the melting temperature $T_m = 24$ K is in good agreement with the μSR-relaxation peak, confirming the extended fluctuation regime. This is also supported by neutron-scattering detecting long-range order within the triangular planes only, but no definite magnetic periodicity along the c direction in $NaCrO_2$, due to a high number of short-range defects [Soubeyroux 1979]. Recent high-resolution neutron scattering reveals a weak incommensurate modulation along the c axis, suggesting interlayer frustration [Hsieh 2008]. It is important to note that the two-dimensional melting transition – from a well-ordered solid into a disordered liquid – is characterized by an intermediate liquid-crystal phase for $T_m \leq T \leq T_i$. The above evaluation suggests that in the two-dimensional magnetic systems under consideration T_N corresponds to T_i. So far, the spin-spin relaxation in

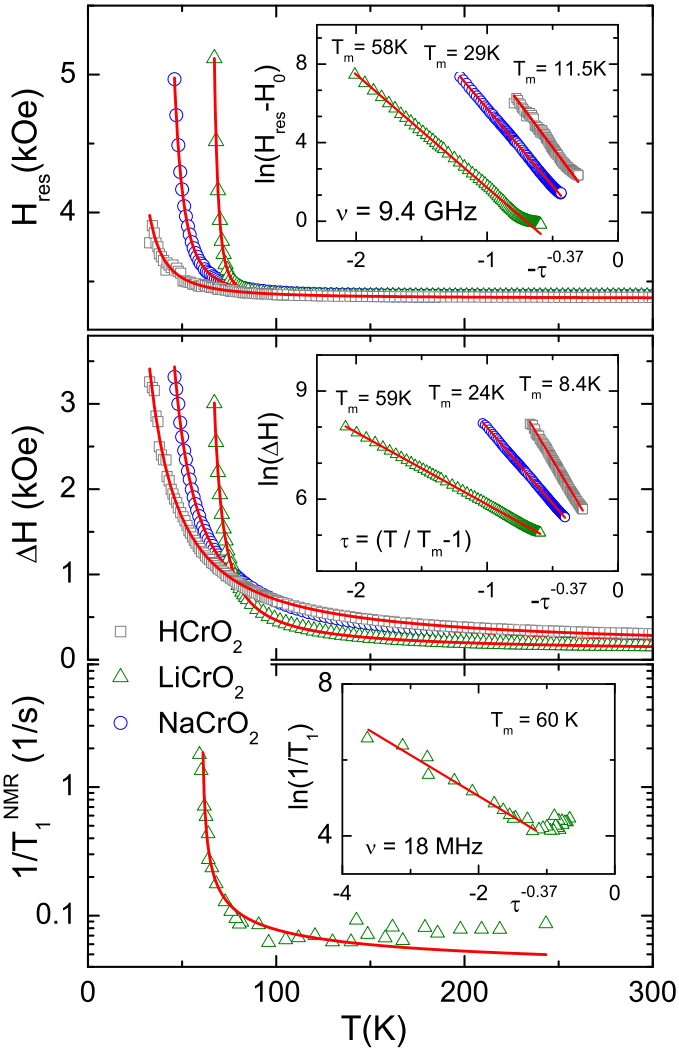

Figure 4.6: The first and the second frames from above show the temperature dependence of resonance field, and linewidth in $HCrO_2$, $LiCrO_2$, and $NaCrO_2$ at 9.4 GHz. The third frame exhibits a logarithmic representation of the nuclear spin-lattice relaxation rate $(1/T_1)$ versus temperature. $1/T_1$ was obtained via nuclear magnetic resonance (NMR) measurement technique in $LiCrO_2$ at 18 MHz. The fit in terms of KTHNY scenario is described in the text. Insets: Logarithmic plots of the linewidth in $HCrO_2$, $LiCrO_2$, and $NaCrO_2$ in the full accessible temperature range; upper frame: $\ln(H_{\rm res} - H_0)$ vs $-\tau^{-0.37}$, where H_0 denotes the resonance field without interaction, middle frame: $\ln(\Delta H)$ vs $-\tau^{-0.37}$, lower frame: $\ln(1/T_1)$ vs $-\tau^{-0.37}$. The KTHNY scenario fits the NMR data as well. The NMR data are the same as in [Alexander 2007].

ordered rock salt compounds favors the KTHNY scenario of two-dimensional melting which is in close relation to the KM scenario in two-dimensional Heisenberg antiferromagnets. This strongly indicates the existence of Z_2-vortices and their dominant role in the spin-spin relaxation mechanism. The universality of the Z_2-vortex induced spin-spin relaxation mechanism will be further corroborated in delafossite compounds in the following section.

4.3 Chromium Delafossite Oxides

4.3.1 Sample Preparations and Magnetic Characterization

Polycrystalline $CuCrO_2$ was prepared by solid-state reaction from the stoichiometric mixture of Cu_2O_3 [Seki 2008]. It was heated at 1000° C for 24 hours in air. Powder x-ray diffraction measurements did not show any detectable impurity. Single crystalline $CuCrO_2$ was grown by the flux technique, following Ref. [Poienar 2010]. $AgCrO_2$ was prepared by solid-state reaction as well but the stoichiometric mixture of Ag and Cr_2O_3 was heated for 48 hours in O_2 at 900° C, then pestled and heated again for 48 hours in O_2 at 900° C. A very small amount of impurity in $AgCrO_2$ has been also detected as in Ref. [Seki 2008]. The lattice constants have been found to be $a = 2.975$ Å, $c = 17.096$ Å, and $a = 2.984(4)$ Å, $c = 18.511(4)$ Å [Shannon 1971] for the Cu and Ag compound, respectively. Very recently, inelastic neutron scattering studies in single crystals of

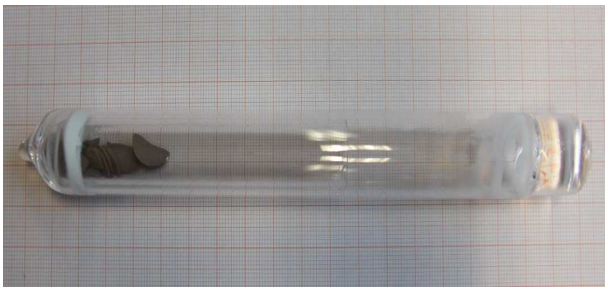

Figure 4.7: $PdCrO_2$ polycrystalline sample in evacuated sealed silica tube which is photographed on millimeter paper.

$CuCrO_2$ [Poienar 2010] showed that there is a weakly dispersive excitation along the c-axis which reflects the two-dimensional character of the magnetic interactions. The spin dynamics can be correctly described by the helicoidal model with a strong planar anisotropy.

In $CuCrO_2$, the magnetic susceptibility follows the Curie-Weiss law at high temperatures. In polycrystalline material, the Curie temperature amounts to $\Theta_{CW} = -213$ K and the corresponding exchange constant $J/k_B \approx -14$ K. A flat broad peak is observed close to the Néel temperature $T_N = 24$ K as characteristic of a quasi-two-dimensional

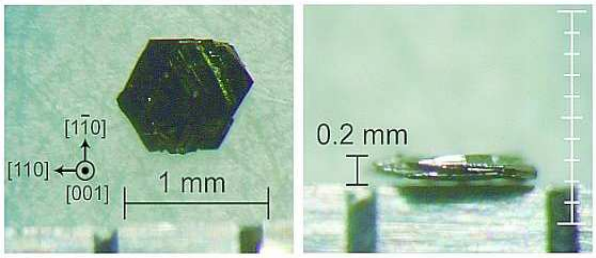

Figure 4.8: Optical microscope images of a single crystal of $PdCrO_2$.

antiferromagnet (Fig. 4.9, the lower frame). The effective magnetic moment is obtained as $P_{\text{eff}} = 4.02\mu_{\text{B}}$ which is somewhat larger than the expected value $3.87\mu_{\text{B}}$. For the single crystal, the Curie temperature amounts to $\Theta_{\text{CW}} = -165$ K and the exchange constant $J/k_{\text{B}} \approx -11$ K, which coincides with that value given in reference [Doumerc 1986] (Fig. 4.10). In fact, successive magnetic phase transitions have been also found at $T_{\text{N}_1} = 23.6$ K and $T_{\text{N}_2} = 24.2$ K [Kimura 2008]. The effective magnetic moment is obtained as $P_{\text{eff}} = 3.68\mu_{\text{B}}$ which is 5% below the expected value $3.87\mu_{\text{B}}$. The magnetic susceptibility of $AgCrO_2$ reveals also the same flat broad maximum at 38 K (Fig. 4.9, the middle frame). At high temperatures, the susceptibility follows a Curie-Weiss law with a high Curie-Weiss temperature $\Theta_{\text{CW}} = -159$ K. The system undergoes a phase transition at $T_{\text{N}} = 21$ K which is close to that in $CuCrO_2$. The effective paramagnetic moment $P_{\text{eff}} = 3.78\mu_{\text{B}}$ roughly corresponds to the expected one. The antiferromagnetic exchange constant is obtained as $J/k_{\text{B}} \approx -9$ K which is comparable to that given in Ref. [Doumerc 1986].

As in Ref. [Doumerc 1986], $PdCrO_2$ was prepared by using an exchange reaction in palladium molten chloride as:

$$Pd + PdCl_2 + 2LiCrO_2 \longrightarrow 2PdCrO_2 + 2LiCl \tag{4.3}$$

The starting mixtures were pressed and heated in an evacuated sealed silica tube for 4 days at 790° C (see Fig. 4.7). The reaction products were recovered as a black powder by washing in water. A further washing in aqua regia (royal water) was done to remove any traces of remained Pd metal and other by-products. Powder x-ray diffraction measurements show a single phase in $PdCrO_2$. Single crystals were grown by Takatsu and Maeno [Takatsu 2010] from the mixture of polycrystalline $PdCrO_2$ and NaCl with a mass ratio of typically 1 : 10. We note here that the minimum mass ratio in which single crystals were formed was 1 : 4. The mixture was sealed in an evacuated quartz tube ($130mm \times \varnothing 20mm$), heated to 880° C in 3.5 h, and kept at this temperature for 24 h. It was then cooled down to 800° C at a cooling rate of 0.25-0.5° C/h and to 700° C at 1° C/h. The melting point of NaCl is 801° C at ambient pressure. After the slow cooling

processes, the quartz tube was furnace-cooled down to room temperature. Single crystals were obtained with by-products such as Cr_2O_3. In order to grow larger crystals, single crystals were added in the mixture as seeds. The largest crystal size obtained is about $0.5 \times 0.5 \times 0.2mm^3$ (see the microscope pictures in Fig. 4.8). The lattice parameters at 25° C have been found to be $a = 2.923(3)$ Å, $c = 18.087(3)$ Å [Shannon 1971]. The observed magnetic susceptibility in the temperature range $2 \leq T \leq 300$ K, continuously increases down to $T = 49$ K (the upper frame in Fig. 4.9) and exhibits a broad peak around 50 K due to prominent short-range order. No anomaly indicating the long-range ordering is apparent. The relatively high negative $\Theta_{CW} = -568$ K and the enhanced paramagnetic moment of $4.19\mu_B$ result from the semi-flat susceptibility curve at high temperatures which in addition contains a Pauli-contribution of the conduction electrons in the Pd-planes. The corresponding in-plane exchange constant $J/k_B \approx -38$ K therefore appears to be enhanced as compared to the value given by Doumerc [Doumerc 1986]. Recent neutron powder diffraction measurements indicated that the system is a Heisenberg spin system and the spins lie in a plane containing the c-axis below T_N, i.e. an easy-axis type 120° structure [Mekata 1995]. Very recent, reported magnetization measurement results on single crystals confirmed that the magnetic susceptibility is nearly isotropic above T_N but becomes slightly anisotropic below T_N ($\chi_{ab} > \chi_c$). According to Takatsu et al. [Takatsu 2010], both χ_c and χ_{ab} in low fields show a strong enhancement at low temperatures below 60 K. This behavior is qualitatively different from χ of the powder sample. Small hysteresis loops are observed in the field dependence of both M_c and M_{ab}. These results may be attributed to a slight canting of the spins.

4.3.2 ESR-Measurements

For the two multiferroic compounds $CuCrO_2$ and $AgCrO_2$, typical ESR spectra are depicted in Fig. 4.11. Both compounds show a single exchange-narrowed resonance line, which is perfectly described by a symmetrical Lorentzian curve. In contrast, metallic $PdCrO_2$ can be well described by an asymmetrical Lorentzian (Dysonian) curve due to the skin effect which appears in the conductive compounds because of the interaction between the applied microwave field and mobile charges. The linewidth at room temperature amounts to about 178 Oe, 205 Oe and 224 Oe for $CuCrO_2$, $AgCrO_2$, and $PdCrO_2$, respectively. The corresponding values of the resonance fields are 3381 Oe, 3382 Oe and 3368 Oe for the same respective order. The single crystal of $CuCrO_2$ reveals a linewidth of 153 Oe and 246 Oe at room temperature for the magnetic field applied in the ab-plane and along the c-axis, respectively (see the lower frame in Fig. 4.15). Note that at temperatures higher than 200 K, ΔH in $PdCrO_2$ starts to increase and to follow a linear Korringa like behavior as typical for metals. The effective "insulator" value of ΔH at room temperature can be roughly estimated as 99 Oe by subtracting the Kor-

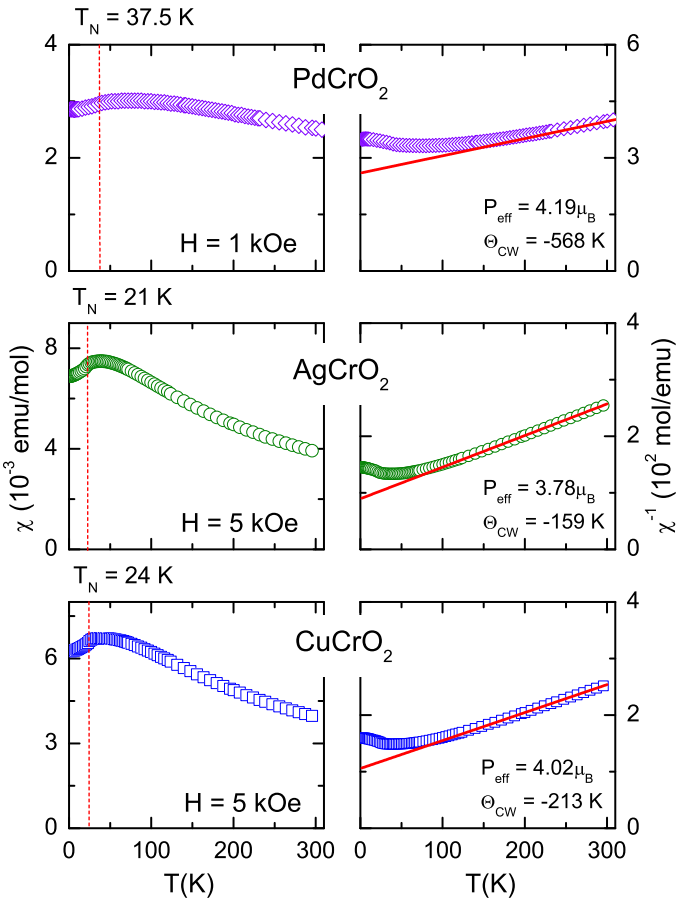

Figure 4.9: Left-hand frames, temperature dependence of the magnetic susceptibility of $CuCrO_2$, $AgCrO_2$, and $PdCrO_2$. Measurements are carried out in an applied field of 5 kOe in the first two compounds between 2 K and 300 K and 1 kOe in $PdCrO_2$ between 2 K and 400 K. The right-hand frames show the inverse susceptibilities. The red solid lines indicate linear fit curves of the data between $200-300$ K in $CuCrO_2$, $AgCrO_2$ and between $300-400$ K in $PdCrO_2$.

ringa contribution. Similar procedures can be done to get the corrected values of ΔH in the $PdCrO_2$ single crystal as well. One obtains 68 Oe and 98 Oe for the field applied in the *ab*-plane and along the *c*-axis (see the lower frame in Fig. 4.16). On decreasing temperature the spectra broaden rapidly, shift to higher resonance fields, and become undetectable on approaching the ground state at T_N. The high-temperature resonance fields of these compounds correspond to a *g*-value of about $g = 1.98$, close to 2 indicative for the nearly quenched orbital moment of Cr^{3+}. In the single crystal of $CuCrO_2$, the resonance fields $H_{res.}$ have been found to be 3388 Oe and 3380 Oe in *ab*-plane and *c*-axis, respectively. This indicates an anisotropy in *g*-value as $\Delta g = g_{ab} - g_c \approx 0.005$. In the single crystal of $PdCrO_2$, $H_{res.} = 3414$ Oe and 3369 Oe in *ab*-plane and *c*-axis, respectively. The corresponding anisotropy of the *g*-value is larger than in $CuCrO_2$: $\Delta g \approx 0.03$.

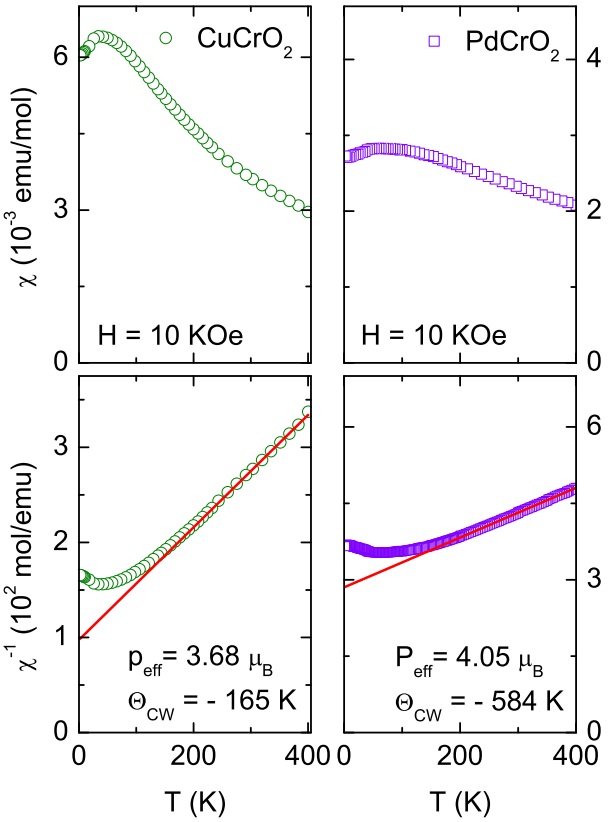

Figure 4.10: The magnetic susceptibility of single crystals of $CuCrO_2$ and $PdCrO_2$. The measurement has been performed in the direction parallel to *ab*-plane.

The temperature dependence of the fit parameters, i.e. intensity, resonance field, and linewidth, is depicted in Fig. 4.12, Fig. 4.13 and Fig. 4.14 for $CuCrO_2$, $AgCrO_2$, and $PdCrO_2$, respectively. The ESR intensities have been plotted together with the static spin susceptibilities, revealing the characteristic maximum of two-dimensional antiferromagnets, which scales with the exchange constant J/k_B. The deviation of the ESR intensities from static spin susceptibilities at low temperatures is similar to that observed in the geometrically frustrated spinel compound $ZnCr_2O_4$, where it has been attributed to the increasing influence of nonresonant relaxational modes with strongly increasing linewidth [Martinho 2001]. For detailed discussion about this point one is referred to section 5.2.2. Considering the linewidth like in $ACrO_2$ rock salts (A: H, Li, Na), the broad fluctuation regime above T_N can be empirically described by $\Delta H = C\varepsilon^{-p}$, with $\varepsilon = (T/T_N - 1)$. Critical exponent values have been obtained as $p \approx 0.9$, 0.8, and 0.7 for $CuCrO_2$, $AgCrO_2$, and $PdCrO_2$, respectively. These values are very close to those in the rock salts (see Table 4.1). Here one recalls that in $NaCrO_2$ μSR and NMR experiments indicated strong magnetic fluctuations even below T_N, which were interpreted as a possible evidence of Z_2-excitations in the chirality vortex regime [Olariu 2006]. Moreover, in

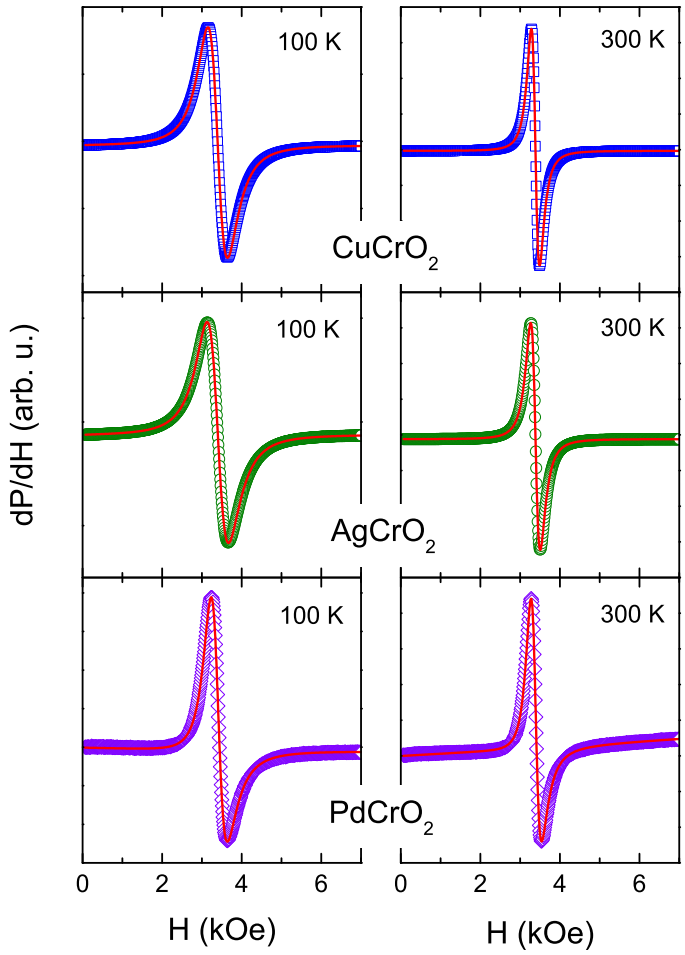

Figure 4.11: ESR spectra of $CuCrO_2$, $AgCrO_2$, and $PdCrO_2$ in X-band for selected temperatures in the paramagnetic regime. The solid line indicates the fit with the field derivative of a Lorentz line (symmetrical in $CuCrO_2$, $AgCrO_2$ and asymmetrical in $PdCrO_2$). The linewidth strongly increases as the temperature approaches T_N.

the triangular lattice antiferromagnetic compound $CsMnBr_3$, such an extended critical region found by neutron scattering is attributed to the dominance of dynamical chirality due to chiral fluctuations. The corresponding fluctuations are related to four-spin correlations, and their direct experimental study is impossible [Plakhty 1999, Plakhty 2000]. Indeed as was pointed before (see section 3.4), the ESR linewidth is determined by four-spin correlation functions, which makes the dynamical chirality or rather chiral fluctuations accessible to ESR technique.

Like in the ordered rock-salt compounds the temperature dependence of the ESR linewidth can be very well described in the whole temperature regime $T_N < T < 300$ K in terms of a BKT- or related scenario without any residual linewidth contribution. Only in $PdCrO_2$ a slight additional linear increase shows up above 200 K due to the

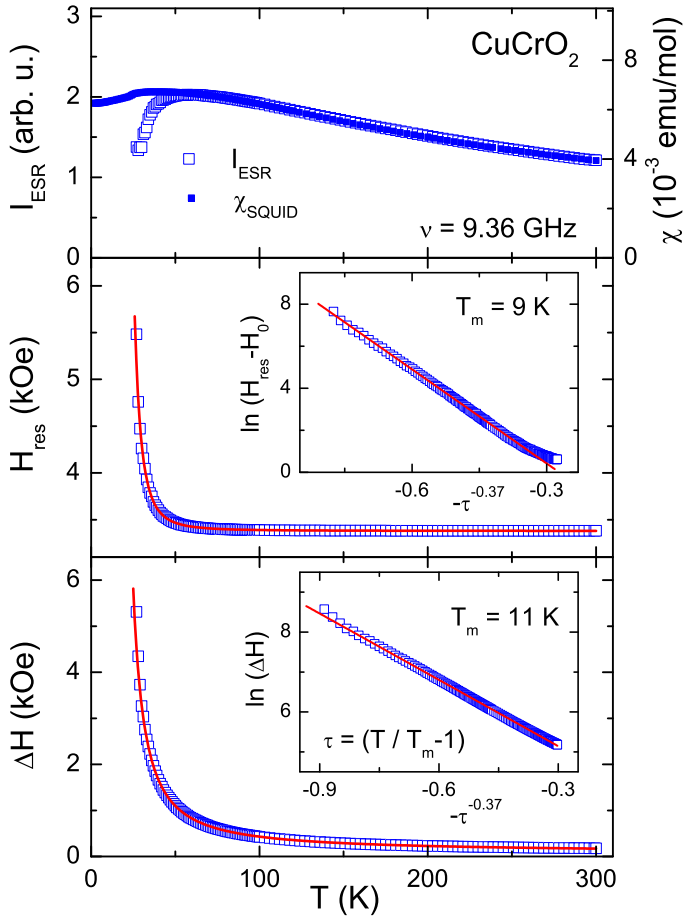

Figure 4.12: Temperature dependence of the intensity, resonance field, and linewidth in $CuCrO_2$. The fit in terms of KTHNY scenario is described in the text. Insets: Logarithmic plots of the linewidth in $CuCrO_2$ in the full accessible temperature range; middle frame: $\ln(H_{\mathrm{res}} - H_0)$ vs $-\tau^{-0.37}$, where H_0 denotes the resonance field without interaction, lower frame: $\ln(\Delta H)$ vs $-\tau^{-0.37}$.

conductivity of the sample and the corresponding Korringa relaxation of the Cr spins via the conduction electrons. Starting from the pure BKT fit with $\nu = 0.5$ one finds a significantly improved fit quality as compared to the critical behaviour in $CuCuO_2$ and $AgCrO_2$. However, the KT temperature is significantly below T_{N} in both compounds, like in $NaCrO_2$ and $HCrO_2$. Only in $PdCrO_2$ the ratio $T_{\mathrm{KT}}/T_{\mathrm{N}} = 0.85$ is similar to the expected value for a BKT-transition. The same holds for the value of the b parameter, which exceeds the theoretical value of 1.5 both in the copper and silver compound, but remains below this maximum value in $PdCrO_2$, which behaves comparable to $LiCrO_2$. Giving the exponent ν free in the BKT-like scenario results in exponents smaller than 0.5 for all three compounds, where $CuCrO_2$ approaches closest to the KTHNY behavior. Fixing now the exponent to $\nu = 0.37$ for the KTHNY model or $\nu = 0.42$ following the

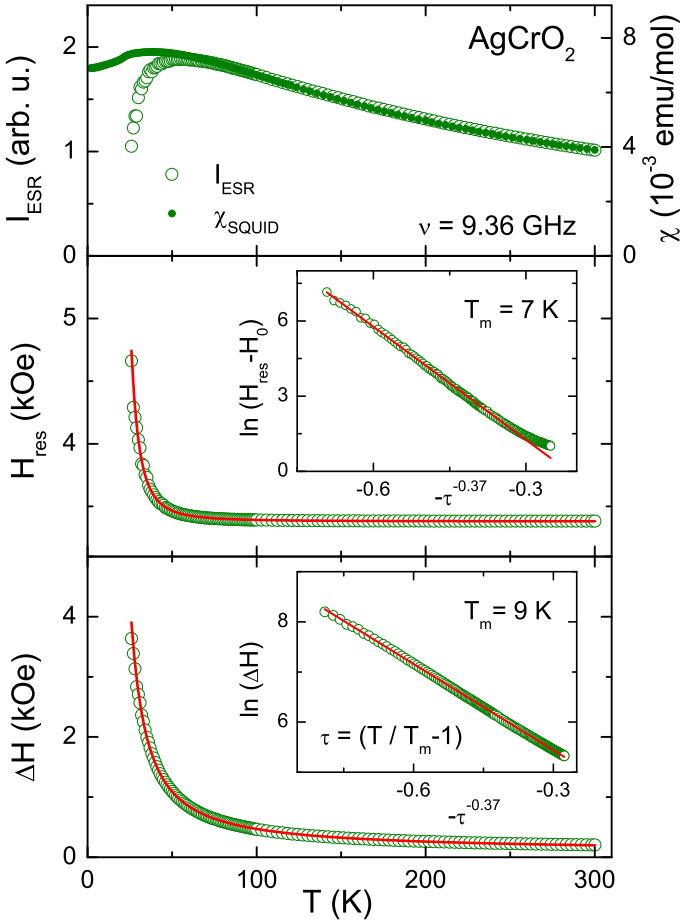

Figure 4.13: Temperature dependence of the intensity, resonance field, and linewidth in $AgCrO_2$. The fit in terms of KTHNY scenario is described in the text. Insets: Logarithmic plots of the linewidth in $AgCrO_2$ in the full accessible temperature range; middle frame: $\ln(H_{\rm res} - H_0)$ vs $-\tau^{-0.37}$, where H_0 denotes the resonance field without interaction, lower frame: $\ln(\Delta H)$ vs $-\tau^{-0.37}$.

KM model yields a comparable high fitting quality. In $CuCrO_2$ and $AgCrO_2$ the melting temperature $T_{\rm m}$ derived from the KTHNY fit even better approximates the theoretically expected KM temperature than using the exponent $\nu = 0.42$. In the single crystal of $CuCrO_2$, the melting transition temperature $T_{\rm m} \approx 15$ K and 13 K are obtained for the magnetic field applied parallel and perpendicular to c-axis, respectively (see Fig. 4.15). Both values are close to that obtained in the polycrystalline sample (see table 4.2) and in very good agreement with the theoretical KM-temperature. On the other hand, in $PdCrO_2$ the experimental value of $T_{\rm m} = 33.4$ K lies in between the numerically estimated value of $T_{\rm m}$ and $T_{\rm N}$. This implies that the phase transition is largely affected by the interplane (out-of-plane) coupling or the anisotropy. Early studies by means of neutron-powder diffraction suggested that the strong competition between the intraplane (in-

	$CuCrO_2$	$AgCrO_2$	$PdCrO_2$
J/k_B (K)(*Literatures*)*	-11.4	-9	-23
T_N (K) (*Literatures*)*	24	21	37.5
Critical behavior			
C (Oe)	1230	1330	527(4)
p	0.86(1)	0.80(1)	0.66(1)
T_N(K)	23.30(4)	21.84(8)	37.15(6)
R^2	0.99858	0.9983	0.99639
BKT model			
ΔH_∞(Oe)	57.2(4)	68.5(3)	110(2)
b	2.45(3)	3.15(5)	0.56(1)
T_{KT}(K)	6.97(1)	3.97(9)	31.73(3)
R^2	0.99983	0.99982	0.99739
KTHNY model			
ΔH_∞(Oe)	31.66(1)	40.10(9)	73(2)
b	1.86(1)	1.93(2)	0.68(1)
T_m(K)	11.33(1)	9.01(3)	33.37(9)
R^2	0.99989	0.99985	0.99808
KM model			
T_{KM} (K) [Theory]**	14.62	11.54	29.50
ΔH_∞(Oe)	43.35(9)	47.21(4)	88.53(7)
b	1.90(2)	2.54(4)	0.62(1)
T_{KM}(K)	10.30(4)	5.44(5)	32.75(1)
R^2	0.99974	0.99973	0.99784
BKT model with free ν			
ΔH_∞(Oe)	29(4)	60(5)	26(7)
ν	0.35(2)	0.47(2)	0.23(2)
b	1.80(2)	3.13(7)	1.01(9)
T_{KT}(K)	12.25(5)	3.88(1)	34.99(3)
R^2	0.99976	0.99979	0.99841

Table 4.2: Fit parameters for the temperature dependence of the ESR linewidth corresponding to critical behavior $\Delta H = C/(T/T_N - 1)^p$, BKT model $\Delta H = \Delta H_\infty \exp(3b/\tau^{0.5})$ with $\tau = T/T_{KT} - 1$, KTHNY model $\Delta H = \Delta H_\infty \exp(3b/\tau^{0.37})$ with $\tau = T/T_m - 1$, and KM model $\Delta H = \Delta H_\infty \exp(3b/\tau^{0.42})$ with $\tau = T/T_{KM} - 1$. In the last part of the table, the exponent ν was given free. The quality of the fit is characterized by the coefficient of determination $R^2 = 1 - \sum_i (y_i - f_i)^2 / \sum_i (y_i - \bar{y})^2$, where y_i, f_i, and $\bar{y}$ denote the data, the corresponding fit values, and the total average of the data, respectively. *[Doumerc 1986],**[Kawamura 2010].

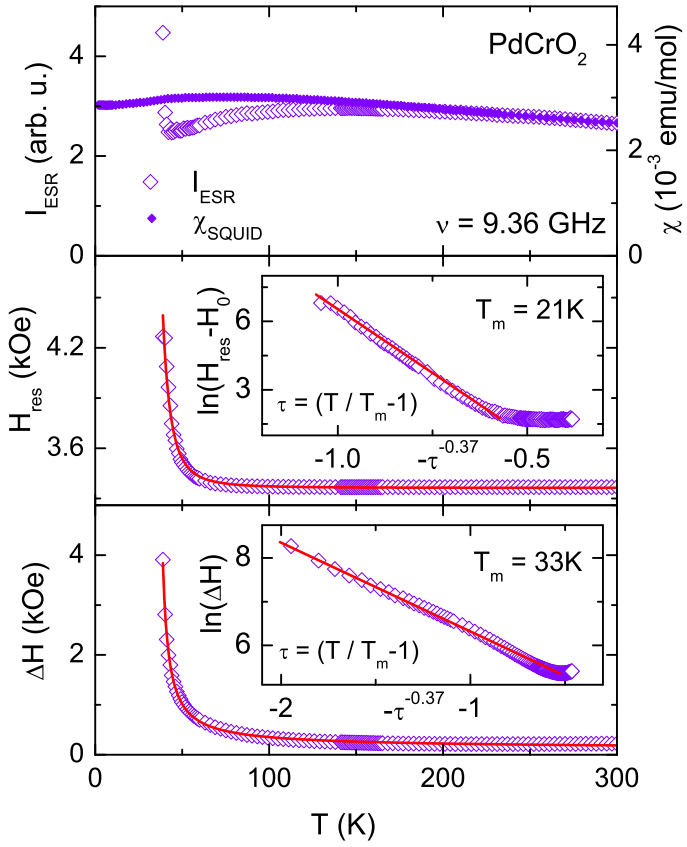

Figure 4.14: Temperature dependence of the intensity, resonance field, and linewidth in $PdCrO_2$. The fit in terms of KTHNY scenario is described in the text. Insets: Logarithmic plots of the linewidth in $PdCrO_2$ in the full accessible temperature range; middle frame: $\ln(H_{\rm res} - H_0)$ vs $-\tau^{-0.37}$, where H_0 denotes the resonance field without interaction, lower frame: $\ln(\Delta H)$ vs $-\tau^{-0.37}$.

plane) and the interplane (out-of-plane) interactions suppresses the development of the true long-range order below $T_{\rm N}$ and therefore is responsible for the fact that $T_{\rm N}$ increases $T_{\rm KM}$ [Kadowaki 1990, Oohara 1994, Mekata 1995]. In the single crystal of $PdCrO_2$, the melting transition temperature is obtained as $T_{\rm m} \approx 35(3)$ K and 29(3) K for the magnetic field applied parallel and perpendicular to the c-axis, respectively (see Fig. 4.16). Both values are comparable to that obtained in the polycrystalline sample (see table 4.2), the latter even matches the theoretical value of $T_{\rm KM}$. Like in the rock salts these data indicate that in delafossites the spin relaxation is governed by the presence of Z_2-vortices. Also the temperature dependence of the resonance field measured in the polycrystalline samples is well described in terms of the KTHNY scenario with slightly smaller $T_{\rm m}$ values than obtained from the linewidth. For the single crystals the reliable determination of the resonance field becomes more and more uncertain on approaching $T_{\rm N}$ from above, because of the smallness of the single crystals and strongly increasing linewidth, resulting

in a noisy signal. Therefore, the data only indicate the incipient increase of the resonance field on decreasing temperature but do not allow a satisfactory fit. Especially in the $PdCrO_2$ single crystal the skin effect serves for additional uncertainties concerning the dispersion to absorption ratio, which itself affects the resonance field.

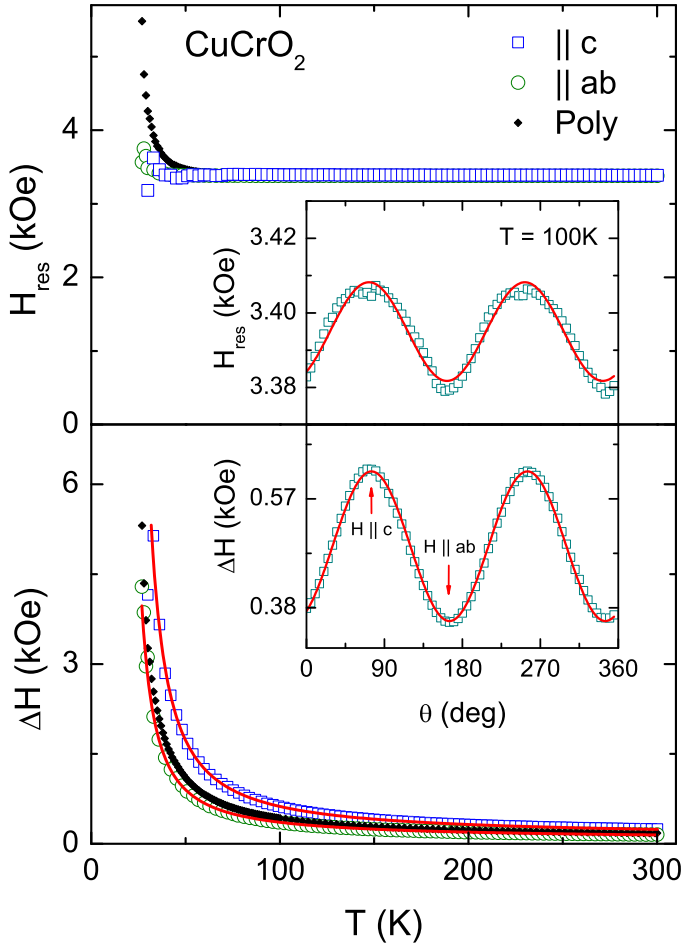

Figure 4.15: ESR parameters of a single crystal $CuCrO_2$. The average of the resonance fields in the *ab*-plane and along *c*-axis corresponds to the polycrystalline data at high temperatures. The inset exhibits the angular dependence of the ESR linewidth and the resonance field. The solid line indicates the fit using the following equation: $\Delta H = A + B\cos^2(\theta - C)$, where A, B, and C are arbitrary constants. H_{res} was fitted following the same equation. The *g*-value is nearly 2 as expected and shows a slight shift (0.005) from 2 in both directions at room temperature. The lower frame shows the melting scenario applied both in plane and out-of-plane.

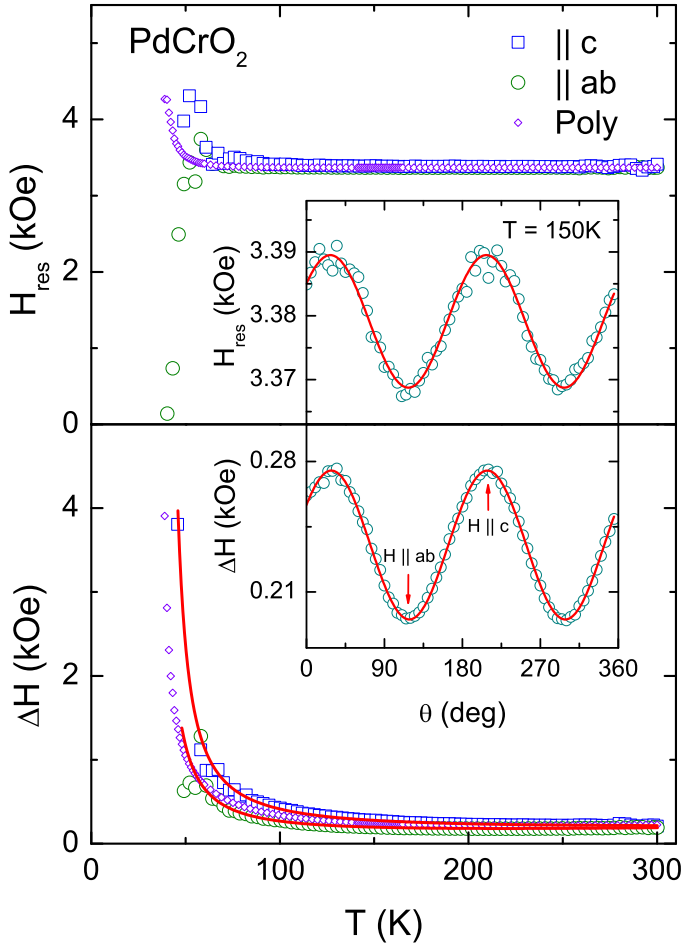

Figure 4.16: Temperature dependence of the resonance field H_{res} (upper frame) and linewidth ΔH (lower frame) of the ESR line in a single crystal $PdCrO_2$ compared to the powder sample. The insets illustrate the anisotropies of H_{res} and ΔH for rotation of the magnetic field from the c-axes into the ab-plane. The rotation of the magnetic field within the ab-plane does not reveal any kind of anisotropy. The solid lines indicate the fit using the following equation: $A + B\cos^2(\theta - C)$, where A, B, and C are arbitrary constants for both ΔH and H_{res}. In the lower frame, the melting scenario is applied both in the ab-plane and along the c-axis.

4.3.3 Estimation of the Linewidth at Room Temperature

To estimate the linewidth at room temperature, one has to calculate both dipolar and crystal field anisotropy contributions to the linewidth. The most difficult issue is to determine the crystal field anisotropy parameter D. To do that, one needs to prepare a single crystal, which is not always possible. The single crystal can be measured by antiferromagnetic resonance technique and, hence, the D parameter could be estimated. Another possibility is to derive the D value from optical measurement data, using theo-

retical outlines given by Angelov et al. [Angelov 1984], following Abragam and Bleaney [Abragam 1970], as:

$$D \propto \lambda^2 \frac{\Delta_{\text{trig}}}{\Delta_0^2} = 8\lambda^2 k^2 (\frac{\Delta_1 - \Delta_0}{\Delta_0^2}) \tag{4.4}$$

where $\Delta_0 \equiv 10Dq$, λ is the spin-orbit coupling and k is the coefficient of orbital reduction due to covalency. Early optical absorption measurements found that $10Dq$ values in chromium ordered rock salt and delafossite oxides are equal or slightly more than 17000 cm^{-1} [Elliston 1975, Dance 1988, Doumerc 1986], while in $NaCrS_2$ it is much smaller (14660 cm^{-1}) than in the corresponding oxide [Elliston 1975]. This is due to the reduced ionicity of the sulphide. The trigonal distortion of the octahedra, Δ_{trig}, is characterized by the $d'_{\text{O-O}}/d''_{\text{O-O}}$ ratio where $d'_{\text{O-O}}$ is the edge length of an octahedron within an oxygen double layer and $d''_{\text{O-O}}$ is the edge length along the c-axis. Using this expression leads to $D = 1000 - 1200$ Oe in ordered rock salts and delafossites [Meisenheimer 1961, Angelov 1984]. These values lead to smaller values in the crystal field contributions to the ESR linewidths than the dipolar contributions, which contradicts the data in the single crystals. A larger value of $D \approx 3535$ Oe is suggested by Dance et al. in the delafossite compounds $CuCrO_2$ and $AgCrO_2$ [Dance 1988]. This value is equal to that one, which is obtained with help of antiferromagnetic resonance technique in a single crystal of $CuCrO_2$ [Yamaguchi 2010]. Alternatively, using the expression $M_{2\text{ab}}^{CF} = \frac{6D^2}{5}$, where $M_{2\text{ab}}^{CF}$ can be obtained empirically from Eq. 2.48, one can give a rough estimation of the D-parameter from paramagnetic resonance measurements of the linewidth anisotropy at room temperature. In the available single crystals of $CuCrO_2$ and $PdCrO_2$, D is found to be about 7000 Oe, and 5800 Oe, respectively. Earlier measurements in a single crystal of $NaCrO_2$ given by Elliston and coworkers [Elliston 1975], are also used to give an estimation of D as 6800 Oe which is close to that value obtained in $CuCrO_2$. The exchange field H_{ex} values in polycrystalline compounds are determined by applying Eq. 2.29 as 29×10^4 Oe, 96×10^4 Oe, 49×10^4 Oe, 28×10^4 Oe, 22×10^4 Oe, and 56×10^4 Oe for $HCrO_2$, $LiCrO_2$, $NaCrO_2$, $CuCrO_2$, $AgCrO_2$, and $PdCrO_2$, respectively. Experimentally determined values of H_{ex}, (see Eq. 2.47), in single crystals of $NaCrO_2$, $CuCrO_2$, and $PdCrO_2$ are found to be 36×10^4 Oe, 72×10^4 Oe, and 45×10^4 Oe, respectively.

The calculated values of dipolar as well as crystal-field contributions, which are listed in table 4.3, have shown that the main contribution to the exchange-narrowed ESR linewidth comes from the crystal field. The total contributions from dipolar and crystal field are comparable to those values which were measured at room temperature.

Compound	$\Delta H_{\mathrm{DD}}[Oe]$	$\Delta H_{\mathrm{CF}}[Oe]$	$\Delta H_{\mathrm{Total}}[Oe]$	$\Delta H_{\mathrm{Observed}}[Oe]$
$HCrO_2$	74	252	326	305
$LiCrO_2$	27	77	104	158
$NaCrO_2$	44	150	195	287
$CuCrO_2$	78	109	187	178
$AgCrO_2$	97	109	206	205
$PdCrO_2$	44	96	140	99

Table 4.3: In the first two columns, the listed values are obtained by using Eqs. 2.44, 2.24. The last column exhibits the observed linewidth values at room temperature.

4.4 $CuCrS_2$

Ternary chromium dichalcogenides have been less intensively studied, and show a variety of different magnetic structures ranging from a 120° spin structure in $LiCrS_2$ [Lafond 2001] over a commensurate magnetic structure in $KCrS_2$ to a helix with an in-plane spin orientation in $NaCrS_2$ [Engelsman 1973]. Other interesting properties like ferroelectricity and electronic-ionic conductivity have been found in $AgCrS_2$ and $CuCrS_2$, respectively [Singh 2009, Engelsman 1973]. The compound under investigation, $CuCrS_2$ undergoes a transition to a super-ionic state at 670 K [Abramova 2006]. It is also assumed to exhibit a spin-glass state under the substitution of chromium ions by vanadium [Tsujii 2007].

4.4.1 Crystal Structure and Magnetic Properties

Ceramic material of $CuCrS_2$ was synthesized by solid-state reaction of the pure elements as described in detail in [Almukhametov 2003]. It crystallizes in space group $R\bar{3}m$ at room temperature. The basic atomic structure consists of covalent-ionic bound S-Cr-S layers separated by a van der Waals gap causing strong crystalline anisotropy perpendicular to the layers. Isolated CrS_2 is metastable and occurs only with an electron donor, therefore monovalent Cu^+ cations are intercalated between CrS_2 sandwiches [Rasch 2009]. The nearest-neighbor intralayer Cr-Cr distance of 3.48 Å is small compared to the interlayer Cr-Cr distance of 6.55 Å. The magnetic exchange within the layers over Cr-S-Cr pathways is expected to be much stronger than the interlayer exchange via Cr-S-Cu-S-Cr bonds. Early neutron-powder-diffraction experiments on $CuCrS_2$ revealed a three-dimensional magnetic ordering below T_{N} into a complex helical structure with

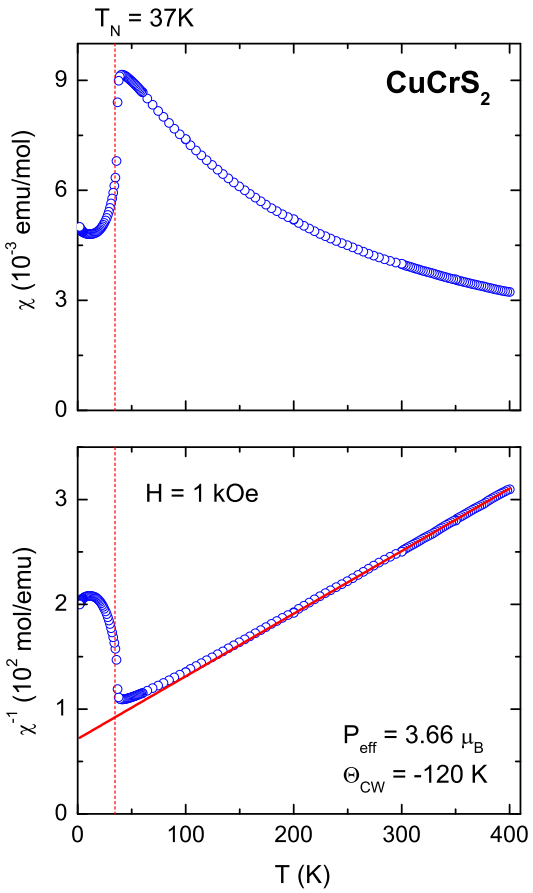

Figure 4.17: Magnetic susceptibility of polycrystalline $CuCrS_2$ in the temperature range $4 \leq T \leq 400$ K.

an incommensurate magnetic propagation vector [Winterberger 1987]. As the ordering of magnetic moments and the lattice distortion occur simultaneously, $CuCrS_2$ has been identified as magnetoelastic material [Rasch 2009]. Magnetic susceptibility measurements show a negative Curie-Weiss temperature of $\theta_{\mathrm{CW}} = -120$ K. The system undergoes a magnetic phase transition at $T_{\mathrm{N}} = 37$ K (Fig. 4.17). The effective magnetic moment $3.66\mu_{\mathrm{B}}$ is slightly smaller than the expected one but very close to that found in the single crystal of $CuCrO_2$. The ESR measurements were performed in the temperature range $4 \leq T \leq 300$ K. Typical ESR spectra are depicted in Fig. 4.18. All spectra show a single exchange-narrowed resonance line, which is satisfactorily described by a Lorentz curve. The resonance field (the middle frame in Fig. 4.19) increases as the temperature increases and reaches ≈ 3383 Oe at room temperature. This behavior is different from that observed in ordered rock salt and delafossite oxides which are investigated in this work. The corresponding g-value is ≈ 1.977 which is close to $g = 2$ (the middle frame in Fig. 4.19), indicating the quenched orbital moment of the half-filled t_{2g}^3 state in Cr^{3+} (spin $S = 3/2$). As the temperature decreases, the spectra broaden rapidly

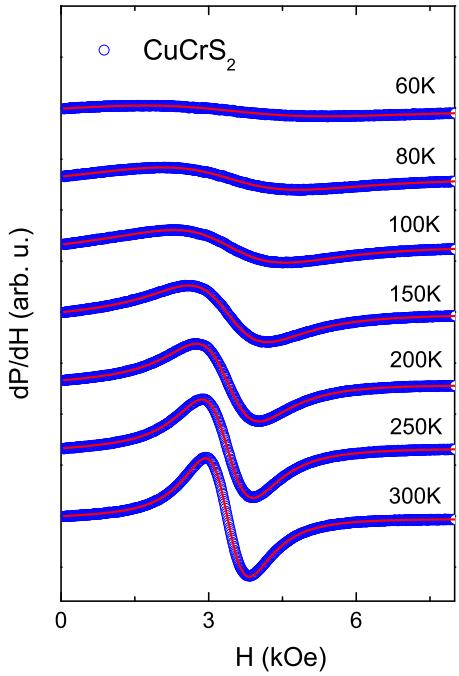

Figure 4.18: ESR spectra of $CuCrS_2$ in X-band for selected temperatures in the paramagnetic regime. Solid line: fit with the field derivative of a Lorentz line. At low temperatures, spectra becoming very broad and not any more observable below $T_N = 37$ K.

(Fig. 4.18), and become undetectable on approaching the Néel temperature $T_N = 37$ K. The linewidth at room temperature is about 770 Oe. The ESR intensity nicely matches the magnetic susceptibility which shows a bump at 50 K (the upper frame in Fig. 4.19). The temperature dependence of the linewidth approximately follows a critical behavior $\Delta H \propto (T - T_N)^{-p}$ in the whole temperature range with an exponent of $p \approx 0.65$ (the lower frame in Fig. 4.19). Previous ESR studies in the iso-structural single crystal $NaCrS_2$ at 36 GHz (Q-band), reveal a critical divergence of the linewidth with exponent values $p \approx 0.71, 0.67$ for the applied magnetic field along the c-axis and in the plane, respectively [Elliston 1974]. $AgCrS_2$ shows a critical exponent close to 0.66 [Benfield 1987]. The value of $T_N = 33$ K which is obtained from the fit of the linewidth is comparable to that observed by the susceptibility. In contrast to the other two-dimensional systems discussed above, the resonance field behaves different from the linewidth (the third frame in Fig. 4.19). The fitting in terms of a melting scenario was also successful, but the quality of the fit was only slightly below that of the critical behavior in contrast to the oxides, where the fit quality always was significantly improved when applying the melting scenario. Therefore a conclusive statement on the role of the magnetic vortices in $CuCrS_2$ cannot be given on the base of the data at hand.

Using ESR technique, Guy et al. [Guy 1985] have obtained a D-value from a single

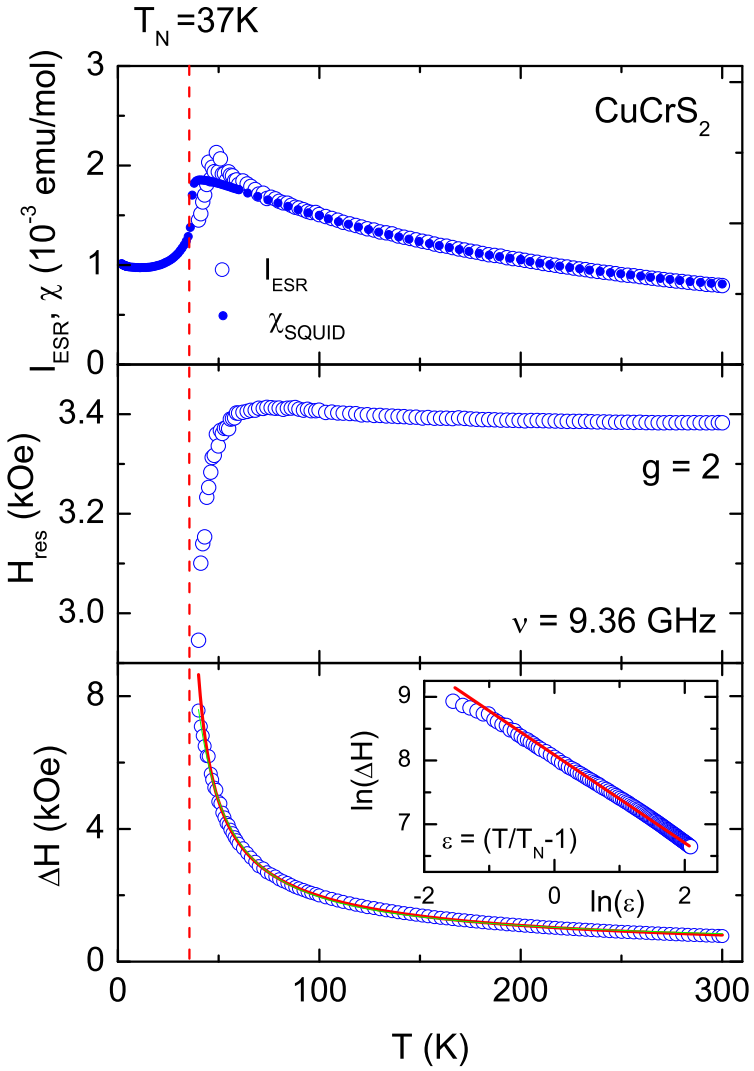

Figure 4.19: Solid lines: fit in terms of the critical behavior, the red line, as described in the text. The inset reveals the logarithmic plot of the linewidth versus the reduced critical temperature. The green line shows the melting scenario. Comparison between both critical behavior and melting scenario, i.e. the quality of the fit, shows that the former is favorite.

crystal of $CuCrS_2$ as 3100 Oe. This value is smaller than in the oxide compounds. The exchange field is smaller than in the oxides as well: $H_{ex} \approx 19 \times 10^4$ Oe. The total contributions from the dipolar and crystal field is 185 Oe which is significantly lower than the observed value at room temperature: 770 Oe. The reason is still unclear, whether there are other sources of anisotropy such as Dzyaloshinskii-Moriya interaction which should be included, or a rigorous estimation of D parameter is needed, or both.

4.5 Discussion

To summarize, the universal relaxation law in a two-dimensional frustrated triangular lattice under focus is dominated by magnetic vortex dynamics. The search for magnetic vortex dynamics and a corresponding BKT scenario was successful in the honey-comb layer antiferromagnet $BaNi_2V_2O_8$ [Heinrich 2003]. The divergence of the paramagnetic linewidth on approaching the antiferromagnetic order, was well described in terms of the divergent vortex correlation length which is characteristic for free unpaired vortices. The paramagnetic linewidth in the isostructural compounds $BaNi_2P_2O_8$ and $BaNi_2As_2O_8$ diverges in a similar way [Heinrich 2004]. However, due to the large linewidths in both compounds the fit parameters yielded values which were not in the same range as in $BaNi_2V_2O_8$. Therefore, it was not clear, whether these compounds reveal a BKT scenario as well. This question is left for further research in future to be more clarified. Recently, unconventional dynamics in the two-dimensional triangular lattice antiferromagnet $NaCrO_2$ was observed. Muon spin rotation and NMR revealed a fluctuating crossover regime extending well bellow T_N, with a peak of the relaxation rate $1/T_1$ around $T \approx 25$ K [Olariu 2006]. This novel finding was discussed within the context of excitations in the triangular Heisenberg antiferromagnets. It was suggested that the dynamical regime could be an evidence for "Z_2" excitations in the chirality vortex regime. In addition shortly after, based on the temperature dependence of NMR $1/T_1$ measurements in the isostructural compound $LiCrO_2$, a possible occurrence of a BKT transition taking place at $T \approx 54$ K was reported [Alexander 2007]. It is important here to note that this discussion was treated in the frame that freely moving vortices through lattice induce spin flipping. These findings in both compounds have motivated the author to search for a vortex driven universal relaxation law in the family of ordered chromium rock salt and some similar compounds such as chromium delafossites. Starting with ordered rock salts, $HCrO_2$, $LiCrO_2$, and $NaCrO_2$ exhibit a BKT-like scenario which is in agreement with the other results which are obtained by different measurement technique. As was mentioned already above, in $NaCrO_2$ the peak in the relaxation rate around 25 K corresponds to the BKT-like or rather KTHNY transition temperature T_m. Reinvestigating the NMR data in $LiCrO_2$ using the same model, KTHNY, leads to a transition temperature close to that obtained in the ESR linewidth (see the lower frame in Fig. 4.6). This scenario can give a good result in $HCrO_2$ as well. Remarkably, it is possible to describe the data without any residual contribution (which was necessary in $BaNi_2V_2O_8$), i.e. only with the divergence of the correlation length ξ as the theory states. Further investigations of chromium delafossites $CuCrO_2$, $AgCrO_2$, and $PdCrO_2$ lead to values close to the universal exponent value $\nu = 0.37$. On the other hand, current theoretical studies in the two-dimensional triangular Heisenberg model obtained a close exponent value 0.42. This value is used to fit the recent high-field ESR data at lower tem-

peratures (below 20 K) in the triangular antiferromagnet $NiGa_2S_4$ which suggested also the occurrence of Z_2-vortices [Yamaguchi 2008]. Very recently, the same authors found that the BKT scenario ($\nu = 0.5$) deviates from the their ESR data [Yamaguchi 2010]. However, the exponent value 0.42 as well as 0.37; i.e. $\nu < 0.5$ lead to a more convenient description of the data in $NiGa_2S_4$ (T. Okubo: Private Communication). This again corroborates that in a two-dimensional triangular antiferromagnetic lattice the KTHNY scenario describes the paramagnetic data successfully. Therefore, a universal exponent in this class of compounds is now so far well known. These new results in this work can be considered as a milestone for further research investigations in two-dimensional frustrated triangular antiferromagnetic oxides.

5 Chromium Spinels

5.1 Structure and Exchange Interactions

Chromium spinels have the composition ACr_2X_4 where A represents a divalent ion such as Mg, Zn, Hg, or Cd, and X^{2-} represents O^{2-}, S^{2-}, or Se^{2-} ions. The smallest unit cell that has cubic symmetry contains eight ACr_2X_4 molecules and, therefore, thirty-two anions and twenty-four cations. The X^{2-} anions constitute a fcc lattice which contains a total of sixty-four tetrahedral voids and thirty-two octahedral voids per unit cell.

In a stoichiometric crystal eight of the tetrahedral and sixteen of the octahedral voids are occupied by cations. They are called A and B (Cr in this work) sites, respectively. B^{3+} forms a pyrochlore lattice which occupies 1/2 of the octahedral voids. A diamond lattice is formed by A^{2+} and includes 1/8 of the tetrahedral voids. Two octants of the spinel structure are shown on the left-hand side of Fig. 5.1. From the left-hand octant of this figure one recognizes that the A site is tetrahedrally surrounded by four X^{2-} ions. It is also surrounded by a perfect tetrahedron of nearest neighbor metal ions A^{2+}. The adjacent octant has no A ion in the center. The octahedral Cr sites are found in this adjacent octant only. The position of each Cr^{3+} ion is on a body diagonal with a symmetrically placed X^{2-} ion on the same diagonal. In a perfect spinel the point symmetry of the A site is cubic, since it is surrounded both by a perfect tetrahedron of X^{2-} and A^{2+} metal ions, while this is not the case for the Cr site. Each Cr site is surrounded by an octahedron of X^{2-} ions. However, the nearest-neighbor Cr^{3+} ions surrounding a given Cr site induce an axis of symmetry in the $\langle 111 \rangle$ direction. Since any of the directions along the four-body diagonals occurs equally as symmetry axis,

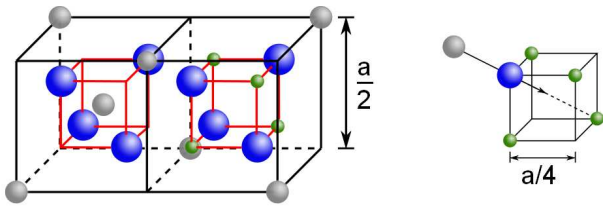

Figure 5.1: Crystal structure of spinel ACr_2X_4. A sites are the tetrahedrally coordinated ions and are indicated by gray spheres. Octahedrally coordinated Cr^{3+} ions are shown as small green spheres and anions (O^{2-}, S^{2-}, or Se^{2-} ions) as large blue spheres.

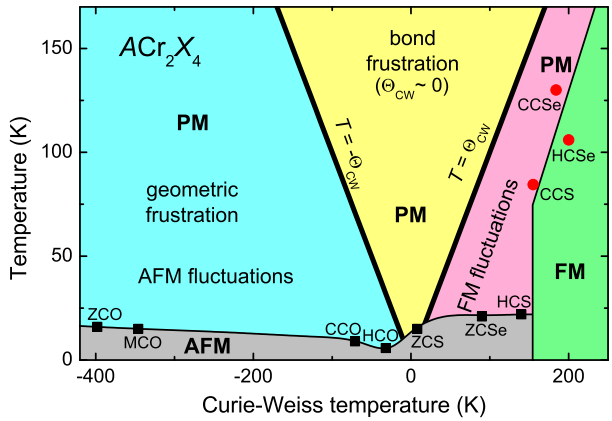

Figure 5.2: Schematic magnetic phase diagram of ACr_2X_4, where characteristic temperatures are plotted versus the Curie-Weiss temperature (Θ_{CW}). In this diagram the abbreviations of $ZnCr_2O_4$, $MgCr_2O_4$, $CdCr_2O_4$, $HgCr_2O_4$, $ZnCr_2S_4$, $CdCr_2S_4$, $HgCr_2S_4$, $ZnCr_2Se_4$, $CdCr_2Se_4$, and $HgCr_2Se_4$ are given as ZCO, MCO, CCO, HCO, ZCS, CCS, HCS, ZCSe, CCSe, HCSe, respectively. Ferromagnetic (FM) (red circles) and antiferromagnetic (AFM) (black squares) ordering temperatures are depicted. Hypothetical magnetic ordering temperatures ($T = \pm\Theta_{\mathrm{CW}}$) are indicated by thick solid lines. Thin solid lines separate magnetically ordered from paramagnetic (PM) phases and are drawn to guide the eye [Rudolf 2007].

the overall symmetry remains cubic. However, if the Cr^{3+} ion was exposed to a trigonal field, there would be four magnetically inequivalent sites.

The perfect spinel structure is seldom maintained. Often one finds deviations in the anion sublattice, in part because of considerations of relative size. The A sites have a volume too small for some of the metal ions which can be substituted at this site and tend to force out the four X^{2-} ions along the body diagonals. While the cubic symmetry is maintained for the A site, the anion octahedron becomes distorted and tends to reinforce the trigonal component at the Cr site (the right-hand side of Fig. 5.1). As it was mentioned in Section (2.5.2), the parameter x measures the distortion. If $x = 0.25$, the spinel is non-distorted. In a perfect spinel there are eight divalent ions in the A site and sixteen Cr^{3+} (trivalent) ions on the B-site. Such a spinel is called normal spinel, which holds for the compounds under focus in this work. There exist also spinels in which eight trivalent ions are distributed at random at the B sites, with the remaining eight trivalent ions at the A sites. Such a spinel is called an inverse spinel. It was often found that if the divalent ion is a transition metal ion, the spinel is inverse. In case of only partial inversion one speaks about intermediate spinels.

The evolution of the magnetic properties of the chromium spinels is schematically shown in Fig. 5.2. In the complete regime from strongly negative Θ_{CW} temperatures (-400 K) to positive Θ_{CW} temperatures of almost 150 K, the ground states of all spinels

exhibit antiferromagnetism with different spin arrangements, whereas a ferromagnetic ground-state is realized only for $\Theta_{\mathrm{CW}} > 150$ K.

Generally, the diversity of magnetic properties can hardly be explained without understanding the mechanism of exchange interactions between the Cr spins, their range, and relative strength. The estimation of the exchange constant is not an easy matter because of competing contributions from several nearest and next nearest neighbors. Such a competition leads to a complicated nature of the ground state as well. Anderson [Anderson 1956] has shown that the nearest-neighbor $Cr^{3+} - Cr^{3+}$ exchange interactions alone cannot produce any long-range antiferromagnetic order on the Cr site due to the geometrical frustration of the pyrochlore lattice. He has drawn attention to the next-nearest-neighbor interactions of type $Cr^{3+} - X^{2-} - X^{2-} - Cr^{3+}$ which can give antiferromagnetic long-range ordering, and T_{N} will depend on these interactions in a complicated way. This may explain the great difference between Θ_{CW} and T_{N} in $ZnCr_2O_4$, $MgCr_2O_4$, and $CdCr_2O_4$: the large negative Θ_{CW} arises from strongly antiferromagnetic nearest-neighbor interactions, whereas T_{N} is determined mainly by the much weaker antiferromagnetic next-nearest-neighbor interactions. Baltzer et al. [Baltzer 1966] have developed a model to explain the magnetism of the spinels on the basis of a Heisenberg spin Hamiltonian of the form:

$$\mathcal{H} = -2J \sum_{i,j} \mathbf{S}_i \cdot \mathbf{S}_j - 2K \sum_{i,k} \mathbf{S}_i \cdot \mathbf{S}_k \tag{5.1}$$

The first term includes six nearest-neighbor $Cr^{3+} - X^{2-} - Cr^{3+}$ superexchange interactions with an exchange constant J. Note that the interaction contains a direct antiferromagnetic $Cr^{3+} - Cr^{3+}$ exchange contribution, which dominates for small $Cr^{3+} - Cr^{3+}$ distance, as realized in the oxides. The 90° $Cr^{3+} - X^{2-} - Cr^{3+}$ super-exchange itself is expected to be ferromagnetic due to the Goodenough-Kanamori-Anderson rules and dominates for larger $Cr^{3+} - Cr^{3+}$ distance [Menyuk 1966]. The second term includes more-distant pair interactions which are assumed to have identical strength K. They considered 30 more-distant interactions including 12 second-nearest-neighbors at a distance $(a/4)\sqrt{6}$, 6 third-nearest-neighbors at a distance $(a/4)\sqrt{8}$, and 12 fourth-nearest-neighbors at a distance $(a/4)\sqrt{10}$. These interactions occur by the same type of extended super-exchange path, $Cr^{3+} - X^{2-} - A^{2+} - X^{2-} - Cr^{3+}$. Six third-nearest-neighbor interactions with a different path $Cr^{3+} - X^{2-} - Cr^{3+} - X^{2-} - Cr^{3+}$, are neglected. Other authors, see for example [Lotgering 1964], propose a $Cr^{3+} - X^{2-} - X^{2-} - Cr^{3+}$ interaction between second, third, and fourth neighbor pairs. In both cases, the calculated magnitudes of the more distant neighbor interactions could be of overriding significance, because of their much larger number.

In $ZnCr_2O_4$ considering the tetragonal symmetry and using the generalized constant

coupling model (GCC) to fit the magnetic susceptibility, one obtained ≈ -25 K for the nearest-neighbor $Cr^{3+} - Cr^{3+}$ interaction and approximately -3 K for the next-nearest-neighbors [Kant 2010]. The first value is very close to that estimated by applying molecular field theory, as approximately -26 K taking into account only the six nearest neighbors [Martinho 2001]. For the path $Cr^{3+} - O^{2-} - Cr^{3+}$, in both $ZnCr_2O_4$ and $MgCr_2O_4$, J/k_B has approximately the same value: -25 K [Lotgering 1971]. In $CdCr_2O_4$, the antiferromagnetic nearest-neighbor $Cr^{3+} - Cr^{3+}$ exchange interaction is weaker than in $ZnCr_2O_4$ and $MgCr_2O_4$, ≈ -15 K, while the next-nearest-neighbor exchange is ferromagnetic and yields ≈ 4 K [Kant 2010]. The role of next-nearest-neighbor ferromagnetic exchange coupling increases and becomes more important in chromium chalcognides [Rudolf 2007].

In sulfide compounds, antiferromagnetic next-nearest-neighbor interactions compete directly with ferromagnetic super-exchange $Cr^{3+} - S^{2-} - Cr^{3+}$ interactions. In $CdCr_2S_4$ the ferromagnetic exchange constant $J/k_B \approx 12$ K clearly dominates the antiferromagnetic one $K/k_B \approx -0.3$ K indicating that the ground state is obviously ferromagnetic [Baltzer 1966]. Within the frame of Weiss's molecular field theory, analogous values for the exchange constants have been obtained [Holland 1972]. In $HgCr_2S_4$ the ground state is a non-collinear antiferromagnet, although the ferromagnetic exchange interaction is the dominant one [Akino 1971](the ferromagnetic exchange constant $J/k_B \approx 13$ K is noticeable larger than the antiferromagnetic one $K/k_B \approx -0.6$ K) [Baltzer 1966]. It seems that the $Cr^{3+} - X^{2-} - Cr^{3+}$ angle is the factor which controls the nature of the magnetic ground state. In $HgCr_2S_4$ this angle is 98° (at room temperature), i.e. larger than for ferromagnetic $CdCr_2S_4$, for which the value is 96.9°. This is in agreement with Goodenough-Kanamori-Anderson superexchange rules since larger deviation from the 90° angle, for which antiferromagnetic correlation due to electron transfer is forbidden by symmetry, will increase the orbital overlap in favor of antiferromagnetic superexchange [Chapon 2006]. It is important to note that in the chromium spinel oxides $MgCr_2O_4$, $ZnCr_2O_4$, and $CdCr_2O_4$, the angle of $Cr^{3+} - O^{2-} - Cr^{3+}$ is larger than 90° as well: 95.5°, 95.4°, 99.9°, respectively [Motida 1970]. However, the dominant magnetic interaction is the direct antiferromagnetic exchange $Cr^{3+} - Cr^{3+}$ as was mentioned above.

Similar to sulfide compounds, the exchange interactions in selenides are all of the superexchange type ($Cr^{3+} - Se^{2-} - Cr^{3+}$), J/k_B, because the distance between the magnetic ions is too large for direct interactions. In fact, the interactions between more distant neighbors ($Cr^{3+} - Se^{2-} - Se^{2-} - Cr^{3+}$), K/k_B, should be taken into account. It was found $J/k_B \approx 10, 14, 16$ K while $K/k_B \approx -1, -0.1, -0.5$ K for $ZnCr_2Se_4$, $CdCr_2Se_4$, and $HgCr_2Se_4$, respectively [Lotgering 1971].

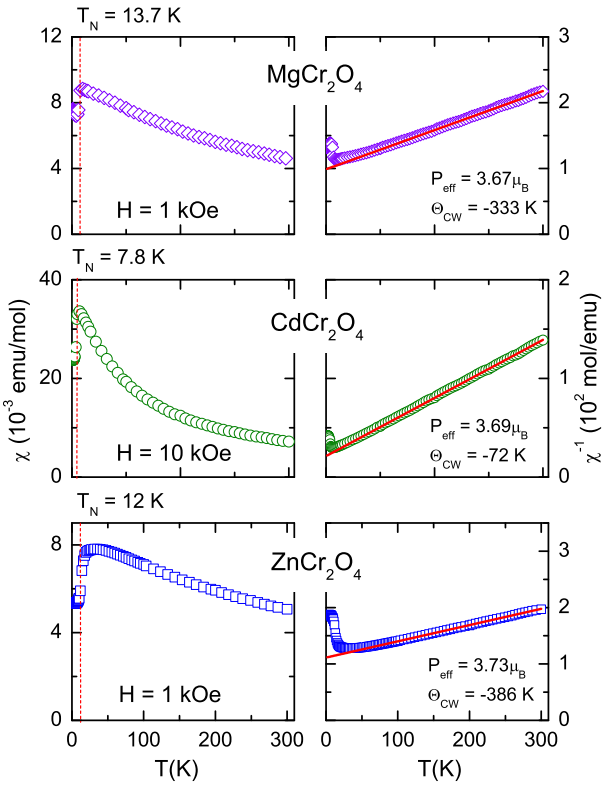

Figure 5.3: Temperature dependence of the magnetic susceptibility and its inverse of $ZnCr_2O_4$, $MgCr_2O_4$, and $CdCr_2O_4$ in the temperature range $4 \leq T \leq 300$ K.

5.2 Chromium Oxides

5.2.1 Sample Preparations and Magnetic Characterization

Polycrystalline $ZnCr_2O_4$, $MgCr_2O_4$, and $CdCr_2O_4$ samples were prepared by solid-state reaction from high-purity elements in evacuated quartz ampoules. The synthesis was repeated several times in order to reach good homogeneity.

Among all chromium spinels considered in this work, $ZnCr_2O_4$ and $MgCr_2O_4$ exhibit the smallest lattice constants $a = 8.317(2)$ Å, $a = 8.319(3)$ Å [Rudolf 2007], the highest negative Curie-Weiss temperatures $\Theta_{\rm CW} = -386$ K, $\Theta_{\rm CW} = -333$ K as well as the highest frustration parameters $f = \frac{|\Theta_{\rm CW}|}{T_{\rm N}} \approx 32$, and 24, respectively (usually $f = 10$ is taken as a minimum value to characterize geometrically frustrated magnets). Both compounds reveal an antiferromagnetic order at $T_{\rm N} = 12$ K for the *Zn*- and $T_{\rm N} = 13.7$ K for the *Mg*-system. The effective paramagnetic moments $P_{\rm eff}$ were estimated from the magnetic susceptibilities as $3.73\mu_{\rm B}$ in $ZnCr_2O_4$ and $3.67\mu_{\rm B}$ in $MgCr_2O_4$ which are about $4-5\%$ below the theoretical value $3.87\mu_{\rm B}$ see also Fig. 5.3. On the other hand, $CdCr_2O_4$ reveals a clear negative low $\Theta_{\rm CW} = -72$ K and relatively small $T_{\rm N} = 7.8$ K with a slight increase of the lattice constant $a = 8.596(2)$ Å [Rudolf 2007]. The frustration parameter

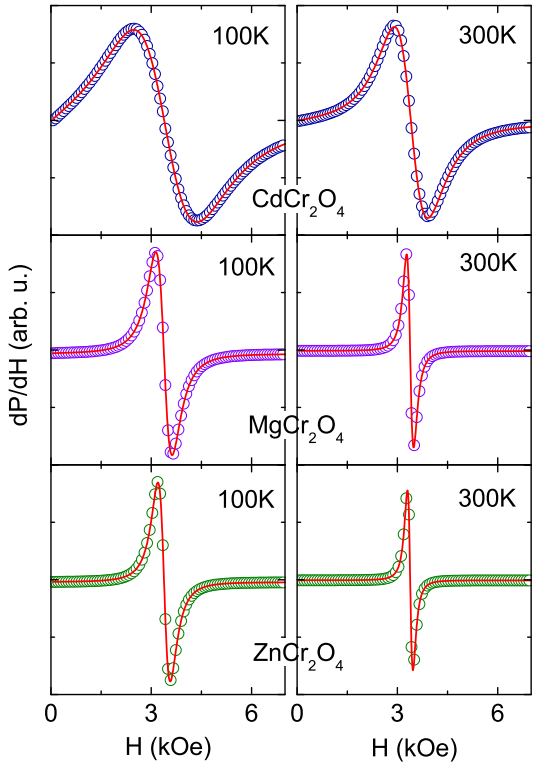

Figure 5.4: ESR spectra of $ZnCr_2O_4$, $MgCr_2O_4$, and $CdCr_2O_4$ in X-band for selected temperatures in the paramagnetic regime. The solid line indicates the fit with the field derivative of a Lorentz line.

$f \approx 9 < 10$ which is just at the border of geometrical frustration. The effective magnetic moment is obtained as $P_{\text{eff}} = 3.69\mu_{\text{B}}$ which is $\approx 5\%$ below the theoretical value.

5.2.2 ESR Results and Discussion

Typical ESR spectra of chromium oxides are shown in Fig. 5.4. All compounds reveal a single exchange-narrowed resonance line, which is perfectly described by a Lorentzian curve. At elevated temperatures the resonance fields of all three compounds correspond to a g-value of about $g = 2$ indicating the quenched orbital moment of the half-filled t_{2g} state in Cr^{3+} with pure spin $S = 3/2$. The spectra broaden rapidly and become undetectable on approaching T_{N}. According to Martinho and coworkers's study in $ZnCr_2O_4$ [Martinho 2001], the integrated intensity of the ESR below 100 K is unusual due to the fact that its temperature dependence is qualitatively different from the temperature dependence of the susceptibility. They pointed out that the ESR susceptibility $\chi(T)$ (compare with section 2.4.1):

$$\chi(T) = \frac{2}{\pi} \int_0^\infty \frac{\chi''(\omega) d\omega}{\omega} \tag{5.2}$$

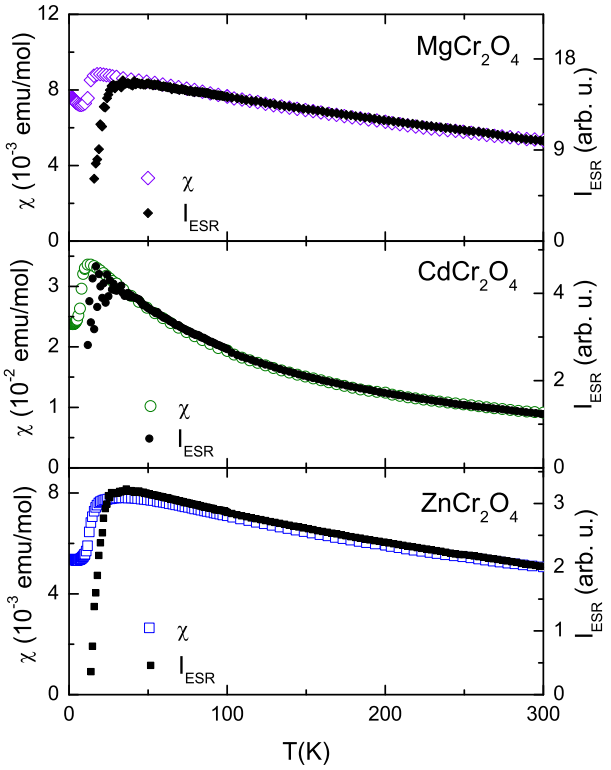

Figure 5.5: Temperature dependence of the ESR intensities of $ZnCr_2O_4$, $MgCr_2O_4$ and $CdCr_2O_4$ in X-band in the paramagnetic regime. The open symbols indicate the corresponding static susceptibilities.

where $\chi''(\omega, T)$ denotes the imaginary part of the dynamic susceptibility and $\chi(T)$ is identified with the static limit of the real part of the dynamic susceptibility $\chi'(\omega, T)$. Since the absorbed power is proportional to

$$\int_{\omega_0-\delta}^{\omega_0+\delta} d\omega\omega\chi'' \tag{5.3}$$

where ω_0 is the resonance frequency and δ the linewidth, one would expect that the susceptibility and the integrated intensity would have a similar temperature dependence, if the resonance is narrow, $\delta \ll \omega_0$, provided χ'' has significant spectral weight only near ω_0. Such would appear to be the case in $ZnCr_2O_4$ above 90 K. The behavior at lower temperatures provides evidence for a growing contribution to the Kramers-Kronig integral for $\chi(T)$ coming from nonresonant modes. Such modes, which are likely to be relaxational in nature, are characteristic of a frustrated paramagnet at low temperatures. This behavior has been observed in all two-dimensional oxides investigated in this work, in which geometrical frustration plays a dominant role. The temperature dependence of the resonance fields shows nearly constant behavior above 50 K. At 300 K, the resonance fields $H_{\rm res} \approx 3381$ Oe, 3382 Oe, and 3382 Oe are obtained for $MgCr_2O_4$, $ZnCr_2O_4$, and

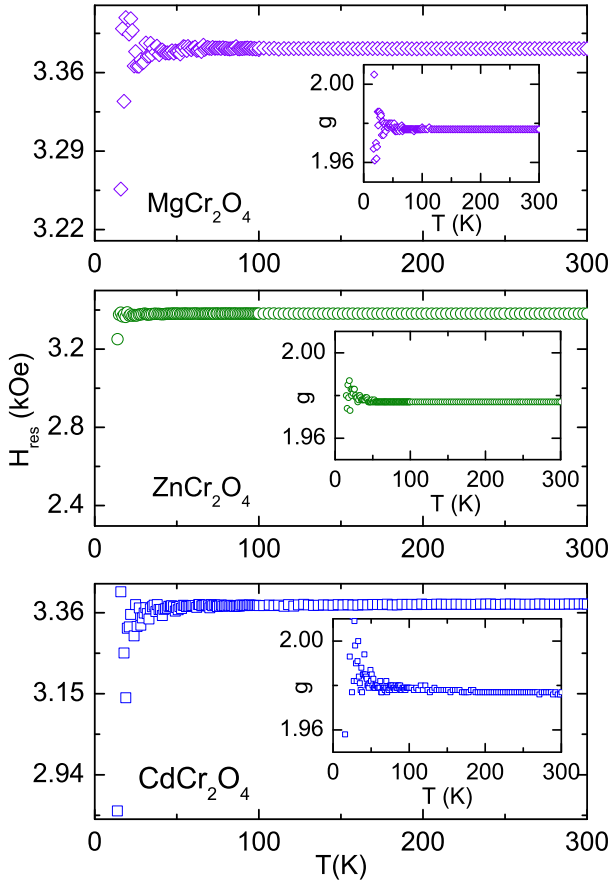

Figure 5.6: Resonance fields and g-factors of $MgCr_2O_4$, $ZnCr_2O_4$, and $CdCr_2O_4$ in the temperature range $4 \leq T \leq 300$ K. Above 50 K, resonance fields stay constant as the temperature increases. The insets illustrate the behavior of the g-factors as a function of temperature.

$CdCr_2O_4$, respectively. The g-factor values at the same temperature have been found to be the same: 1.977. In contrast to the case of two-dimensional chromium ordered rock salt and delafossite oxides in which the resonance fields behave similar to the linewidths, a different behavior has been detected in the spinels where the resonance fields only slightly increase at the beginning as the temperature increases till 50 K. Then no clear changes in these resonance fields have been observed as the temperature further increases to approach 300 K. On the other hand, the ESR linewidths in these compounds follow a comparable relaxation behavior as in two-dimensional chromium ordered rock salt and delafossite oxides. At room temperature, the ESR linewidths have the following values: 180 Oe, 142 Oe, and 848 Oe for $MgCr_2O_4$, $ZnCr_2O_4$, and $CdCr_2O_4$, respectively. They are of the same order as those of the two-dimensional ordered rock salts and delafossites (see for example table. 4.3). The critical exponent attains values of $p \approx 0.63 - 0.83$ (see table 5.1), comparable to the critical exponent values in two-dimensional triangular

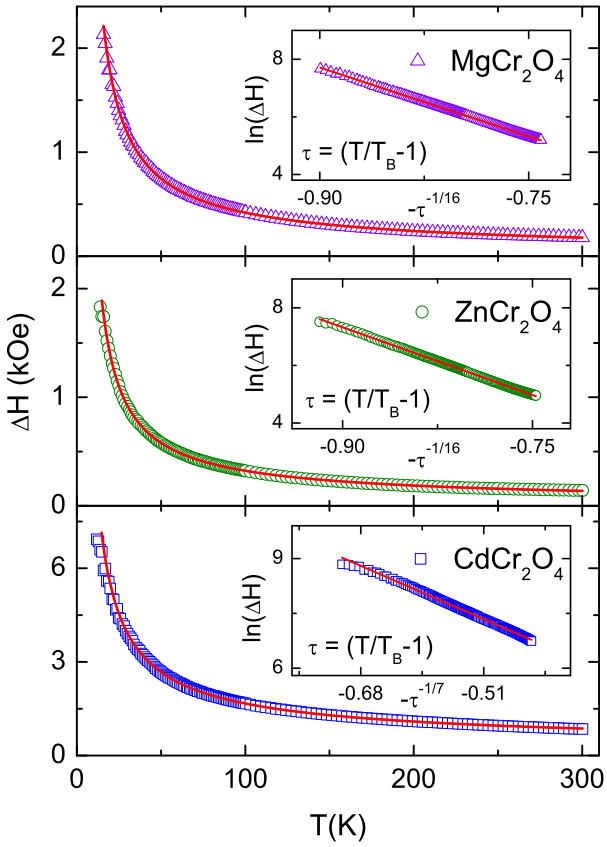

Figure 5.7: The temperature dependance of the linewidth of $MgCr_2O_4$, $ZnCr_2O_4$, and $CdCr_2O_4$. Insets: Logarithmic plots of ΔH as $\ln(\Delta H)$ vs $-\tau^{-\nu}$, where ν values are 1/16 for $MgCr_2O_4$ and $ZnCr_2O_4$, and 1/7 in the case of $CdCr_2O_4$. The transition temperature T_B named by the author after Bulgadaev [Bulgadaev 1999] who treated the BKT model in the frame of higher symmetries.

antiferromagnets which are discussed in chapter four. Inspired by this similarity to the two-dimensional antiferromagnets, it seems to be reasonable to try to fit the linewidth data with a BKT-like scenario. Indeed, this scenario turned out to describe successfully the data in the full temperature range without any residual contributions. Only exponent ν had to be chosen much smaller than 0.37. For the Mg and Zn compound $\nu = 1/16$ yielded the optimum fit while for $CdCr_2O_4$ $\nu = 1/7$ was preferable. These results are in line with the generalized Bulgadaev model. As it was discussed in chapter four in which the discrepancy of the ESR linewidths behavior from the usual BKT scenario in these compounds was attributed to the strong influence of the geometrical frustration, one can follow the same way to clarify the same behavior despite the difference in the dimensionality. In $MgCr_2O_4$ the ratio $T_B \approx 0.2T_N$ is very small and not typical for that value expected in the case of a conventional BKT transition. The large value of $b = 5.29(5)$ and the small value of $T_B \approx 2.47(2)$ K are also unconventional. In

	$MgCr_2O_4$	$ZnCr_2O_4$	$CdCr_2O_4$
T_N (K)	13.7	12	7.8
Critical behavior			
C (Oe)	5682(290)	7241(883)	12031(621)
p	0.79(1)	0.83(1)	0.63(1)
T_N(K)	3.64(7)	2.33(6)	4.26(5)
R^2	0.99954	0.99871	0.99908
Bulgadaev model			
ΔH_∞(Oe)	0.001(1)	0.001(1)	17.19(6)
ν	0.0625	0.0625	0.14
b	5.29(5)	5.27(3)	2.94(1)
T_B(K)	2.47(2)	2.82(4)	0.91(1)
R^2	0.99967	0.99981	0.99984

Table 5.1: T_N values have been taken from Fig. 5.3. Fit parameters for the temperature dependence of the ESR linewidth corresponding to critical behavior: $\Delta H = C/(T/T_N - 1)^p$, Bulgadaev model: $\Delta H = \Delta H_\infty \exp(3b/\tau^\nu)$ with $\tau = T/T_B - 1$. The quality of the fit is characterized by the coefficient of determination $R^2 = 1 - \sum_i (y_i - f_i)^2 / \sum_i (y_i - \bar{y})^2$, where y_i, f_i, and $\bar{y}$ denote the data, the corresponding fit values, and the total average of the data, respectively.

$ZnCr_2O_4$ the ratio $T_B \approx 0.2T_N$ as well. Both values of b and T_B have been found to be 5.27(3) and 2.82(4) K, respectively. Smaller values have been even obtained in $CdCr_2O_4$: $T_B \approx 0.1T_N$, $b \approx 2.94(1)$ and $T_B \approx 0.9$ K. A comparable value has been found in $HCrO_2$ with the ratio $T_{KT} \approx 0.13T_N$ as well as a large value of $b \approx 4.1$ (see also section 4.1.3). At the moment it is not clear, whether the kind of symmetry, i.e. the values of ν, belong to the exceptional Lie groups E_6 and E_8 or to the classical groups A_{29} and A_{11} (see also Table 3.1). In the following chapter the spin structures, which are probably related to the BKT-like scenario, will be discussed.

5.2.3 Local Spin-Spin Correlations, Vortices, and Oligomers

Below T_N, $CdCr_2O_4$ exhibits a spin-driven Jahn-Teller-distortion and an incommensurate spin order. The lattice distortion lowers the lattice symmetry from cubic to tetragonal with lattice constants $a = b \neq c$ (an elongation along the c-axis). In contrast, $ZnCr_2O_4$ undergoes a c-axis contraction and a commensurate spin order [Chung 2005]. A theory has been developed to describe the lattice distortion and the incommensurate magnetic order in a unified model. As a result it was found that the distortion stabilizes a collinear magnetic order with a certain propagation wave vector q. Due to the lack of inversion symmetry, the crystal structure becomes chiral. The chirality is transferred to the magnetic order by the relativistic spin-orbit coupling in such a way that

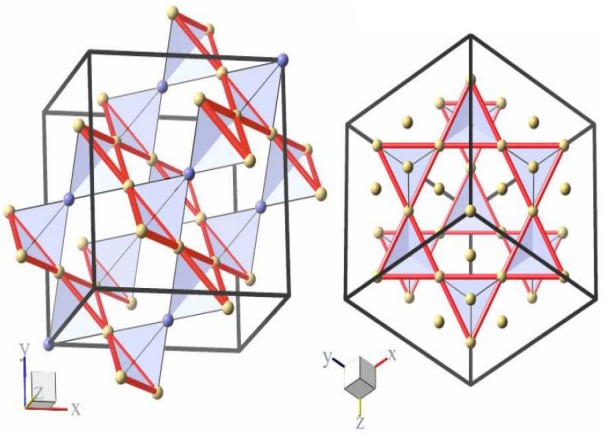

Figure 5.8: Left: The cubic pyrochlore lattice, showing the positions of magnetic ions. This structure can be decomposed into alternating triangular (blue or dark atoms) and kagome planes (gold or light atoms), along the ⟨111⟩ directions. The bonds within the kagome planes are shown in red (dark) lines. Right: a view along [111] shows the structure of the kagome planes [Ross 2009].

the collinear state is twisted into a long spiral associated with a shift in q [Chern 2006]. Inelastic neutron-scattering measurements in $ZnCr_2O_4$ pointed out that the magnetic transition is strongly correlated to the structural one [Lee 2000, Lee 2002]. The calculated form factor was convincingly interpreted as antiferromagnetic hexagonal loops (hexamers), made up of six tetrahedra where two spins of each tetrahedron occupy the vertices of the hexamers. The remaining two spins of a given tetrahedron belong to a different hexamer. Currently, new data of magnetic scattering showed that there are around 10^{12} allowed magnetic ground states. Assuming that all spins have the same amount and the total magnetic moment per tetrahedron equals to zero, 32 possible spin configurations are expected [Ji 2009]. On the other hand inelastic neutron-scattering measurements on single crystals of $MgCr_2O_4$ showed not only the presence of hexamers in the antiferromagnetic phase, but also additional seven-spin clusters (heptamers) [Tomiyasua 2008]. Remarkably, recent elastic neutron-scattering and inelastic neutron-scattering studies in $CdCr_2O_4$[Chung 2005, Matsuda 2007] did not reveal any kind of spin loops, probably due to the incommensurate spin order and its consequences. It is important to note that the multi-spin clusters (oligomers) have been observed in many other spinel compounds like dimers and octamers in $CuIr_2S_4$ [Radaelli 2002], heptamers in AlV_2O_4 [Matsuda 2006], hexamers in $NiCr_2O_4$ and $FeCr_2O_4$ [Tomiyasub 2008]. Remarkably, the three-dimensional pyrochlore lattice can be naturally decomposed along ⟨111⟩ directions into interleaved kagome and triangular planes [Anderson 1956]. According to Ross and coworkers [Ross 2009], one can argue that the two-dimensional spin correlations form within the kagome planes (Fig. 5.8). They performed neutron scattering measurements in the ferromagnetic XY pyrochlore $Yb_2Ti_2O_7$, which showed at

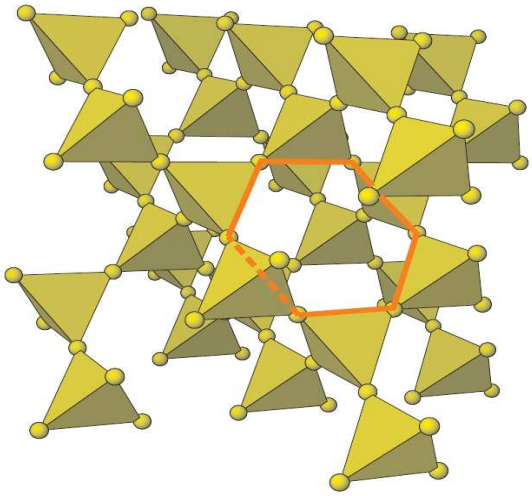

Figure 5.9: The pyrochlore lattice is a network of vertex-sharing tetrahedra. The hexagonal loop is made up of six tetrahedra where two spins of each tetrahedron occupy the vertices of the hexamers. The remaining two spins of a given tetrahedron belong to a different hexamer. The picture is taken from [Moessner 2006].

low temperatures strong quasi-two-dimensional spin correlations, which give way to long range order under the application of magnetic fields. Rods of scattering along $\langle 111 \rangle$ directions due to these two-dimensional spin correlations imply a magnetic decomposition of the cubic pyrochlore system into decoupled kagome planes. High-field ESR measurements performed in $ZnCr_2O_4$ and $MgCr_2O_4$ clearly showed an easy-plane type antiferromagnet (an easy-plane type appears when the single-ion anisotropy constant D satisfies $D > 0$). An antiferromagnetic gap of about 114 GHz and 120 GHz opens below T_N for Zn- and Mg-compounds, respectively, in coincidence with the first order structural phase transition [Yoshida 2006]. In $CdCr_2O_4$, high-field ESR revealed resonance modes below $H_c \approx 5.7 \times 10^4$ Oe (≈ 4 K) explained by molecular-field theory assuming a helical spin structure. Higher-harmonic modes have been also observed indicating that a variation of the spin structure from the helical to the four-sublattice canted one takes place around H_c. The variation of the spin structure from helical to a canted one can be attributed to the lattice transformation which relaxes the competition between the nearest neighbor and next-nearest-neighbor interactions and might require some relaxation time giving rise to the hysteresis which was already observed in the magnetization measurement as a small anomaly at $H_c \approx 5.7 \times 10^4$ Oe. Furthermore, an antiferromagnetic gap of about 150 GHz was observed close to the paramagnetic phase [Kimura 2006]. Now it is necessary to discuss the relationship between hexamer structure (Fig. 5.9) and the spin-lattice coupled model in some details. Tchernyshyov et al. considered a model in which spin rearrangements around such hexagons are dominant [Tchernyshyov 2002].

They discuss a mechanism for lifting the frustration through a coupling between spin and lattice degrees of freedom. The high symmetry of the pyrochlore lattice and the spin degeneracy drive a distortion of tetrahedra via a magnetic Jahn-Teller ("spin-Teller") effect. The resulting state exhibits a reduction from cubic to tetragonal symmetry and the development of bond order in the spin system with unequal spin correlations $\langle \mathbf{S}_i \cdot \mathbf{S}_j \rangle$ on different bonds of a tetrahedron. The spectrum of spin excitations in the distorted antiferromagnet contains a large number of modes clustered near a finite frequency. These magnons, a remnant of pyrochlore zero modes, are confined to strings of parallel spins. They called them string modes. The resonance is a local spin wave reminiscent of the weather-vane mode of the kagome antiferromagnet. The mode is confined to any line of parallel spins. Such lines are abundant in collinearly ordered states: each spin has exactly two parallel neighbors. When successive spins on the string precess with a phase shift of π, spins adjacent to that line can remain unaffected because the exchange field at their locations does not precess. It can be shown that, despite the magnetoelastic coupling, harmonic spin waves and phonons are decoupled in any collinearly ordered magnet. For various kinds of collinear ground states, the string mode can live on straight lines of parallel spins, spirals, irregular lines, or even closed loops. A mode living on a short loop is truly a local resonance. Open strings are localized in only two directions and will, therefore, be seen in the local density of states as a strong van Hove singularity. The shape of the strings determines the form factor of the resonance observable, e.g., by inelastic neutron scattering. In fact a resonance was shortly before observed in the neutron scattering measurements in $ZnCr_2O_4$ [Lee 2002]. It has the form factor of a hexagonal string mode: the shortest possible loop in Tchernyshyov and coauthors's treatment [Tchernyshyov 2002]. This theory has direct relevance to the observed magnetic and structural phase transitions and local modes in the pyrochlore antiferromagnet $MgCr_2O_4$ as well [Tomiyasua 2008]. Recalling the paramagnetic measurements and the two-dimensional character in chromium oxides under focus, one can suggest a relation between these hexagonal loops and highly impact symmetrical vortices which govern the spin-spin relaxation mechanism in the ESR linewidths. To the best knowledge of the author, no theoretical treatment in condensed-matter physics exists which gives any information about the nature of the symmetry of these strings modes. Taking into account the results that are obtained in this work concerning the generalized model given by Bulgadaev, it is possible to speculate that chromium oxides can even realize some kind of superstrings aspects!

5.3 Chromium Chalcogenides

The chromium chalcogenide spinels show a large variety of magnetic properties: ferromagnetic, antiferromagnetic, ferrimagnetic, Pauli-paramagnetic. Also many of them are metals or semiconductors [Haas 1970]. $CdCr_2S_4$ exhibits ferromagnetic and relaxor ferroelectric order as well as a huge magnetocapacitive effect [Hemberger 2005]. The strong magnetocapacitive coupling in $CdCr_2S_4$ is related to the dramatic changes in the relaxation dynamics which is drilled by the ferromagnetic long-range-order [Hemberger 2006]. Similar to the classical Heisenberg ferromagnet $CdCr_2S_4$, metamagnetic $HgCr_2S_4$ reveals colossal magnetocapacitance, colossal magnetoresistance, and also a short-range ferroelectric order [Weber 2006].

5.3.1 Sample Preparations and Magnetic Characterization

Polycrystalline $ZnCr_2S_4$, $CdCr_2S_4$, $HgCr_2S_4$, $ZnCr_2Se_4$, $CdCr_2Se_4$, $HgCr_2Se_4$ samples were prepared by solid-state reaction from high-purity elements in evacuated quartz ampoules. The synthesis was repeated several times in order to reach good homogeneity. For the sulfides and selenides, single crystals have also been grown by gas transport using chlorine as transport agent or by liquid-transport methods.

$ZnCr_2S_4$ is a prototype system for strong bond-frustration in which $\Theta_{CW} = 18$ K slightly exceeds $T_N = 15$ K and, hence, the frustration parameter $f \approx 1$. As expected, the FM interaction increases to equal the antiferromagnetic one [Kant 2010]. Due to the strong competition between ferromagnetic and antiferromagnetic interactions and the strong coupling to the lattice, $ZnCr_2S_4$ undergoes two structural phase transitions at $T_{N_1} = 15$ K and $T_{N_2} = 8$ K [Rudolf 2007]. A hysteresis-effect indicates the transition T_{N_2} as a first order transition. The spin-driven Jahn-Teller-effect lowers the lattice symmetry from cubic to tetragonal at T_{N_1} and from tetragonal to orthorhombic at T_{N_2} [Yokaichiya 2009]. The effective paramagnetic moment $P_{eff} = 3.67\mu_B$ is 5% below the spin-only-value $3.87\mu_B$. Below 100 K, susceptibility measurements show a deviation from the high-temperature ferromagnetic Θ_{CW} which is a signature of the presence of antiferromagnetic correlations. At $T_{N_1} = 15$ K, the spins start to order in an antiferromagnetic long-range-order in a helical form. Between $12 - 8$ K, a second phase appears as a commensurable collinear antiferromagnetic phase, very similar to those observed in $ZnCr_2O_4$ and $CdCr_2O_4$ [Yokaichiya 2009].

$CdCr_2S_4$ orders ferromagnetically below the Curie temperature $T_c = 84.5$ K and exhibits the asymptotic paramagnetic $\Theta_{CW} = 141$ K at high temperatures. A structural phase transition was not observed, even below 4 K, and the lattice remains cubic both in the ferromagnetic phase and in the paramagnetic one.

$HgCr_2S_4$ exhibits a high positive $\Theta_{CW} = 136$ K and an incommensurable antiferro-

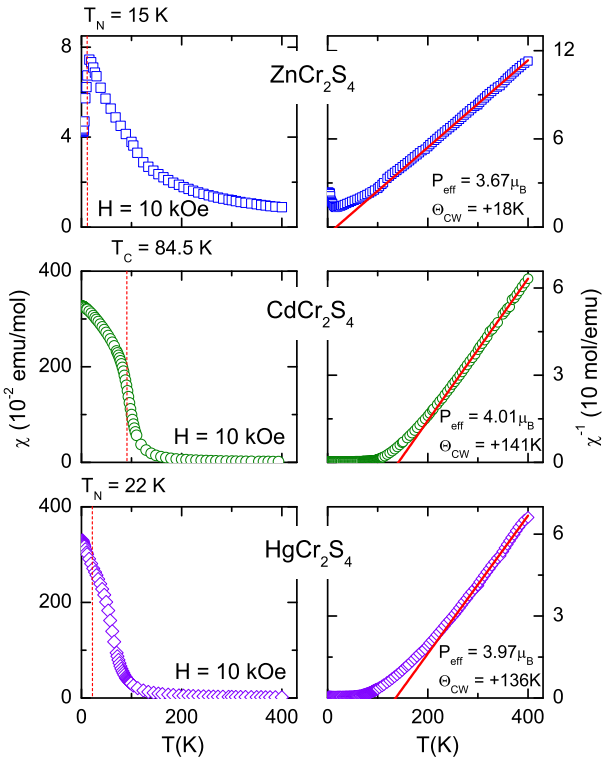

Figure 5.10: Magnetic susceptibility and its inverse of $ZnCr_2S_4$, $CdCr_2S_4$, and $HgCr_2S_4$ in the temperature range $4 \leq T \leq 400$ K.

magnetic order at $T_N = 22$ K. The effective paramagnetic moment is slightly higher than expected, $P_{\text{eff}} = 4.01\mu_B$, $3.97\mu_B$ for $CdCr_2S_4$, and $HgCr_2S_4$, respectively (Fig. 5.10). In ACr_2Se_4 (A: $Zn^{2+}, Cd^{2+}, Hg^{2+}$), high temperature magnetic susceptibility leads to effective paramagnetic moments $P_{\text{eff}} = 3.94\mu_B$, $4.09\mu_B$, and $4.06\mu_B$ which are higher than those expected for Cr^{3+}-ions. $ZnCr_2Se_4$ is an antiferromagnet with a helical spin structure while $CdCr_2Se_4$ and $HgCr_2Se_4$ order ferromagnetically at $T_N = 21$ K, $T_c = 130$ K, and $T_c = 106$ K with $\Theta_{CW} = 97$ K, $\Theta_{CW} = 183$ K, and $\Theta_{CW} = 176$ K, respectively (Fig. 5.11).

5.3.2 ESR Results and Discussion

Typical ESR spectra of chromium chalcogenides are shown in Fig. 5.12. All compounds reveal a single exchange-narrowed resonance line, which is perfectly described by a Lorentzian curve. At elevated temperatures the resonance field values, Fig. 5.13 and Fig. 5.14 exhibit a constant behavior over a wide temperature range.

At room temperature they are obtained as 3372 Oe, 3370 Oe, 3372 Oe, 3355 Oe, 3347 Oe, and 3350 Oe for $ZnCr_2S_4$, $CdCr_2S_4$, $HgCr_2S_4$, $ZnCr_2Se_4$, $CdCr_2Se_4$, and $HgCr_2Se_4$, respectively. The corresponding g-factor values are 1.983, 1.984, 1.983, 1.992, 1.997, and 1.996 as typical for the nearly quenched orbital moment of the half-filled Cr

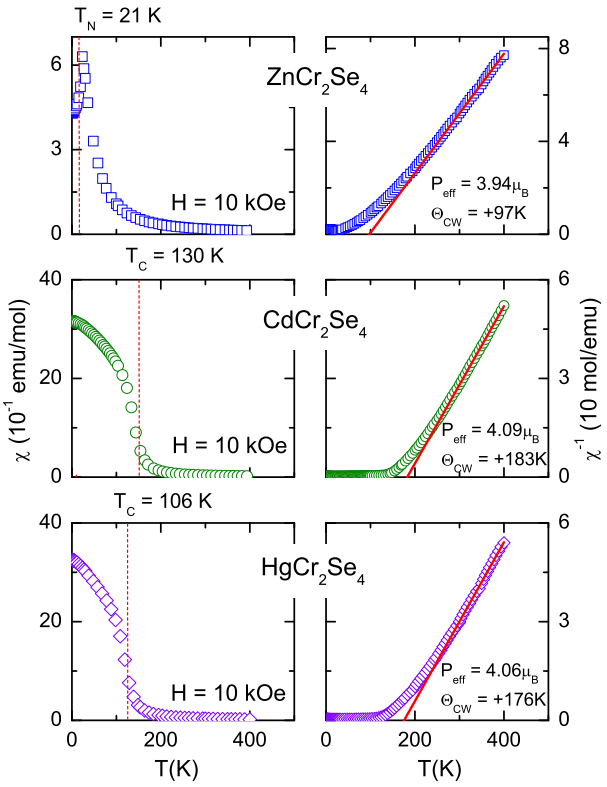

Figure 5.11: Magnetic susceptibility and its inverse of $ZnCr_2Se_4$, $CdCr_2Se_4$, and $HgCr_2Se_4$ in the temperature range $4 \leq T \leq 400$ K.

t_{2g} shell. On decreasing temperature the spectra at first slightly narrow (with exception of $ZnCr_2S_4$) but then strongly broaden and shift to lower resonance fields on approaching the ordering temperature. For antiferromagnetic $ZnCr_2S_4$ and $ZnCr_2Se_4$ the linewidth diverges and the resonance shifts to zero field becoming undetectable below T_N due to the opening of the antiferromagnetic excitation gap, which is larger than the microwave frequency. The intensities match the susceptibility down to T_N. In the ferromagnetic compounds the resonance shifts proportional to the magnetization on approaching the Curie temperature T_c. Strong signals are detected even below T_c, but the results strongly depend on the sample shape due to the demagnetization effect. This is topic of a current diploma thesis [Ehlers 2011]. Here the focus is on the behavior in the paramagnetic regime.

In $CdCr_2S_4$, $HgCr_2S_4$, $CdCr_2Se_4$, and $HgCr_2Se_4$, at temperatures within the range $T_c \leq T \lessapprox 2T_c$, the ESR intensities change proportional to ε^{-p} where p is the critical exponent and $\varepsilon = (T - T_c)/T_c$ is the reduced temperature (see Fig. 5.15, and Fig. 5.16). At temperatures on approaching T_c from above, the short-range order occurs gradually and motions of spins become correlated. For a Heisenberg-type ferromagnet at temperatures $T_c \leq T \leqq 1.5T_c$ [Domb 1963], the static susceptibility is expected to follow

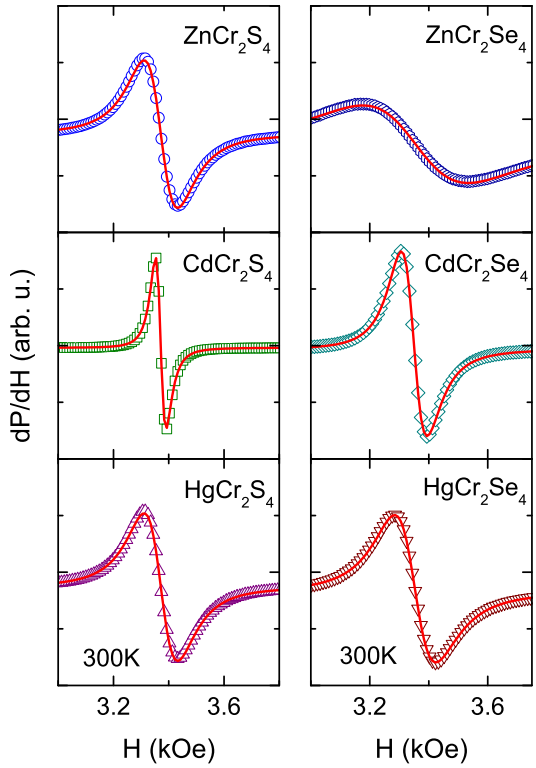

Figure 5.12: ESR spectra of $ZnCr_2X_4$, $CdCr_2X_4$, and $HgCr_2X_4$, where X: S^{2-}, Se^{2-}, in X-band at 300 K. The solid line indicates the fit with the field derivative of a Lorentz line.

$\chi \sim I \propto ((T - T_c)/T_c)^{-4/3}$ for zero-field. The experimental values obtained for the exponent p are larger than $4/3 = 1.33$. For the resonance field of about $H \approx 3$ kOe, it was found that $p = 1.73$, 2.74, 1.35, 1.97 for $CdCr_2S_4$, $HgCr_2S_4$, $CdCr_2Se_4$, and $HgCr_2Se_4$, respectively. The associate critical temperatures obtained from the fit are 81.42 K, 19.95 K, 130.56 K, 93.34 K in the same respective order as mentioned above. These values are in a good agreement with the literature values obtained in these compounds. The enhanced exponent p is related to the strong sensitivity of the critical fluctuations to the external field, while the theoretical value holds for zero-field. Deviations from the static susceptibilities result from the fact that those data were taken at 10 kOe, where saturation is reached already close to T_c. Different theoretical approaches exist to treat the spin relaxation in ferromagnets. In general, to describe the linewidth data in a ferromagnet, one is referred to the work of Kawasaki [Kawasaki 1968]. He predicted that, as the temperature T approaches T_c from above, the ESR linewidth ΔH in a ferromagnet should increase as $\kappa^{-3/2}$ in small-field limit, i.e.,

$$\Delta H \propto \kappa^{-3/2} = \varepsilon^{-1}, \quad H_{res} \ll H_{ex}(\kappa a)^{5/2} \tag{5.4}$$

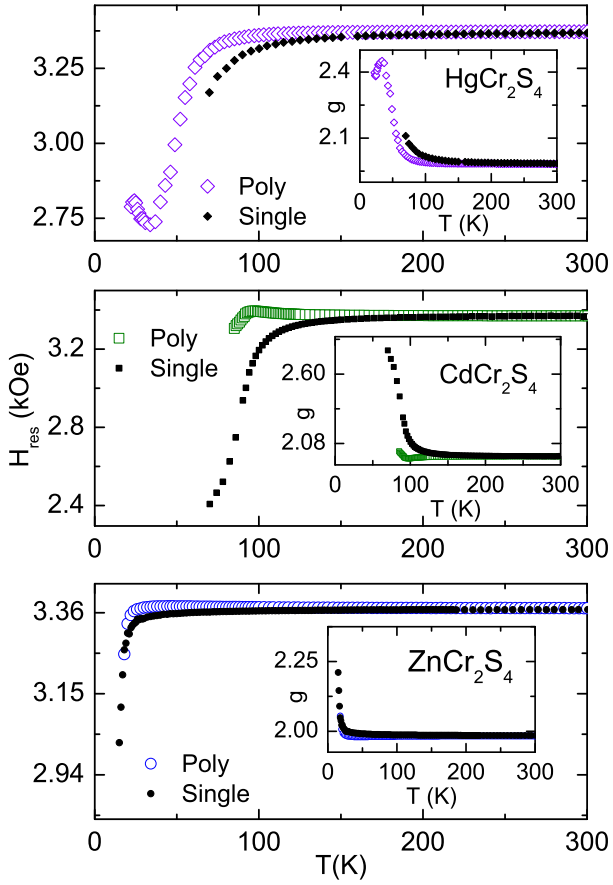

Figure 5.13: Temperature dependence of resonance fields and g-factors of polycrystals and single crystals of $ZnCr_2S_4$, $CdCr_2S_4$, and $HgCr_2S_4$. As expected in the case of Cr^{3+}, the g-factor values are nearly 2 indicating the quenched orbital effect.

where κ is the inverse correlation length, a is the lattice constant, and H_{res} and H_{ex} are, respectively, the resonance and the exchange fields. Shortly after, Huber [Huber 1971] has derived the same relation above for the zero-field case. Both calculations have been done for a Heisenberg system with dipole-dipole interaction as a perturbation and are valid only in the critical region above T_{c}.

Tomita and Kawasaki [Tomita 1970], on the other hand, have investigated the ESR linewidth in zero-field for a uniaxial ferromagnet in the whole paramagnetic regime. Their results pointed out that, as the temperature is lowered toward T_{c}, the ESR line should first narrow and then broaden as the temperature approaches T_{c}, the crossover occurs near the reduced temperature $((T - T_{\mathrm{c}})/T_{\mathrm{c}}) \approx 0.5$. Furthermore, the crossover temperature is independent of the non-zero magnitude of the uniaxial anisotropy. According to Seehra and Gupta [Seehra 1974], several ferromagnets like EuO, $CrBr_3$, and $K_2CuCl_4{\cdot}2H_2O$ have realized those calculations near T_{c} for ESR measurements. In these

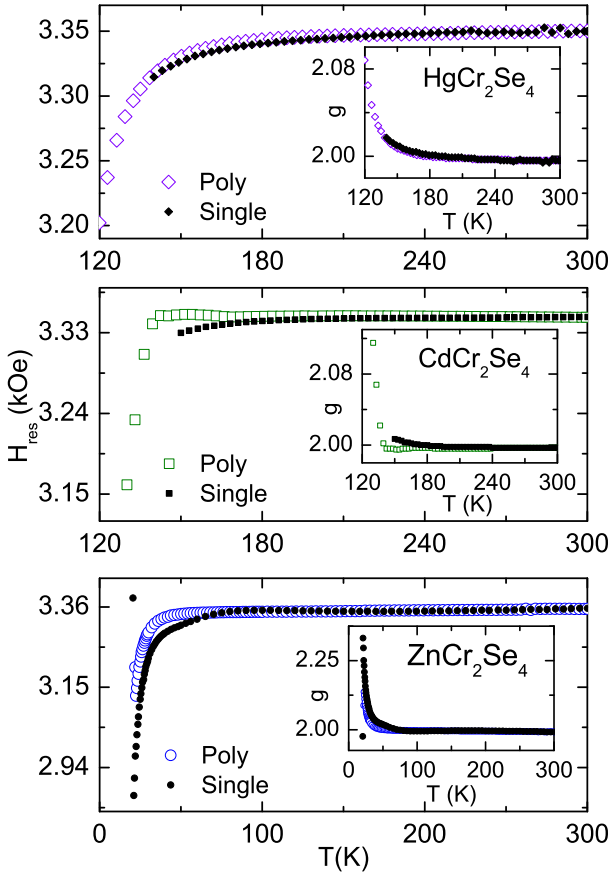

Figure 5.14: Temperature dependence of resonance fields and g-factors of polycrystals and single crystals of $ZnCr_2Se_4$, $CdCr_2Se_4$, and $HgCr_2Se_4$. As expected in the case of Cr^{3+}, the g-factor values are nearly 2 indicating the quenched orbital effect.

compounds, only narrowing of the ESR line has been observed as the temperature approaches T_c from above. In other words, the predicted crossover from narrowing to broadening above T_c has not been observed. However, in $CdCr_2S_4$ and $HgCr_2S_4$ as well as in all selenides under investigation such a crossover seems to exist. But the underlying physical mechanism is different for sulfides and selenides as will be shown now.

As a starting point, following the discussion that was given by Huber [Huber 1971], one has to consider the general expression of the zero-field spin-spin relaxation time T_2^α ($\alpha = x, y$) which reads:

$$\gamma \Delta H = \frac{1}{T_2^\alpha} = \frac{g^2 \mu_B^2}{\chi_\alpha(0)} \int_0^\infty dt (\dot{S}_\alpha(0,t), \dot{S}_\alpha(0)) \tag{5.5}$$

Here $\dot{S}_\alpha = \frac{i}{\hbar}[S_\alpha, \mathcal{H}]$ with $\mathcal{H}$ as the spin Hamiltonian, and $\chi_\alpha(0)$ is the uniform field susceptibility along the α-direction. One important aspect of Eq. 5.5 is that the product $\Delta H \cdot T \cdot \chi_\alpha(0)$ carries the critical contribution which should vary as $((T - T_c)/T_c)^{-7/3}$ for

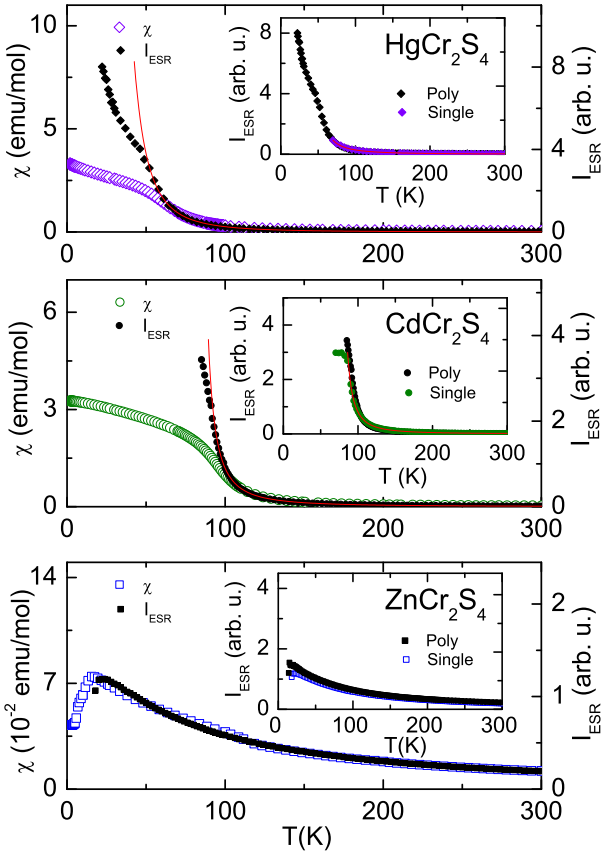

Figure 5.15: Temperature dependence of ESR intensities and magnetic susceptibilities of polycrystals and single crystals of $ZnCr_2S_4$, $CdCr_2S_4$, and $HgCr_2S_4$. In the main frames only polycrystalline data are shown. The solid lines indicate the critical behavior fit (see also the description in the text).

$0.5 < ((T - T_c)/T_c) < 1$ and as $((T - T_c)/T_c)^{-2/3}$ for $((T - T_c)/T_c) < 0.1$ [Huber 1971, Maleev 1974]. Seehra and Gupta [Seehra 1974] have extended the relation of Huber to include critical and non-critical terms as $\Delta H \cdot T \cdot \chi_\alpha(0) \propto f[(T - T_c)/T_c] + C$, where $f[(T - T_c)/T_c]$ is a critical function and C represents the non-critical term. Near T_c, the critical function is larger than C and was shown to vary as $\chi^{7/4}$ [Seehra 1974].

For $T \gg T_c$, the linewidth is primarily due to the non-critical contribution. In general the non-critical contribution is expected to behave linear as a function of temperature. The origin of this linear temperature dependence term was attributed to single-phonon absorption and emission processes, in which the energy of one phonon must match the splitting between two energy levels [Castner 1971]. At high temperatures, single-phonon processes are much more important in magnetically concentrated systems than for the single-ion case, which leads to a phonon modulation of the crystal field [Huber 1975]. The modulation of the crystal-electric field arises from the motion of the electrically charged ions under the action of the lattice vibrations. This produces a fluctuating electric

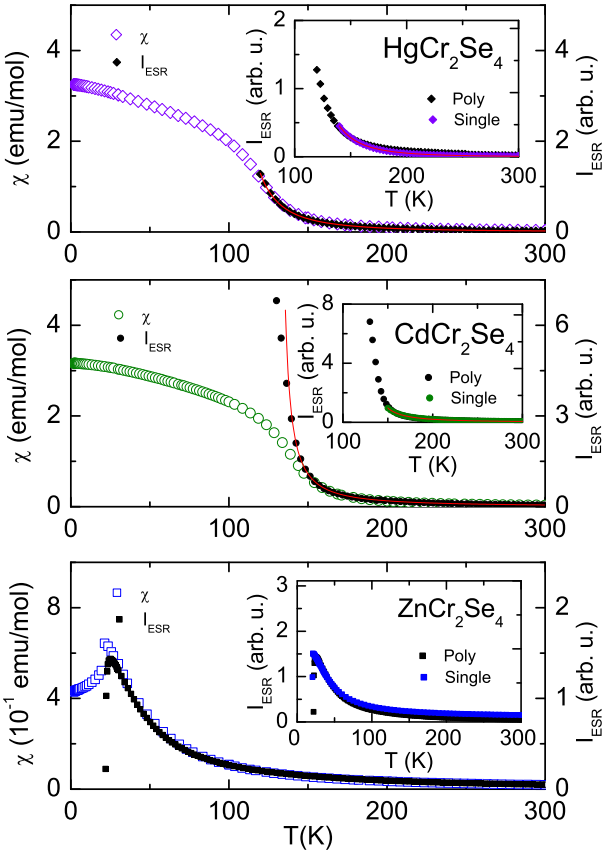

Figure 5.16: Temperature dependence of ESR intensities and magnetic susceptibilities of polycrystals and single crystals of $ZnCr_2Se_4$, $CdCr_2Se_4$, and $HgCr_2Se_4$. In the main frames only polycrystalline data are shown. The solid lines indicate the critical behavior fit (see also the description in the text).

field that is essentially a dynamic orbital-lattice interaction, with no direct interaction with the electron spin. These processes involve spin flips and changes in the exchange energy. However, just as a static ligand field splits the orbital states of a magnetic ion and indirectly influences the spin levels through the spin-orbit coupling, so a fluctuating ligand field can cause transitions between these levels [Abragam 1970]. In addition to the single-phonon processes, there are two-phonon Raman processes which involve absorption of a phonon together with a spin transition followed by emission of a phonon. In fact, the spin-spin correlation functions allow a broad band of phonons to produce spin-lattice relaxation. As the single-phonon process involves only resonant phonons and as such only a restricted number of phonons can take part, the two-phonon processes are expected to dominate at higher temperatures. This is because the two-phonon processes involve the entire phonon spectrum. However, Castner and Seehra [Castner 1971] have pointed out that at temperatures of the order of the Debye temperature Θ_D, the single-phonon process dominates over two-phonon Raman processes because of the very large

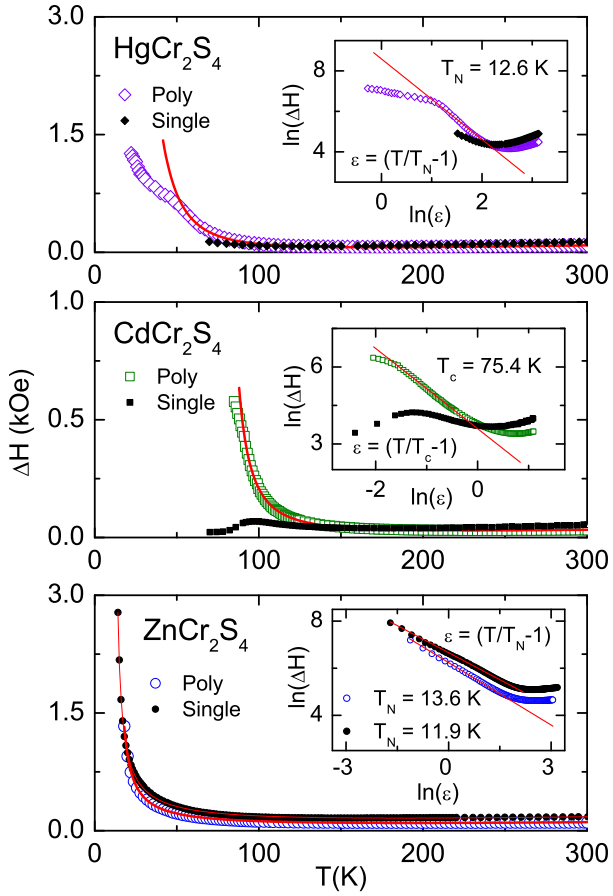

Figure 5.17: Temperature dependence of ESR linewidths of polycrystals and single crystals of $ZnCr_2S_4$, $CdCr_2S_4$, and $HgCr_2S_4$. The solid lines indicate the critical behavior fit. The insets show a logarithmic plot of the linewidths versus reduced critical temperatures obtained directly from the fit (see also the description in the text).

density of phonon states [$\rho(\omega = J/\hbar)$]. It is important to note that the spin-lattice relaxation rate is expected to be proportional to T and T^7 for single-phonon and two-phonon Raman processes, respectively. The reader is referred to the books of Abragam and Bleaney [Abragam 1970] and Sinha and Kumar [Sinha 1980] in which many cases of single-phonon and two-phonon Raman processes as well as other spin-lattice relaxation processes have been discussed in more details which are out of the scope of this work.

If there is no contribution to the linewidth from sources other than spin-spin interactions, a plot of $\Delta H \cdot T \cdot \chi_\alpha(0)$ versus T would approach a constant value for $T \gg T_c$ (generally, one expects approximately constant values for $T \geq 2-3T_c$) [Huber 1975]. To test these predictions in chromium spinel chalcogenides, one has to plot $\Delta H \cdot T \cdot I_{\mathrm{ESR}}$ versus the temperature as depicted in the right hand side of Fig. 5.19, where the ESR line intensities substitute the initial uniform susceptibilities $\chi_\alpha(0)$. This substitution

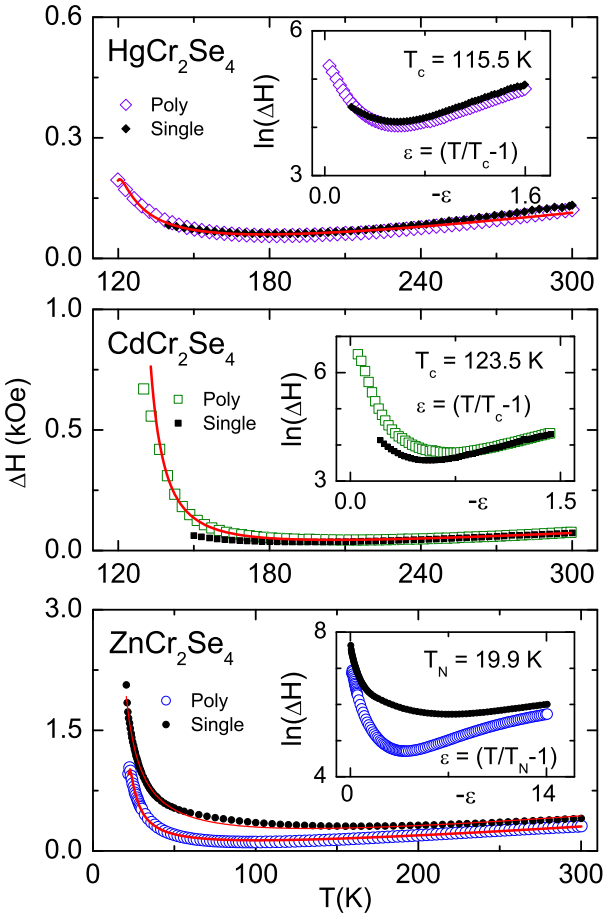

Figure 5.18: Temperature dependence of ESR linewidths of polycrystals and single crystals of $ZnCr_2Se_4$, $CdCr_2Se_4$, and $HgCr_2Se_4$. The solid lines indicate the critical behavior fit. The insets show a logarithmic plot of the linewidths versus reduced critical temperatures obtained directly from the fit (see also the description in the text).

can be justified because above the critical temperatures magnetic susceptibilities behave the same as ESR intensities (see Fig. 5.15, and Fig. 5.16). To obtain significant results, the measurements shown in Fig. 5.19 were extended up to 550 K. All sulfides as well as $ZnCr_2Se_4$ approach a constant value of $\Delta H \cdot T \cdot I_{\mathrm{ESR}}$ at high temperatures, whereas $CdCr_2Se_4$ and $HgCr_2Se_4$ exhibit a monotonous increase. This means that in the former group the pure spin-spin relaxation dominates while in the latter two compounds spin-phonon relaxation becomes important due to the heavy atomic masses and correspondingly small Debye temperatures Θ_{D}. $\Theta_{\mathrm{D}} \approx 392$ K and 361 K for $ZnCr_2S_4$ and $HgCr_2S_4$, respectively, while $\Theta_{\mathrm{D}} \approx 309$ K and 281 K for $ZnCr_2Se_4$ and $HgCr_2Se_4$, respectively [Rudolf 2007, Rudolf 2009].

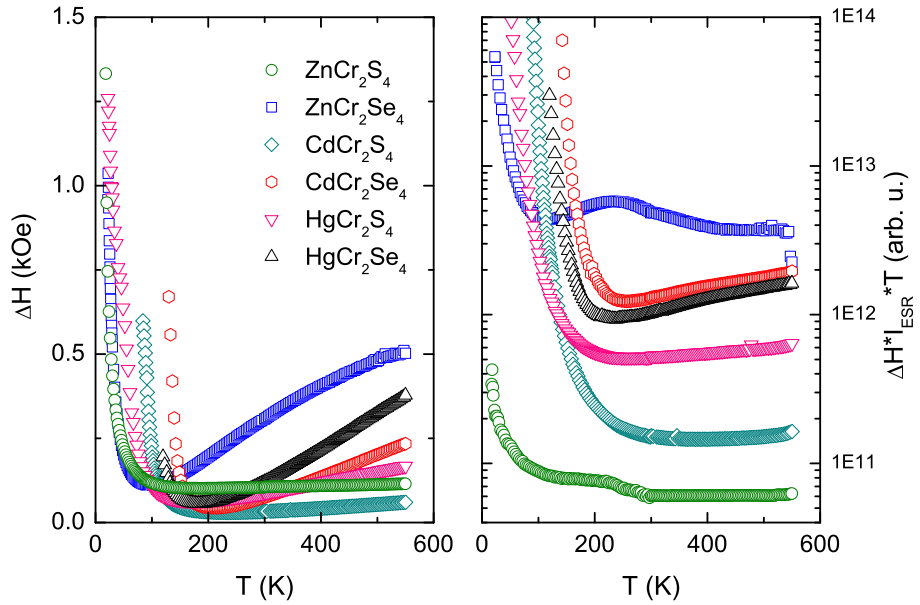

Figure 5.19: Left hand plot: ESR linewidths of all sulfide and selenide spinels under investigation are shown in the temperature range $T_c \leq T \leq 550$ K for the polycrystalline compounds. Right hand plot: a logarithmic plot of $\Delta H \cdot T \cdot I_{ESR}$ versus T for the same compounds. $ZnCr_2S_4$, $CdCr_2S_4$, and $HgCr_2S_4$ reveal a constant behavior for temperatures $T \geq 2 - 3T_c$, while $ZnCr_2Se_4$, $CdCr_2Se_4$, and $HgCr_2Se_4$ do not reveal this behavior.

Now turning back to the critical regime, the linewidth can be approximated by:

$$\Delta H = a \cdot (T/T_c - 1)^{-p} + b \cdot T + c \tag{5.6}$$

where a, b, and c are arbitrary constants. The last two terms refer to the non-critical contribution to the linewidth. One obtained $p = 0.79$, 0.88, 1.72, 2.62 for single crystalline $ZnCr_2S_4$ and polycrystalline $ZnCr_2S_4$, $CdCr_2S_4$, and $HgCr_2S_4$, respectively (Fig. 5.17). b and T_c values are determined as: $b \approx 0.40$ Oe/K, 0.25 Oe/K, 0.09 Oe/K, 0.28 Oe/K and $T_c \approx 12$ K, 14 K, 75 K, 13 K for all compounds mentioned above in the same respective order. The transition temperature values correspond to the expected magnetic transition values in these compounds. Otherwise, no additional constant term c is needed to perfect the fit. The exponent p is expected to be ≈ 1 for a three-dimensional Heisenberg ferromagnet [Benner 1990]. This value is satisfied for $ZnCr_2S_4$ ($p \approx 0.8$). However in the ferromagnets $CdCr_2S_4$, and $HgCr_2S_4$ one observes $p = 1.7$ and $p = 2.6$, respectively, which are close to the exponents observed in the ESR intensities. This indicates that the main source of broadening comes from scattering of the magnetization on pits and pores in the sample. So far the sulfide spinels are satisfactorily evaluated. However, applying Eq. 5.6 in spinel chromium selenides was not successful to describe the data.

In spinel chromium selenide compounds, the single-phonon process starts to play an

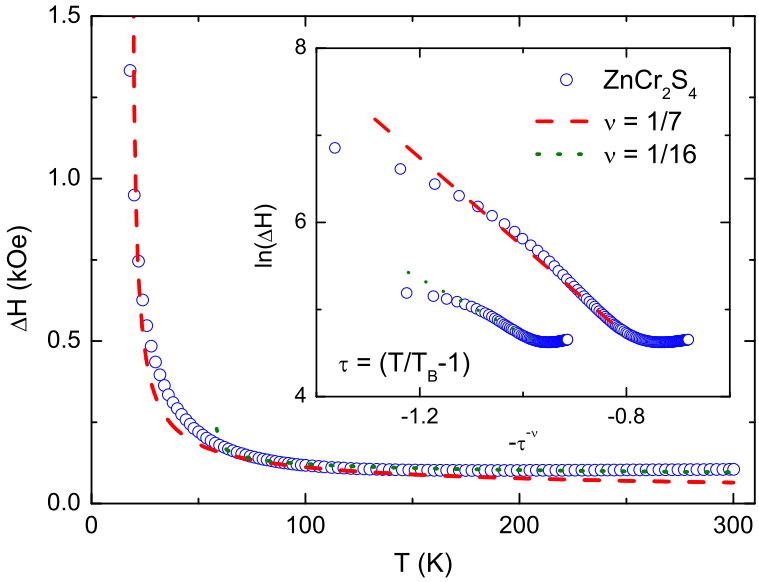

Figure 5.20: The temperature dependance of the linewidth of $ZnCr_2S_4$. Inset: Logarithmic plots of ΔH as $\ln(\Delta H)$ vs $-\tau^{-\nu}$, where ν values are 1/7 and 1/16. The transition temperature T_B substitutes T_{KT} temperature in the BKT scenario.

important role in contrast to sulfides. This leads to a further broadening due to the spin-lattice relaxation, which increases monotonically with temperature. Following the refined expression used by Berzhansky [Berzhansky 1982] who considered, in addition to the spin-lattice relaxation term, a zero-field dipolar spin-spin interaction term as well as a magnetic field dependent dipolar spin-spin interaction term due to the spin diffusion effect, the ESR linewidth can be expressed as:

$$\Delta H = a \cdot (T/T_c - 1)^{\gamma} + b \cdot (T/T_c - 1)^{-3\gamma/4} - c \cdot (T/T_c - 1)^{-[\gamma + 3\rho/2]} \qquad (5.7)$$

where $\gamma \approx 1.30$ and the critical exponent for spin diffusion $\rho \approx 0.30$. A successful test of this equation has been done in $CdCr_2S_4$ and $CdCr_2Se_4$ [Berzhansky 1982]. Furthermore, application to ESR measurement data of $CdCr_2Se_4$ and the mixed-composition system $CdCr_2(Se_{1-x}S_x)_4$ under hydrostatic pressure up to 8 GPa led to reasonable results [Sakai 1986]. As one applies Eq. 5.7 to the spinel chromium selenide compounds under focus, the exponent values that are given above have been kept constant. This implies that $T_c \approx 20$ K, 123 K, 115 K for polycrystallines $ZnCr_2Se_4$, $CdCr_2Se_4$, and $HgCr_2Se_4$, respectively. These values are in a good agreement with those expected in these compounds. Finally, it is necessary to check, whatever a BKT-like scenario is realized in the frustrated sulfides or selenide compounds. Here $ZnCr_2S_4$ seems to be the most promising candidate, because its linewidth monotonously decreases up to high temperatures under consideration. The dashed and dotted line in Fig. 5.20 indicate fits

with the possible exponents $\nu = 1/7$ and $\nu = 1/16$, respectively. Both scenarios clearly fail to describe the data points. This indicates that the BKT-like scenarios are restricted to the systems of strong geometric frustration realized for the oxide spinels, only.

5.4 Estimation of the Linewidth at Room Temperature

To estimate the crystal field contribution to the ESR linewidth at room temperature, the spectroscopic parameters which are obtained from optical measurements data are required, in order to calculate the D parameter. Previous optical absorption measurements found that $10Dq$ values are 17450 cm^{-1}, 14195 cm^{-1}, 18041 cm^{-1}, and 19900 cm^{-1} as well as B values are 525 cm^{-1}, 220 cm^{-1}, 431 cm^{-1}, and 303 cm^{-1} in $ZnCr_2O_4$, $ZnCr_2S_4$, $ZnCr_2Se_4$, and $CdCr_2S_4$ [Rudolf 2009]. In $MgCr_2O_4$ and $CdCr_2O_4$ one obtained 17300 cm^{-1} and 17000 cm^{-1} for $10Dq$ and $\approx$ 638 cm^{-1} and 465 cm^{-1} for B, respectively [Pavlov 2002, Deisenhofer 2010]. If D parameter values are calculated following Eq. 2.35, large D values have been obtained: 0.82×10^4 Oe, 1.06×10^4 Oe, 0.93×10^4 Oe, 0.85×10^4 Oe, 1.18×10^4 Oe, and 1.44×10^4 Oe, for $MgCr_2O_4$, $ZnCr_2O_4$, $ZnCr_2S_4$, $ZnCr_2Se_4$, $CdCr_2O_4$, and $CdCr_2S_4$, respectively. However, these values lead to a too large crystal-field contribution term to the ESR linewidths in these compounds. Taking into account only the first two terms in this equation, which include the trigonal crystal field parameter ν only, it follows that $D \approx 0.11 \times 10^4$ Oe in $MgCr_2O_4$, $ZnCr_2O_4$, and $CdCr_2O_4$, which turns out to be too small. Even smaller values of 0.04×10^4 Oe, 0.06×10^4 Oe, and 0.07×10^4 Oe have been found in $ZnCr_2S_4$, $CdCr_2S_4$, and $ZnCr_2Se_4$, respectively. The exchange field H_{ex} values are determined approximately by applying Eq. 2.29 as 54×10^4 Oe, 62×10^4 Oe, 12×10^4 Oe, 3×10^4 Oe, 23×10^4 Oe, 22×10^4 Oe, 16×10^4 Oe, 30×10^4 Oe, and 28×10^4 Oe for $MgCr_2O_4$, $ZnCr_2O_4$, $CdCr_2O_4$, $ZnCr_2S_4$, $CdCr_2S_4$, $HgCr_2S_4$, $ZnCr_2Se_4$, $CdCr_2Se_4$, and $HgCr_2Se_4$, respectively. Furthermore, measurements in slightly Cr^{3+} doped spinel $MgAl_2O_4$ showed that $D \approx 0.5 \times 10^4$ Oe [Stahl 1959].

Using this latter value in $MgCr_2O_4$, $ZnCr_2O_4$, and $CdCr_2O_4$, close values to the linewidths at room temperature are found. On the other hand, using a simple concept to estimate D values is also empirically possible. In Fig. 5.21, a line which has a slope equal to one and the intercept $H^2_{fine} = 0$ can be drawn through the origin point. H^2_{fine} represents the mean square width of the fine structure. This fine structure is due the to crystal-field splittings and to the nuclear hyperfine splitting. Now, assuming that only second moments of dipolar and crystal field are the main sources of the linewidth, as the line intercepts the $H_{ex} \cdot \Delta H_{obs.}$ axis, only the second moment of the crystal field is obtained. Therefore, it is easy to give estimations of D values as $H^2_{fine} = \frac{12}{5} D^2$. Following this way, one can plot parallel lines through all the points above the origin

point in order to determine the intercepts. This leads to $D \approx 0.55\times10^4$ Oe, 0.56×10^4 Oe, 0.55×10^4 Oe, 0.41×10^4 Oe, 0.34×10^4 Oe, 0.25×10^4 Oe, and 0.20×10^4 Oe, for $MgCr_2O_4$, $ZnCr_2O_4$, $CdCr_2O_4$, $ZnCr_2Se_4$, $HgCr_2Se_4$, $CdCr_2Se_4$, and $HgCr_2S_4$, respectively. The agreement is good considering the variations of crystal structure effects from compound to compound. The total calculated linewidths are in a very good agreement with the observed values at room temperature (see table 5.2). However, the linewidth in $ZnCr_2S_4$ shows a large discrepancy from the observed value at 300 K. In fact, $ZnCr_2S_4$ is a bond frustrated compound in which both ferromagnetic and antiferromagnetic interactions become important. This leads to a small Θ_{CW} while the competing exchange interactions are strong. As the dipolar contribution is calculated with help of Θ_{CW} (see Eq. 2.31), the large value of ΔH_{DD} seems to be fictitious. In fact, lattice distortions can influence the hyperfine structure. A trigonal distortion along the $\langle 111\rangle$ crystal direction leads to an axial field H_{ax} at the Cr sites. This quantity represents the axially symmetric hyperfine field and it is angular dependent. A theoretical expression of the axial hyperfine field is:

$$H_{ax} = (6/7)\mu_B \Delta g \langle r^{-3}\rangle \tag{5.8}$$

where $\langle r^{-3}\rangle$ is the average value for the Cr^{3+} $3d$ wave function [Stauss 1969]. Another probe of the crystal-field contribution is the Cr-NMR which measures the local axial field (Eq. 5.8) at the Cr nucleus.

Δg is defined like in Eq. 2.39. It is found that the Δg values the of chromium spinel compounds under focus lie approximately between 0.006 and 0.01. For $\langle r^{-3}\rangle = N^{-3}\langle r_0^{-3}\rangle$ where $\langle r_0^{-3}\rangle = 3.0841$ (a.u.)$^{-3}$ [Zhou 1983]. The estimated values of H_{ax} are obtained as ≈ 3 kOe in both $CdCr_2O_4$ and $ZnCr_2S_4$. A larger value of 3.6 kOe has been obtained in $CdCr_2S_4$ while smaller values of 1.9 kOe, 2.1 kOe, and 2.6 kOe have been found in $MgCr_2O_4$, $ZnCr_2Se_4$, and $ZnCr_2O_4$, respectively. In addition, it is also very close to those values of H_{ax} which were found by NMR technique in $CdCr_2S_4$, $HgCr_2S_4$, $CdCr_2Se_4$ and $HgCr_2Se_4$ between $2.1 - 2.3$ kOe [Stauss 1969]. The second root of the intercept values in Fig. 5.21 gives values between $8.6 - 3.2$ kOe which are slightly larger than those values obtained theoretically as well as experimentally.

Additional sources of further splittings such as hyperfine splittings will be now discussed. Following Eq. 2.51, it is easy to determine κ values in the chromium spinel compounds as $\kappa \approx 0.43$, 0.22, 0.37, 0.39, 0.28, and 0.49 for $ZnCr_2O_4$, $ZnCr_2S_4$, $ZnCr_2Se_4$, $CdCr_2O_4$, $CdCr_2S_4$, and $MgCr_2O_4$, respectively. In all spinel compounds in this work except $HgCr_2O_4$, the angle is smaller than 54.7° which is a clear indication of the elongated distortion effect. In contrast $HgCr_2O_4$ reveals clearly a larger angle $\approx 61.4°$. This leads to a compressed octahedron. By applying the normalization condition $a^2 + b^2 = 1$, testing Eq. 2.53 for chromium spinels would lead to negative values, as expected, of $(1 - 2a^2 + b^2)$: -0.57, -0.86, -0.98, -0.93, and -0.71 in $MgCr_2O_4$, $ZnCr_2O_4$, $CdCr_2O_4$,

Compound	$\Delta H_{\mathrm{DD}}[Oe]$	$\Delta H_{\mathrm{CF}}[Oe]$	$\Delta H_{\mathrm{Total}}[Oe]$	$\Delta H_{\mathrm{Observed}}[Oe]$
$MgCr_2O_4$	63	134	197	180
$ZnCr_2O_4$	54	121	175	142
$CdCr_2O_4$	239	605	844	848
$ZnCr_2S_4$	390	–	390	105
$CdCr_2S_4$	43	–	43	33
$HgCr_2S_4$	44	44	88	89
$ZnCr_2Se_4$	54	252	306	310
$CdCr_2Se_4$	25	50	75	76
$HgCr_2Se_4$	26	99	125	121

Table 5.2: The listed values in the first column are obtained by using Eqs. 2.25 and 2.27. The crystal field contributions are calculated as described in the text. The exchange field H_{ex} values are determined by applying Eq. 2.29. The values of ΔH_{CF} in all compounds, except in $ZnCr_2S_4$ and $CdCr_2S_4$, are obtained empirically from Fig. 5.21.

$ZnCr_2S_4$, and $ZnCr_2Se_4$, respectively. Substituting these values and κ values in Eq. 2.53, finally, it is possible to give estimations of the hyperfine constants $A_{\parallel} \approx 19$ Oe, 8 Oe, 15 Oe, 18 Oe, and 22 Oe as well as $A_{\perp} \approx 11$ Oe, 3 Oe, 9 Oe, 9 Oe, and 16 Oe in $ZnCr_2O_4$, $ZnCr_2S_4$, $ZnCr_2Se_4$, $CdCr_2O_4$, and $MgCr_2O_4$, respectively. This again satisfies the condition that for $A_{\parallel} > A_{\perp}$, the octahedra should exert elongations along the $\langle 111 \rangle$ crystal direction. On the other hand, the broadening effect of the hyperfine structure in the ESR linewidth can be approximately neglected taking into account the relatively small natural abundance of ^{53}Cr which is only 9%, whereas 91% are even isotopes with no spin and no magnetic moment. The small value of the hyperfine coupling constant, $A \approx 20$ Oe, is resonable [Angelov 1984]. The hyperfine spacing is given by $\Delta H_{\mathrm{h.f.}} = A_{\parallel}/g_{\parallel}\mu_{\mathrm{B}}$ [Morrish 1965]. Therefore, $\Delta H_{\mathrm{h.f.}} \approx 11$ Oe, 10 Oe, 9 Oe, 4 Oe, and 8 Oe, in $MgCr_2O_4$, $ZnCr_2O_4$, $CdCr_2O_4$, $ZnCr_2S_4$, and $ZnCr_2Se_4$, respectively. Both $A_{\parallel}$ and $A_{\perp}$ can be combined as an isotropic constant $A_{\mathrm{iso}} = (A_{\parallel} + 2A_{\perp})/3$. It is found that $A_{\mathrm{iso}} \approx 9$ Oe, 7 Oe, 6 Oe, 3 Oe, and 6 Oe in $MgCr_2O_4$, $ZnCr_2O_4$, $CdCr_2O_4$, $ZnCr_2S_4$, and $ZnCr_2Se_4$, respectively. These values of A_{iso} are comparable to that found as ≈ 47.44 MHz $\equiv 17$ Oe for Cr^{3+} ions incorporated in a single crystal of natural $MgAl_2O_4$ spinel [Bravo 1992].

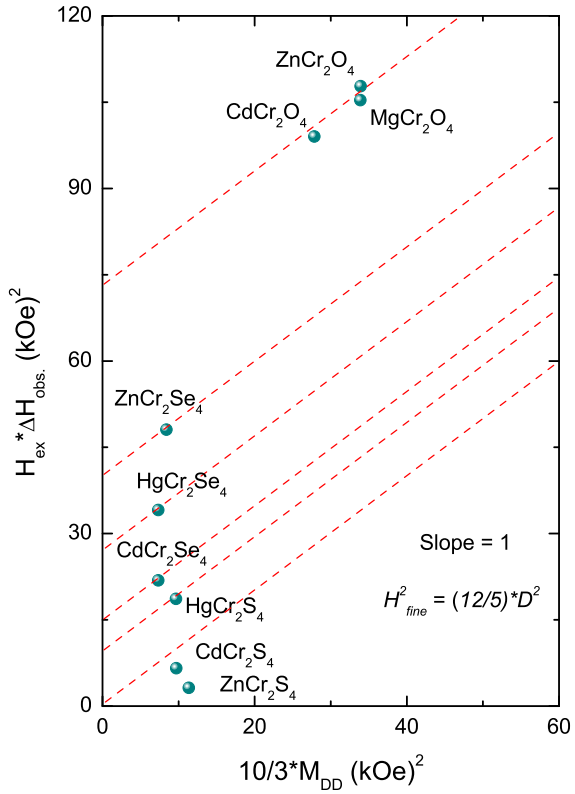

Figure 5.21: A linear plot of $H_{\text{ex}} \cdot \Delta H_{\text{obs.}}$ versus the extreme narrowed dipolar second moment. The values of the intercept $H_{\text{fine}} = \sqrt{\frac{12}{5}} D$ are obtained as parallel lines which cross the $H_{\text{ex}} \cdot \Delta H_{\text{obs.}}$ axis in non-zero points. Only positive values of H_{fine} are taken into account; i.e. all compounds except in $ZnCr_2S_4$, $CdCr_2S_4$ (see also table 5.2).

6 Conclusions and Perspectives

The aim of the present thesis was to give an overview on the abilities of electron spin resonance (ESR) as a microscopic probe for spin correlation phenomena in Cr^{3+} based two- and three-dimensional oxides and chalcogenides. The physics of these series of compounds is intimately connected with the partially filled electronic $3d$ shell of the Cr^{3+} ions. Direct information on the local susceptibility and the dominant magnetic interactions are accessible from the respective parameters: ESR intensity, g value, and linewidth.

Triangular lattice antiferromagnetic ordered rock salts $HCrO_2$, $LiCrO_2$, $NaCrO_2$ and delafossites $CuCrO_2$, $AgCrO_2$, $PdCrO_2$, $CuCrS_2$ are very interesting from the point of view of spin frustration and related ground state. The search for magnetic vortex dynamics and a corresponding Berezinsky-Kosterlitz-Thouless-like (BKT) scenario was successful in these compounds, except in $CuCrS_2$ in which conventional critical behavior dominates the temperature dependence of the ESR linewidth. A universal behavior of the ESR linewidth, $\Delta H \propto \xi^3$ where the vortex correlation length $\xi = \xi_0 \exp[\frac{b}{(T/T_m - 1)^\nu}]$ with $\nu = 0.37$, was discovered in the paramagnetic temperature regime $T > T_N$ for $ACrO_2$ delafossite as well as rock-salt compounds. Remarkably, the exponent $\nu = 0.37$ derived from the linewidth data deviates from the usual BKT-value $\nu = 0.5$ expected in the XY-model. But this can be anticipated to result from the spin relaxation via Z_2-vortices, because it agrees very well with recent theoretical predictions for the temperature dependence of the Z_2-vortex correlation length $\xi(T)$ in two-dimensional frustrated Heisenberg triangular lattice antiferromagnets [Okubo 2010]. This discovery strongly indicates the existence of the Z_2-vortices in the exotic ground-state properties observed in these materials. Except in $LiCrO_2$ and $PdCrO_2$, a wide fluctuation regime $T_m \leq T \leq T_N$ with T_m about 50% lower than T_N due to the coexistence of vortices is supposed to govern the ordered state. The finger print of the vortex dynamics extends over the whole paramagnetic regime and can be observed even at room temperature. Also these findings are in excellent agreement with the very recently theoretically predicted divergence of the BKT-critical regime for the isotropic two-dimensional Heisenberg antiferromagnet [Misawa 2010]. Further analysis of the data delivered additional interesting results. For example, the b parameter which is restricted to $b < 1.57$ in the BKT model but can take any arbitrary value in the generalized case, is found to reveal values between $0.7 \leq b \leq 2$. The microscopic meaning of this strong variation within a group of very

similar compounds needs further theoretical investigation.

Similar to two-dimensional antiferromagnetic oxides, the three-dimensional antiferromagnetic pyrochlore lattice of the B-site Cr-spinel oxides reveals a BKT-like scenario of the spin relaxation derived from the temperature dependence of the ESR linewidth. However, the exponent ν had to be chosen much smaller than 0.37. For the Mg and Zn compound $\nu = 1/16$ yielded the optimum fit while for $CdCr_2O_4$ $\nu = 1/7$ was preferable. A wide spin-fluctuation regime $T_B \leq T \leq T_N$ was derived from the fitting with the generalized BKT correlation length, where T_B is located more than 80% below T_N. The b parameter values are found to be larger than 2. This evaluation is an advanced step in the path to understand the extended divergent behavior of the linewidths in the paramagnetic regime in spinel oxides $ZnCr_2O_4$, $MgCr_2O_4$, and $CdCr_2O_4$. The applied generalized BKT idea following Bulgadaev, which considers the different internal local symmetries of spins, seems to be connected to the multi-spin clusters (oligomers), which were observed by other measurement techniques in these compounds. So far no theoretical treatment has related these oligomers to any kind of vortex structure. Here advanced theoretical investigations are highly needed to clarify this point. Note that in the related sulfide and selenide compounds only conventional critical broadening without indication of the presence of vortices was found in agreement with the neutron-scattering experiments which did not reveal any oligomer structures.

As a future task for searching new frustrated materials which can realize a BKT-like scenario, the jarosite compound family appears as a prominent candidate. This family has the chemical formula $AM_3(OH)_6(SO_4)_2$ where A: Na^+, K^+, Rb^+, Ag^+, Tl^+, NH_4^+, H_3O^+, $1/2Pb^+$, or $1/2Hg^+$, and M: Al^{3+}, Fe^{3+}, Cr^{3+}, Gd^{3+}. The large chemical variability makes the jarosites an unusually rich series to study geometrical frustration. Here the magnetic ions, M, lie on the vertices of a kagome lattice which is separated from the other kagome layers by sulfate, hydroxide, and A cations. Typical in-plane M-M distances are 3.6 Å and interplane M-M distances are 6 Å [Ramirez 2001]. In fact, it was found that above 20 K $KCr_3(OH)_6(SO_4)_2$, $T_N \approx 4$ K, realizes the two-dimensional classical Heisenberg antiferromagnet on the kagome lattice. The exchange interactions are estimated to be around 5 K which is five times smaller than that of the Fe-jarosite compounds. It is well known that a Fe-jarosite compound $H_3OFe_3(OH)_6(SO_4)_2$ reveals an unconventional spin glass-like phase [Bisson 2008]. In Cr-jarosite, the transition temperatures are lower by one order of magnitude than in Fe-jarosite. The Cr^{3+} spins form a 120° spin structure with small canting angles from the kagome plane. The net moments on the kagome planes which are created by the canting of the spins align ferromagnetically along the c-axis. The existence of the hysteresis loop in the magnetization is attributed to this weak ferromagnetism in the canted antiferromagnets [Morimoto 2003]. Preliminary ESR measurements in this compound in the temperature range between

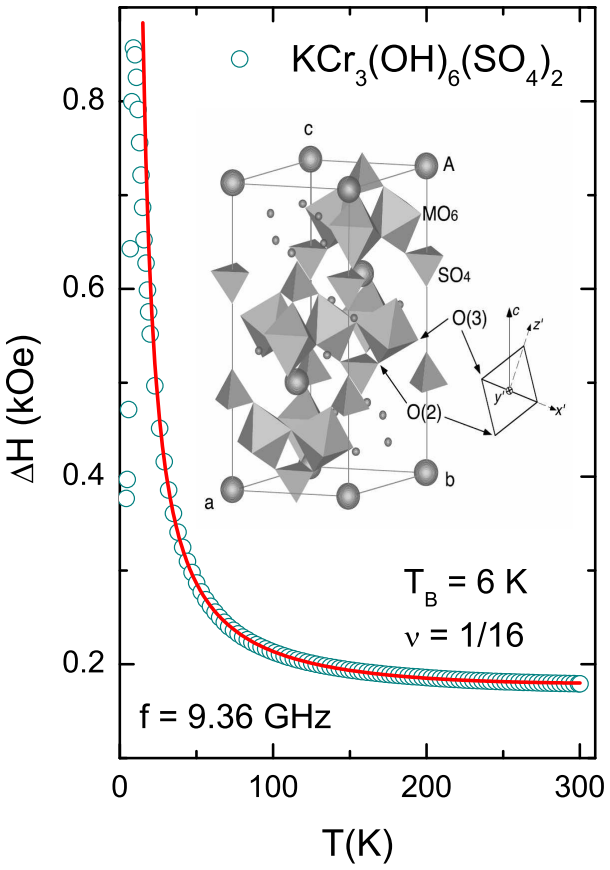

Figure 6.1: The ESR linewidth in the jarosite compound $KCr_3(OH)_6(SO_4)_2$ shows a BKT-like scenario comparable to the Cr-oxide spinels. However in contrast to $ZnCr_2O_4$ and $MgCr_2O_4$ spinels, an additional linear term is required to get an optimal fit. The inset shows the general crystal structure of $AM_3(OH)_6(SO_4)_2$ (A: monovalent ion Na^+, K^+, Rb^+, Ag^+, Tl^+, NH_4^+, H_3O^+, $1/2Pb^+$, or $1/2Hg^+$, M: trivalent ion Al^{3+}, Fe^{3+}, Cr^{3+}, Gd^{3+}) with kagome lattice in the *ab*-plane. The M^{3+} ions, which are coordinated by two O(2) oxygen atoms and four O(3) oxygen atoms, reside at the vertices of the kagome lattice. Octahedra and tetrahedra indicate MO_6 and SO_4 groups, respectively. The neighboring MO_6 octahedra share an O(3) oxygen atom at the corner. The kagome layers are well separated by nonmagnetic A^+ ions and $SO_4{}^{2-}$ groups. Therefore, as M^{3+} is a magnetic ion, the compound is expected to be a good candidate for a two-dimensional kagome lattice antiferromagnet. Note that the principal axis of the octahedron O(2)-M-O(2) is not parallel to the *c*-axis [Inami 2001].

$4 - 300$ K, showed that the linewidth can be analyzed in the frame of a BKT-like scenario (Fig. 6.1). The interesting matter is that the exponent $\nu = 1/16$ is found to be the same as in $ZnCr_2O_4$ and $MgCr_2O_4$ spinels, in which the three-dimensional pyrochlore lattice can be naturally decomposed along $\langle 111 \rangle$ directions into interleaved kagome and triangular planes [Anderson 1956]. Further research in jarosite compounds can clarify whether the BKT-like scenario is a universal behavior of the kagome lattice.

Bibliography

[Abragam 1951] A. Abragam and H. M. L. Pryce, *Theory of the Nuclear Hyperfine Structure of Paramagnetic Resonance Spectra in Crystals*, Proc. Roy. Soc. **A205**, 135 (1951).

[Abragam 1955] A. Abragam, J. Horowitz, H. M. L. Pryce, and K. W. Morton, *On the Hyperfine Structure of Paramagnetic Resonance: The s-Electron Effect*, Proc. Roy. Soc. **A230**, 169 (1955).

[Abragam 1970] A. Abragam and B. Bleaney, *Electron Paramagnetic Resonance of Transition Ions*, Clarendon Press, Oxford (1970).

[Abramova 2006] G. M. Abramovaa, and G. A. Petrakovskii, *Metal-Insulator Transition, Magnetoresistance, and Magnetic Properties of 3d-Sulfides*, Low Temp. Phys. **32**, 725 (2006).

[Ajiro 1988] Y. Ajiro Y. Ajiro, H. Kikuchi, S. Sugiyama, T. Nakashima, S. Shamoto, N. Nakayama, M. Kiyama, N. Yamamoto and Y. Oka, *Z_2 Vortex-Induced Broadening of the EPR Linewidth in the Two-Dimensional Triangular Lattice Antiferromagnets, $HCrO_2$ and $LiCrO_2$*, J. Phys. Soc. Jpn. **57**, 2268 (1988).

[Akino 1971] T. Akino and K. Motizuki, *Spin Configuration of Magnetic Ions on B-Sites in Normal Cubic Spinels*, J. Phys. Soc. Japan **31**, 691 (1971).

[Alexander 2007] L. K. Alexander, N. Buttgen, R. Nath, A. V. Mahajan, and A. Loidl, *^7Li* NMR Studies on the Triangular Lattice System *$LiCrO_2$*, Phys. Rev. B **76**, 064429 (2007).

[Almukhametov 2003] R. F. Almukhametov, R. A. Yakshibayev, E. V. Gabitov, A. R. Abdullin, R. M. Kutusheva, Structural Properties and Ionic Conductivities of $CuCr_{1-x}V_xS_2$ Solid Solutions, Phys. Status Solidi B **236**, 29 (2003).

[Altshuler 1974] S. A. Altschuler und B. M. Kosyrew, *Electron Paramagnetic Resonance in Compounds of Transition Elements*, Second revised edition, John Wiley and Sons, New York (1974).

[Anderson 1953] P. W. Anderson and P. R. Weiss, *Exchange Narrowing in Paramagnetic Resonance*, Rev. Mod. Phys. **25**, 269 (1953).

[Anderson 1954] P. W. Anderson, *A Mathematical Model for the Narrowing of Spectral Lines by Exchange or Motion* , J. Phys. Soc. Jpn. **9**, 316 (1954).

[Anderson 1956] P. W. Anderson, *Ordering and Antiferromagnetism in Ferrites*, Phys. Rev. **102**, 1008 (1956).

[Anderson 1959] P. W. Anderson, *New Approach to the Theory of Superexchange Interactions*, Phys. Rev. **115**, 2 (1959).

[Anderson 1963] P. W. Anderson, *Theory of Magnetic Exchange Interactions: Exchange in Insulators and Semiconductors*, Solid State Phys. **14**, 99 (1963).

[Anderson 1973] P. W. Anderson, *Resonating Valence Bonds: A New Kind of Insulator?*, Mater. Res. Bull. **8**, 153 (1973).

[Angelov 1984] S. Angelov, J. Darriet, C. Delmas and G. Le Flem, *Relation Between the EPR Linewidths and the Exchange Integrals in $ACrO_2$ (A = Li, Na and K)*, Solid State Communications, **50**, 4 (1984).

[Arima 2007] T. Arima, *Ferroelectricity Induced by Proper-Screw Type Magnetic Order*, J. Phys. Soc. Jpn. **76**, 073702 (2007).

[Bajpai 2005] A. Bajpai and A. K. Nigam, *Synthesis of High-Purity Samples of CrO_2 by a Simple Route*, Appl. Phys. Lett. **87**, 222502 (2005).

[Balents 2010] L. Balents, *Spin Liquids in frustrated Magnets* , Nature (London) **464**, 199 (2010).

[Baltzer 1966] P. K. Baltzer, P. J. Wojtowicz, M. Robbins, and E. Lopatin, *Exchange Interactions in Ferromagnetic Chromium Chalcogenide Spinels*, Phys. Rev. **151**, 367 (1966).

[Becker 1996] J. Becker, *Untersuchungen der Spindynamik in den Zweidimensionalen Antiferromagneten Bariumnickelphosphat und Manganthiophosphat*, PhD tesis, TU Darmstadt (1996).

[Benfield 1987] R. E. Benfield, P. P. Edwards, A. M. Stacy, *Electron Spin Resonance Spectroscopy of Layered Chromium Silver Chalcogenides*, J. Chem. Soc. Faraday Trans. 1, **83**(12), 3527 (1987).

[Benner 1990] H. Benner and J. P. Boucher, *Spin Dynamics in the Paramagnetic Regime: NMR and EPR in Two-Dimensional Magnets* in *Magnetic Properties of Layered Transition Metal Compounds*, pp. 323-378, Editor L. J. de Jongh, Kluwer Academic Publishers, Dordrecht, Boston, London (1990).

[Berezinskii 1972] V. L. Berezinskii, *An Overview of Problems with Continuous Symmetry*, Sov. Phys. JETP **34**, 610 (1972).

[Berge 1986] B. Berge, T. Diep, A. Ghazali, and P. Lallemand, *Phase Transitions in Two-Dimensional Uniformly Frustrated XY Spin Systems*, Phys. Rev. B **34**, 3177 (1986).

[Berger 1970] L. Berger, *Side-Jump Mechanism for the Hall Effect of Ferromagnets*, Phys. Rev. B **2**, 4559 (1970).

[Bersohn 1952] R. Bersohn, *Nuclear Electric-Quadrupole Spectra in Solids* , J. Chem. Phys. **20**, 1508 (1952).

[Berzhansky 1982] V. N. Berzhansky, V. I. Ivanov, and A. V. Lazuta, *Magnetic Field Effect on the Critical EPR-Dynamics of the Cubic Ferromagnets $CdCr_2Se_4$ and $CdCr_2S_4$*, Solid State Commun. **44**, 771 (1982).

[Bethe 1929] H.-A. Bethe, *Termaufspaltung in Kristallen*, Ann. Physik [5], **3**, 133 (1929).

[Bisson 2008] W. G. Bisson and A. S. Wills, *Anisotropy-Driven Spin Glass Transition in the Kagome Antiferromagnet Hydronium Jarosite $H_3OFe_3(OH)_6(SO_4)_2$*, J. Phys.: Condens. Matter **20**, 452204 (2008).

[Bleaney 1952] B. Bleaney and K. D. Bowers, *Anomalous Paramagnetism of Copper Acetate*, Proc. Roy. Soc. **A214**, 451 (1952).

[Bloch 1946] F. Bloch, *Nuclear induction*, Phys. Rev. **70**, 460 (1946).

[Bravo 1992] D. Bravo and R. Böttcher, *Electron-Nuclear-Double-Resonance Investigations on Cr^{3+} Ions in Natural $MgAl_2O_4$ Spinel*, J. Phys.: Condens. Matter **4**, 7295 (1992).

[Bulgadaev 1999] S. A. Bulgadaev, *Berezinskii-Kosterlitz-Thouless Phase Transitions in Two-Dimensional Systems with Internal Symmetries*, Journal of Experimental and Theoretical Physics **89**, 1107 (1999).

[Castner 1971] T. G. Castner and M. S. Seehra, *Antisymmetric Exchange and Exchange-Narrowed Electron-Paramagnetic-Resonance Linewidths*, Phys. Rev. B **4**, 38 (1971).

[Chapon 2006] L. C. Chapon, P. G. Radaelli, Y. S. Hor, M. T. F. Telling and J. F. *Mitchell, Non-Collinear Long-Range Magnetic Ordering in $HgCr_2S_4$*, Preprint cond-mat/0608031 (2006).

[Chern 2006] G.-W. Chern, C. J. Fennie, and O. Tchernyshov, Broken Parity and a Chiral Ground State in the Frustrated Magnet $CdCr_2O_4$, Phys. Rev. B **74**, 060405(R) (2006).

[Choi 1985] M. Y. Choi and D. Stroud, *Critical Behavior of Pure and Diluted XY Models with Uniform Frustrations*, Phys. Rev. B **32**, 5773 (1985).

[Chung 2005] J.-H. Chung, M. Matsuda, S.-H. Lee, K. Kakurai, H. Ueda, T. J. Sato, H. Takagi, K.-P. Hong, and S. Park, *Statics and Dynamics of Incommensurate Spin Order in a Geometrically Frustrated Antiferromagnet $CdCr_2O_4$*, Phys. rev. Lett. **95**, 247204 (2005).

[Costa 1998] J. E. R. Costa, B. V. Costa, and D. P. Landau, *Dynamic Behavior of Vortices in the Classical Two-Dimensional Anisotropic Heisenberg Model*, Phys. Rev. B **57**, 11510 (1998).

[Coxeter 1973] H. S. M. Coxeter, *Regular Polytopes*, Dover Publications (1973).

[Cuccoli 2003] A. Cuccoli, T. Roscilde, R. Vaia, and R. Verrucchi, *Detection of XY Behavior in Weakly Anisotropic Quantum Antiferromagnets on the Square Lattice*, Phys. Rev. Lett. **90**, 167205 (2003).

[Curie 1894] P. Curie, *On the Symmetry in Physical Phenomena, Symmetry of an Electrical Field and of a Magnetic Field (in French)*, Journal de Physique, **3**, III, 393 (1894).

[Dance 1988] J. M. Dance, A. Wichainchai, P. Dordor, E. Marquestaut, J. P. Doumerc, and A. Ammar, *Determination of the Zero Field Splitting and Exchange Narrowing of EPR Linewidth in Cr^{3+} Delafossite-Type Oxides*, J. Phys. Chem. Solids **49**, 377 (1988).

[Deisenhofer 2010] J. Deisenhofer, Private Communications.

[Delmas 1978] C. Delmas, F. Menil, G. Le Flem, C. Fouassier and P. Hagenmuller, *Etude Comparative des Proprietes Magnetiques des Oxydes Lamellaires $ACrO_2$ (A=Li, Na, K)-II*, J. Phys. Chem. Solids **39**, 55 (1978).

[DLee 1986] D. H. Lee, J. D. Joannopoulos, and J. W. Negele, *Symmetry Analysis and Monte Carlo Study of a Frustrated Antiferromagnetic Planar (XY) Model in Two Dimensions*, Phys. Rev. B **33**, 450 (1986).

[de Jongh 1990] L. J. de Jongh, *Introduction to Low-Dimensional Magnetic Systems* in *Magnetic Properties of Layered Transition Metal Compounds*, pp. 1-51, Editor L. J. de Jongh, Kluwer Academic Publishers, Dordrecht, Boston, London (1990).

[Demokritov 1989] S. O. Demokritov, M. M. Kreines, V. I. Kudinov and S. V. Detra, *Ferromagnetic Resonance and the Phase Diagrams of the Two-Dimensional Easy-plane Ferromagnets $(CH_3NH_3)_2CuCl_4$ and K_2CuF_4*, Zh. Eksp. Teor. Fiz. **95**, 2211 (1989)[Sov. Phys. JETP **68**, 1277] (1989).

[Domb 1963] C. Domb, *Statistical Mechanics of Critical Behaviour in Magnetic Systems, in: Magnetism*, Vol. **IIA**, Ed. T. Rado and E. Suhl, New York (1963).

[Doumerc 1986] J. Doumerc, A. Wichainchai, A. Ammar, M. Pouchard, and P. Hagenmuller, *On Magnetic Properties of Some Oxides with Delafossite-Type Structures*, Mat. Res. Bull., **21**, 745 (1986).

[Eikmans 1989] H. Eikmans, J. E. van Himbergen, H. J. F. Knops, and J. M. Thijssen, *Critical Behavior of an Array of Josephson Junctions with Variable Couplings*, Phys. Rev. B **39**, 11759 (1989).

[Ehlers 2011] Dieter Ehlers, *Ferromagnetische Resonanz an Multiferroika*, Diploma Thesis, Universität Augsburg (2011).

[Elliston 1974] P. R. Elliston, *Electron Paramagnetic Resonance in $NaCrS_2$*, J. Phys. C: Solid State Phys., **7**, 425 (1974).

[Elliston 1975] P.R. Elliston, F. Habbal, N. Saleha, G.E. Watsona, K.W. Blazeyb and H. Rohrerb, *Magnetic and optical study of $NaCrO_2$*, J. Phys. Chem. Solids **36**, 877 (1975).

[Engelsman 1973] F.M.R. Engelsmana, G.A. Wiegersa, F. Jellineka, and B. Van Laarb, *Crystal Structures and Magnetic Structures of Some Metal(I) Chromium(III) Sulfides and Selenides*, J. Solid State Chem. **6**, 574 (1973).

[Fang 2003] Z. Fang, N. Nagaosa, K. S. Takahashi, A. Asamitsu, R. Mathieu, T. Ogasawara, H. Yamada, M. Kawasaki, Y. Tokura and K. Terakura, *The Anomalous Hall Effect and Magnetic Monopoles in Momentum Space*, Science **302**, 92 (2003).

[Folen 1961] V. J. Folen, G. T. Rado, and E. W. Stalder, *Anisotropy of the Magnetoelectric Effect in Cr_2O_3*, Phys. Rev. Lett. **6**, 607 (1961).

[Gaveau 1991] P. Gaveau, J. P. Boucher, L. P. Regnault, and Y. Henry, *Magnetic-Field Dependence of the Phosphorous Nuclear Spin Relaxation Rate in the Quasi-Two-Dimensional XY Antiferromagnet $BaNi_2(PO_4)_2$*, J. Appl. Phys. **69**, 6228 (1991).

[Gekht 1989] R. S. Gekht, *Magnetic states and Phase Transitions in Frustrated Triangular-Lattice Antiferromagnets*, Sov. Phys. Usp. **32**, 871 (1989).

[Goodenough 1955] J. B. Goodenough, *Theor of the Role of Covalence in the Perowskite-Type Magnetites [La, M(II)]MnO_3*, Phys. Rev. **100**, 564 (1955).

[Goodenough 1963] J. B. Goodenough, *Magnetism and the Chemical Bond* Interscience, New York (1963).

[Granato 1991] E. Granato, J. M. Kosterlitz, J. Lee, and M. P. Nightingale, *Phase transitions in Coupled XY-Ising Systems*, Phys. Rev. Lett. **66**, 1090 (1991).

[Granato 1993] E. Granato and M. P. Nightingale, *Chiral Exponents of the Square-Lattice Frustrated XY Model: A Monte Carlo Transfer-Matrix Calculation*, Phys. Rev. B **48**, 7438 (1993).

[Grest 1989] G. S. Grest, *Critical Behavior of the Two-Dimensional Uniformly Frustrated Charged Coulomb Gas*, Phys. Rev. B **39**, 9267 (1989).

[Griffith 1971] J. S. Griffith, *The Theory of Transition Metal Ions*, Cambridge University Press, Cambridge (1971).

[Gutowsky 1952] H. S. Gutowsky and B. R. Mcgarvey, *Nuclear Magnetic Resonance in Metals. I. Broadening of Absorption Lines by Spin-Lattice Interactions*, J. Chem. Phys. **20**, 1472 (1952).

[Guy 1985] D. R. P. Guy, E. A. Marseglia, and S.C. Guy, *Electron Spin Resonance in $CuCrS_2$ and $CuCrSe_2$ Single Crystals*, Mol. Cryst tiq. Cvsr. **121**, 165 (1985).

[Haas 1970] C. Haas, *Magnetic semiconductors* , Crit. Rev. Solid State Sci. **1**, 47 (1970).

[Halperin 1978] B. I. Halperin and D. R. Nelson, *Theory of Two-Dimensional Melting*, Phys. Rev. Lett. **41**, 121 (1978).

[Hamilton 1963] W. C. Hamilton and J. A. Ibers, *Structures of $HCrO_2$, and $DCrO_2$*, Acta Cryst. **16**, 1209 (1963).

[Heinekamp 1985] S. W. Heinekamp and R. A. Pelcovits, *Spin-Correlation Function in Two-Dimensional XY Model*, Phys. Rev. B **32**, 4528 (1985).

[Heinrich 2003] M. Heinrich, H.-A. Krug von Nidda, A. Loidl, N. Rogado, and R. J. Cava, *Potential Signature of a Kosterlitz-Thouless transition in $BaNi_2V_2O_8$ probed by ESR*, Phys. Rev. Lett. **91**, 137601 (2003).

[Heinrich 2004] M. Heinrich, *Dynamische Suszeptibilitaet Niedrigdimensionaler Uebergangsmetalloxide*, PhD thesis, Universität Augsburg (2004).

[Heisenberg 1926] W. Heisenberg, *Mehrkorperproblem und Resonanz in der Quantenmechanik*, Z. Physik **38**, 411 (1926).

[Heisenberg 1928] W. Heisenberg, *Zur Theorie des Ferromagnetismus*, Z. Physik **49**, 619 (1928).

[Hemberger 2005] J. Hemberger, P. Lunkenheimer, R. Fichtl, H.-A. Krug von Nidda, V. Tsurkan, and A. Loidl, *Relaxor Ferroelectricity and Colossal Magnetocapacitive Coupling in Ferromagnetic $CdCr_2S_4$*, Nature (London) **434**, 364 (2005).

[Hemberger 2006] J. Hemberger, P. Lunkenheimer, R. Fichtl, S. Weber, V. Tsurkan, and A. Loidl, *Multiferroic Behavior in $CdCr_2X_4$ (X = S, Se)*, Physica B **378**, 363 (2006).

[Hikami 1980] S. Hikami and T. Tsuneto, *Phase Transition of Quasi-Two-Dimensional Planar System*, Prog. Theor. Phys. **63**, 387 (1980).

[Hill 2000] N. A. Hill, Why Are There so Few Magnetic Ferroelectrics?, J. Phys. Chem. B, **104**, 6694 (2000).

[Hirakawa 1990] K. Hirakawa, and H. Ikeda, *Neutron Scattering Experiments on Two-Dimensional Heisenberg and Ising Magnets*, in *Magnetic Properties of Layered Transition Metal Compounds*, pp. 231, ed. by L. J. deJongh, Kluwer 1990 (Netherlands).

[Holland 1972] W. E. Holland and H. A. Brown, *Application of the Weiss Molecular Field Theory to the B-site Spinel*, Phys. Stat. Sol. **10**, 249 (1972).

[Huber 1971] D. L. Huber, *Spin-Spin Relaxation near the Curie Point*, J. Phys. Chem. Solids **32**, 2145 (1971).

[Huber 1975] D. L. Huber and Seehra, *Contribution of the Spin-Phonon Interaction to the Paramagnetic Resonance Linewidth of $CrBr_3$*, J. Phys. Chem. Solids **36**, 723 (1975).

[Huber 1978] D. L. Huber, *Critical Slowing Down in The Transverse Autocorrelation Function of a Two Dimensional Planar Magnet*, Phys. Lett. **68A**, 125 (1978).

[Huber 1980] D. L. Huber, *Dynamics of Vortices in Quasi-Two-Dimensional Panar Magnets*, Phys. Lett. **78A**, 406 (1980).

[Huber 1982] D. L. Huber, *Dynamics of Spin Vortices in Two-Dimensional Planar Magnets*, Phys. Rev. B **26**, 3758 (1982).

[Huber 1999] D. L. Huber, G. Alejandro, A. Caneiro, M. T. Causa, F. Prado, M. Tovar, and S. B. Oseroff, *EPR linewidths in* $La_{1-x}Ca_xMnO_3$*:* $0 \leq x \leq 1$, Phys. Rev. B **60**, 12155 (1999).

[Hsieh 2008] D. Hsieh, D. Qian, R. F. Berger, R. J. Cava, J. W. Lynn, Q. Huang, M. Z. Hasan, *Unconventional Spin Order in the Triangular Lattice System* $NaCrO_2$*: A Neutron Scattering Study* , Physica B **403**, 1341 (2008).

[Inami 2001] T. Inami, T. Morimoto, M. Nishiyama, S. Maegawa, Y. Oka, and H. Okumura, *Magnetic Ordering in the Kagome Lattice Antiferromagnet* $KCr_3(OD)_6(SO_4)_2$, Phys. Rev. B **64**, 054421 (2001).

[Ising 1925] E. Ising, *Beitrag zur Theorie des Ferromagnetismus*, Z. Physik **31**, 253 (1925).

[Itzykson 1989] Claude Itzykson, and Jean-Michel Drouffe, *Statistical Field Theory: Volume 2, Strong Coupling, Monte Carlo Methods, Conformal Field Theory and Random Systems* , Cambridge Monographs on Mathematical Physics, Cambridge University Press (1989).

[Izyumov 1988] Yu. A. Izyumov and Yu. N. Skryabin, *Statistical Mechanics of Magnetically Ordered Systems*, Kluwer (1988).

[Ji 2009] S. Ji, S.-H. Lee, C. Broholm, T. Y. Koo, W. Ratcliff, S.-W. Cheong, and P. Zschack, *Spin-Lattice Order in Frustrated* $ZnCr_2O_4$, Phys. Rev. Lett. **103**, 037201 (2009).

[JLee 1991] J. M. Kosterlitz, and E. Granato, *Finite-size Scaling and Monte Carlo Simulations of First-Order Phase Transitions*, Phys. Rev. B **43**, 11531 (1991).

[José 1977] Jorge V. José, Leo P. Kadanoff, Scott Kirkpatrick, and David R. Nelson, *Renormalization, Vortices, and Symmetry-Breaking Perturbations in the Two-Dimensional Planar Model*, Phys. Rev. B **16**, 1217 (1977).

[Jungwirth 2002] T. Jungwirth, Q. Niu and A.H. MacDonald, *Anomalous Hall Effect in Ferromagnetic Semiconductors*, Phys. Rev. Lett. **88**, 207208 (2002).

[Kadowaki 1990] H. Kadowaki, H. Kikuchi, and Y. Ajiro, *Neutron Powder Diffraction Study of the Two-Dimensional Triangular Lattice Antiferromagnet* $CuCrO_2$, J. Phys.: Condens. Matter **2**, 4485 (1990).

[Kadowaki 1995] H. Kadowaki, H. Takei and K. Motoya, *Double-Q* 120 *degrees structure in the Heisenberg Antiferromagnet on Rhombohedrally Stacked Triangular Lattice* $LiCrO_2$, J. Phys.: Condens. Matter **7**, 6869 (1995).

[Kanamori 1959] J. Kanamori, Superexchange Interaction and Symmetry Properties of Electron Orbitals, J. Phys.Chem. Solid **10**, 87 (1959).

[Kant 2010] Ch. Kant, J. Deisenhofer, V. Tsurkan, and A. Loidl, *Magnetic Susceptibility of the Frustrated Spinels $ZnCr_2O_4$, $MgCr_2O_4$ and $CdCr_2O_4$*, J. Phy.: Conf. Ser. **200**, 032032 (2010).

[Kaplan 1959] T. A. Kaplan, *Classical Spin-Configuration Stability in the Presence of Competing Exchange Forces*, Phys. Rev. B **116**, 888 (1959).

[Karplus 1954] R. Karplus, and J.M. Luttinger, *Hall Effect in Ferromagnetics*, Phys. Rev. B **95**, 1154 (1954).

[Katsura 2005] H. Katsura, N. Nagaosa, A. V. Balatsky, *Spin Current and Magnetoelectric Effect in Noncollinear Magnets*, Phys. Rev. Lett. **95**, 057205 (2005).

[Kawamura 1984] H. Kawamura, and S. Miyashita, *Phase Transition of the Two-Dimensional Heisenberg Antiferromagnet on the Triangular Lattice*, J. Phys. Soc. Jpn. **53**, 4138 (1984).

[Kawamura 2010] H. Kawamura, A. Yamamoto, and T. Okubo, *Z_2-Vortex Ordering of the Triangular-Lattice Heisenberg Antiferromagnet*, J. Phys. Soc. Jpn. **79**, 023701 (2010).

[Kawasaki 1968] K. Kawasaki, *Dynamics of Critical Fluctuations. I*, Prog. Theor. Phys. **39**, 285 (1968).

[Kimura 2006] S. Kimura, M. Hagiwara, H. Ueda, Y. Narumi, K. Kindo, H. Yashiro, T. Kashiwagi, and H. Takagi, *Observation of Higher-Harmonic Helical Spin-Resonance Modes in the Chromium Spinel $CdCr_2O_4$*, Phys. Rev. Lett. **97**, 257202 (2006).

[Kimura 2008] K. Kimura, H. Nakamura, K. Ohgushi, and T. Kimura, *Magnetoelectric Control of Spin-Chiral Ferroelectric Domains in a Triangular Lattice Antiferromagnet*, Phys. Rev. B **78**, 140401(R) (2008).

[Kimura 2009] K. Kimura, H. Nakamura, S. Kimura, M. Hagiwara, and T. Kimura, *Tuning Ferroelectric Polarization Reversal by Electric and Magnetic Fields in $CuCrO_2$*, Phys. Rev. Lett. **103**, 107201 (2009).

[Kimura 2009] K. Kimura, T. Otani, H. Nakamura, Y. Wakabayashi, and T. Kimura, *Lattice Distortion Coupled with Magnetic Ordering in a Triangular Lattice Antiferromagnet $CuCrO_2$*, J. Phys. Soc. Jpn. **78**, 113710 (2009).

[Knops 1994] Y. M. M. Knops, B. Nienhuis, H. J. F. Knops, and H. W. J. Blote, *19-Vertex Version of the Fully Frustrated XY Model*, Phys. Rev. B **52**, 7402 (1994).

[Kosterlitz 1973] J. M. Kosterlitz and D. J. Thouless, *Ordering, Metastability and Phase Transitions in Two-Dimensional Systems*, J. Phys. C **6**, 1181 (1973).

[Kosterlitz 1974] J. M. Kosterlitz, *The Critical Properties of the Two-Dimensional XY Model*, J. Phys. C **7**, 1046 (1974).

[Kramers 1930] H. A. Kramers, Proc. Amsterdam Acad. Sci. **33**, 959 (1930).

[Kramers 1934] H. A. Kramers, *L'interaction Entre les Atomes Magnetogenes dans un Cristal Paramagnetique*, Physica **1**, 182 (1934).

[Kubo 1954] R. Kubo and K. Tomita, *A General Theory of Magnetic Resonance Absorption*, J. Phys. Soc. Jpn. **9**, 888 (1954).

[Kubo 1961] R. Kubo, in *Fluctuation, Relaxation and Resonance in Magnetic Systems*, ed. by D. ter Haar, Oliver and Boyd, Edinburgh, p. 23 (1961).

[Lafond 2001] A. Lafond, W. Henggeler, H. Mutka, and B. Ouladdiaf, *Alteration of the Stacked $2\pi/3$ Magnetic Structure in the Triangular Lattice Antiferromagnet $LiCrS_2$*, Can. J. Phys./Rev. can. phys. **79** (11-12): 1427 (2001).

[Larmor 1896] J. Larmor, *The Influence of a Magnetic Field on Radiation Frequency*, Proc. R. Soc. London **60**, 514 (1896).

[Lee 2000] S.-H. Lee, C. Broholm, T. H. Kim, W. Ratcliff, and S.-W. Cheong, *Local Spin Resonance and Spin-Peierls-like Phase Transition in a Geometrically Frustrated Antiferromagnet*, Phys. Rev. Lett. **84**, 3718 (2000).

[Lee 2002] S.-H. Lee, C. Broholm, W. Ratcliff, G. Gasparovic, Q. Huang, T. H. Kim, and S.-W. Cheong, *Emergent Excitations in a Geometrically Frustrated Magnet*, Nature (London) **418**, 856 (2002).

[Loison 2004] D. Loisson, *Phase Transitions in Frustrated Vector Spin Systems: Numerical Studies*, pp177, in "*Frustrated Spin Systems*" ed. by H. T. Diep, World Scientific (2004).

[Lotgering 1964] F. K. Lotgering, *Ferromagnetism in Spinels $CuCr_2S_4$ and $CuCr_2Se_4$*, Proc. Int. Conf. on Magnetics p. 533, Nottingham, England (1964).

[Lotgering 1971] F. K. Lotgering, *Exchange Interaction in Semiconducting Chalcogenides with Normal Spinel Structure from an Experimental Point of View*, Journal De Physique **32**, C1-34 (1971).

[Low 1960] W. Low, *Paramagnetic Resonance in Solids*, Solid State Physics: Advances in Research and Applications, Supplement **2**, London (1960).

[Macfarlane 1967] R. M. Macfarlane, *Zero Field Splittings of t_3^2 Cubic Terms*, J. Chem. Phys. **47**, 2066 (1967).

[Macfarlane 1970] R. M. Macfarlane, *Perturbation Methods in the Calculation of Zeeman Interactions and Magnetic Dipole Line Strengths for d^3 Trigonal-Crystal Spectra*, Phys. Rev. B **1**, 989 (1970).

[Machida 2007] Y. Machida, S. Nakatsuji, Y. Maeno, T. Tayama, T. Sakakibara, and S. Onoda, *Unconventional Anomalous Hall Effect Enhanced by a Noncoplanar Spin Texture in the Frustrated Kondo Lattice $Pr_2Ir_2O_7$*, PRL **98**, 057203 (2007).

[Maleev 1974] S. V. Maleyev, *Magnetic Interaction and the Critical Dynamics above the Curie Point*, Phys. Letters A **47**, 111 (1974).

[Maleyev 1995] S. V. Maleyev, *Investigation of Spin Chirality by Polarized Neutrons* , Phys. Rev. Lett. **75**, 4682 (1995).

[Manoogian 1974] A. Manoogian and A. Leclerc, *Electron-Nuclear-Double-Resonance of* $^{53}Cr^{3+}$ *in Guanidinium Aluminum Sulfate Hexahydrate*, Phys. Rev. B **10**, 1052 (1974).

[Martinho 2001] H. Martinho, N. O. Moreno, J. A. Sanjurjo, C. Rettori, A. J. Garcia-Adeva, D. L. Huber, S. B. Oseroff, W. Ratcliff, S.-W. Cheong, P. G. Pagliuso, J. L. Sarrao, and G. B. Martins, *Studies of the Three-Dimensional Frustrated Antiferromagnetic* $ZnCr_2O_4$, J. Appl. Phys. **89**, 7050 (2001).

[Matsuda 2006] K. Matsuda, N. Furukawa, and Y. Motome, *Spin Singlet State in Heptamers Emerging in Spinel Oxide* AlV_2O_4, J. Phys. Soc. Japan **75**, 124716 (2006).

[Matsuda 2007] M. Matsuda, M. Takeda, M. Nakamura, K. Kakurai, A. Oosawa, E. Lelièvre-Berna, J.-H. Chung, H. Ueda, H. Takagi, and S.-H. Lee, *Spiral Spin Structure in the Heisenberg Pyrochlore Magnet* $CdCr_2O_4$, Phys. Rev. B **75**, 104415 (2007).

[McGarvey 1964] B. R. McGarvey, *Anisotropic Hyperfine Interaction of* ^{53}Cr *in Chromium (III) Acetylacetonate*, J. Chem. Phys. **40**, 809 (1964).

[Mehran 1975] F. Mehran, M. W. Shafer, and G. V. Subba Rao, *Examination of the Various Crystal Field Theories of* d^3 *Ions in Trigonal Fields*, Solid State Communications **17**, 1311 (1975).

[Meisenheimer 1961] R. G. Meisenheimer and J. D. Swalen, *Magnetic Properties of* $HCrO_2$ *and* $DCrO_2$, Phys. Rev. **123**, 831 (1961).

[Mekata 1995] M. Mekata, T. Sugino, Y. Oohara, and H. Yoshizawa, *Magnetic Structure of Antiferromagnetic* $PdCrO_2$*: Possible Degenerate Helices on a Rhombohedral Lattice*, Physica B **213**, 221 (1995).

[Menyuk 1966] G. W. Menyuk, K. Dwight, R. J. Arnott, and A. Would, *Ferromagnetism in* $CdCr_2Se_4$ *and* $CdCr_2S_4$, J. appl. Phys. **37**, 1387 (1966).

[Mermin 1966] N. D. Mermin, H. Wagner, *Absence of Ferromagnetism or Antiferomagnetism in One- or Two-Dimensional Isotropic Heisenberg Models*, Phys. Rev. Lett. **17**, 1133 (1966).

[Mertens 1989] F. G. Mertens, A. R. Bishop, G. M. Wysin and C. Kawabata, *Dynamical Correlations from Mobile Vortices in Two-Dimensional Easy-Plane Ferromagnets*, Phys. Rev. B **39**, 591 (1989).

[Mertens 1991] F. G. Mertens, A. Volkel, G. M. Wysin and A. R. Bishop, *Central peak signatures from vortices in 2D easy-plane antiferromagnets*, Nonlinear Coherent Structures in Physics and Biology: Lecture Notes in Physics, Volume **393**, Springer-Verlag Berlin Heidelberg (1991).

[Mertens 2000] F. G. Mertens and A. R. Bishop, *Dynamics of Vortices in Two-Dimensional Magnets*, in *Lecture Notes in Physics*, pp. 137-170, Volume 543, Editors P. L. Christiansen, M. P. Sørensen, and A. C. Scott, Springer-Verlag Berlin Heidelberg (2000).

[Misawa 2010] T. Misawa and Y. Motome, *Nonequilibrium Relaxation Study of the Anisotropic Antiferromagnetic Heisenberg Model on the Triangular Lattice*, J. Phys. Soc. Jpn. **79**, 073001 (2010).

[Moessner 2006] R. Moessner and A. Ramirez, *Geometrical Frustration*, Physics Today **59**, 24 (2006).

[Moreno 2004] N. O. Moreno, C. Israel, P. G. Pagliuso, A. J. Garcia-Adeva, C. Rettori, J. L. Sarraoa, J. D. Thompson, and S. B. Oseroff, *Magnetic Properties of the Frustrated Antiferromagnet* $LiCrO_2$, J. Magn. Magn. Mater. **272**, 1023 (2004).

[Morimoto 2003] T. Morimoto, M. Nishiyama, S. Maegawa, and Y. Oka, *Magnetization of New Kagome Lattice Antiferromagnets: Cr-Jarosites,* $ACr_3(OH)_6(SO_4)_2$ *[A =Na, K, Rb,* NH_4*]*, J. Phys. Soc. Jpn. **72**, 2085 (2003).

[Morrish 1965] Allan H. Morrish, *The Physical Principles of Magnetism*, John Wiley and Sons, New York (1965).

[Motida 1970] K. Motida, and S. Miyahara, *On the* 90° *Exchange Interaction between Cations (*Cr^{3+}*,* Mn^{2+}*,* Fe^{3+}*, and* Ni^{2+}*) in Oxides*, J. Phys. Soc. Jpn. **28**, 1188 (1970).

[Mulliken 1935] R. S. Mulliken, *Electronic Structures of Polyatomic Molecules and Valence* [6], J. Chem. Phys. **3**, 375 (1935).

[Nagaosa 2010] N. Nagaosa, J. Sinova, S. Onoda, A. H. MacDonald, and N. P. Ong, *Anomalous Hall Effect*, Rev. Mod. Phys. **82**, 1539 (2010).

[Néel 1932] L. Néel, Ann. Phys. **18**, 5 (1932).

[Nelson1977] D. R. Nelson and J. M. Kosterlitz, *Universal Jump in the Superfluid Density of Two-Dimensional Superfluids*, Phys. Rev. Lett. **39**, 1201 (1977).

[Nightingale 1995] M. P. Nightingale, E. Granato, and J. M. Kosterlitz, *Conformal Anomaly and Critical Exponents of the XY Ising Model*, Phys. Rev. B **52**, 7402 (1995).

[Ohgushi 2000] K. Ohgushi, S. Murakami, and N. Nagaosa, *Spin Anisotropy and Quantum Hall effect in the Kagomé Lattice: Chiral Spin State Based on a Ferromagnet*, Phys. Rev. B **62**, R6065 (2000).

[Okubo 2010] T. Okubo and H. Kawamura, *Signature of a* Z_2 *Vortex in the Dynamical Correlations of the Triangular-Lattice Heisenberg Antiferromagnet*, J. Phys. Soc. Jpn. **79**, 084706 (2010).

[Olariu 2006] A. Olariu, P. Mendels, F. Bert, B. G. Ueland, P. Schiffer, R. F. Berger, and R. J. Cava, *Unconventional Dynamics in Triangular Heisenberg Antiferromagnet* $NaCrO_2$, Phys. Rev. Lett. **97**, 167203 (2006).

[Olariu 2009] A. Olariu, P. Mendels, F. Bert, L. K. Alexander, A. V. Mahajan, A. D. Hillier, and A. Amato, *Spin Dynamics in Heisenberg Triangular Antiferromagnets: A μSR Study of $LiCrO_2$*, Phys. Rev. B **79**, 224401 (2009).

[Olsson 1995] P. Olsson, *Two Phase Transitions in the Fully Frustrated XY Model*, Phys. Rev. Lett. **75**, 2758 (1995).

[Oohara 1994] Y. Oohara, S. Mitsuda, H. Yoshizawa, N. Yaguchi, H. Kuriyama, T. Asano, and M. Mekata, *Magnetic Phase Transition in $AgCrO_2$*, J. Phys. Soc. Jpn. **63**, 847 (1994).

[Pake 1973] G. E. Pake and T. L. Estle, *The Principles of Paramagnetic Resonance*, Benjamin, London (1973).

[Pavlov 2002] R. Pavlov, V. Marzá, and J. Carda, *Electronic Absorption Spectroscopy and Colour of Chromium-Doped Solids*, J. Mater. Chem. **12**, 2825 (2002).

[Penrose 2007] Roger Penrose, *The Road to Reality: A Complete Guide to the Laws of the Universe* , Vintage (2007).

[Plakhty 1999] V. P. Plakhty, S. V. Maleyev, J. Kulda, J. Wosnitza D. Visser and E. Moskvin, *Inelastic Polarised Neutron Scattering in the Triangular-Lattice Antiferromagnet $CsMnBr_3$: An Experimental Proof of the Chiral Universality*, Europhys. Lett., **48** (2), 215 (1999).

[Plakhty 2000] V. P. Plakhty, J. Kulda, D. Visser, E. V. Moskvin, and J. Wosnitza, *Chiral Critical Exponents of the Triangular-Lattice Antiferromagnet $CsMnBr_3$ as Determined by Polarized Neutron Scattering*, Phys. Rev. Lett. **85**, 3942 (2000).

[Poienar 2009] M. Poienar, F. Damay, C. Martin, V. Hardy, A. Maignan, and G. André, *Structural and Magnetic Properties of $CuCr_{1-x}Mg_xO_2$ by Neutron Powder Diffraction*, Phys. Rev. B **79**, 014412 (2009).

[Poienar 2010] M. Poienar, F. Damay, C. Martin, J. Robert, and S. Petit, *Spin Dynamics in the Geometrically Frustrated Multiferroic $CuCrO_2$*, Phys. Rev. B **81**, 104411 (2010).

[Pokrovsky 1990] V. L. Pokrovsky and G. V. Uimin, in *Magnetic Properties of Layered Transition Metal Compounds*, ed. by L. J. de Jongh, Kluver Academic Publishers, Dordrecht, Boston, London, pp. 53-103 (1990).

[Poole 1997] Charles P. Poole Jr., *Electron Spin Resonance: A Comprehensive Treatise on Experimental Techniques*, Dover Publications, 2 Sub edition (1997).

[Pryce 1950] M. H. L. Pryce, *A Modified Perturbation Procedure for a Problem in Paramagnetism*, Proc. Phys. Soc. A **63**, 25 (1950).

[Radaelli 2002] P. G. Radaelli, Y. Horibe, M. J. Gutmann, H. Ishibashi, C. H. Chen, R. M. Ibberson, Y. Koyama, Y.-S. Hor, V. Kiryushin, and S.-W. Cheong, *Formation of Isomorphic Ir^{3+} and Ir^{4+} Octamers and Spin Dimerization in the Spinel $CuIr_2S_4$*, Nature (London) **416**, 155 (2002).

[Ramirez 2001] A. P. Ramirez, *Geometrical Frustration*, Handbook of Magnetic Materials **13**, 423 (2001).

[Ramirez-Santiago 1992] G. Ramirez-Santiago and J. V. José, *Correlation Functions in the Fully Frustrated 2D XY Model*, Phys. Rev. Lett. **68**, 1224 (1992).

[Ramirez-Santiago 1994] G. Ramirez-Santiago and J. V. José, *Critical Exponents of the Fully Frustrated Two-Dimensional XY Model*, Phys. Rev. B **43**, 11531 (1994).

[Rasch 2009] Julia C. E. Rasch, M. Boehm, C. Ritter, H. Mutka, J. Schefer, L. Keller, G. M. Abramova, A. Cervellino, and J. F. Löffler, *Magnetoelastic Coupling in the Triangular Lattice Antiferromagnet $CuCrS_2$*, Phys. Rev. B **80**, 104431 (2009).

[Rastelli 1986] E. Rastelli and A. Tassi, *The Rhombohedral Heisenberg Antiferromagnet: Infinite Degeneracy of the Ground State and Magnetic Properties of Solid Oxygen*, J. Phys. C: Solid State Phys. **19**, L423 (1986).

[Regnault 1990] L. P. Regnault and J. Rossat-Mignod, *Phase Transitons in Quasi Two-Dimensional Planar Magnets* in *Magnetic Properties of Layered Transition Metal Compounds*, Editor L. J. de Jongh, Kluwer Academic Publishers, Dordrecht, Boston, London, pp. 323-378 (1990).

[Richards 1973] Peter M. Richards, *Critical Exponents for NMR and ESR Linewidths in a Two-Dimensional Antiferromagnet*, Solid State Communications **13**, 253 (1973).

[Richards 1974] Peter M. Richards and M. B. Salamon, *Exchange Narrowing of Electron Spin Resonance in a Two-Dimensional System*, Phys. Rev. B **9**, 32 (1974).

[Rieger 2008] H. Rieger, R. Paul, J. Noh, and G. Schehr, *Computer Simulations of Phase Transitions and Dynamics in Confined Systems*, Z. Phys. Chem. 222, 433 (2008).

[RLee 1994] J.-R. Lee, *Phase Transitions in the Two-Dimensional Classical Lattice Coulomb Gas of Half-Integer Charges*, Phys. Rev. B **49**, 3317 (1994).

[Rønnow 2002] H. M. Rønnow, A. R. Wildes, S. T. Bramwell, *Magnetic correlations in the $2D$ $S = 5/2$ honeycomb antiferromagnet $MnPS_3$*, Physica B **276**, 676 (2000).

[Ross 2009] K. A. Ross, J. P. C. Ruff, C. P. Adams, J. S. Gardner, H. A. Dabkowska, Y. Qiu, J. R. D. Copley, and B. D. Gaulin, *Two-Dimensional Kagome Correlations and Field Induced Order in the Ferromagnetic XY Pyrochlore $Yb_2Ti_2O_7$*, PRL **103**, 227202 (2009).

[Rudolf 2007] T. Rudolf, Ch. Kant, F. Mayr, J. Hemberger, V. Tsurkan, and A. Loidl, *Spin-phonon Coupling in Antiferromagnetic Chromium Spinels*, New J. Phys. **9**, 76 (2007).

[Rudolf 2009] T. Rudolf, Frustration und Ordnung: Infrarotspektroskopie an Chromspinellen, PhD thesis, Universität Augsburg (2009).

[Sakai 1986] N. Sakai and J. H. Pifer, *Effect of Hydrostatic Pressure on the Exchange Interactions in a Ferromagnetic Spinel $CdCr_2Se_4$*, Phys. Rev. B **33**, 1875 (1986).

[Seehra 1974] M. S. Seehra and R. P. Gupta, *Temperature Dependence of the EPR Linewidth of $CrBr_3$ near T_c*, Phys. Rev. B **9**, 197 (1974).

[Seki 2008] S. Seki, Y. Onose, and Y. Tokura, *Spin-Driven Ferroelectricity in Triangular Lattice Antiferromagnets $ACrO_2$ (A=Cu, Ag, Li, or Na)*, Phys. Rev. Lett. **101**, 067204 (2008).

[Shannon 1971] R. D. Shannon, D. B. Rogers, and C. T. Prewitt, *Chemistry of Noble Metal Oxides. I. Syntheses and Properties of ABO_2, Delafossite Compounds*, Inorganic Chemistry, **10** (4), 713 (1971).

[Singh 2009] K. Singh, A. Maignan, C. Martin and Ch. Simon, *$AgCrS_2$: A Spin Driven Ferroelectric*, Chem. Mater., **21** (21), 5007 (2009).

[Sinha 1980] K. P. Sinha and N. Kumar, *Interactions in Magnetically Ordered Solids*, Oxford University Press (1980).

[Smit 1955] J. Smit, *The Spontanuous Hall Effect in Ferromagnetics I*, Physica (Amsterdam) **21**, 877 (1955).

[Soda 2009] M. Soda, K. Kimura, T. Kimura, M. Matsuura, and K. Hirota, *Electric Control of Spin Helicity in Multiferroic Triangular Lattice Antiferromagnet $CuCrO_2$ with Proper-Screw Order*, J. Phys. Soc. Jpn. **78**, 124703 (2009).

[Soubeyroux 1979] J. L. Soubeyroux, D. Fruchart, C. Delmas, and G. Le Flem, *Neutron Powder Diffraction Studies of Two-Dimensional Magnetic Oxides*, Journal of Magnetism and Magnetic Materials **14**, 159 (1979).

[Stahl 1959] R. Stahl-Brada, and W. Low, Paramagnetic Resonance Spectra of Chromium and Manganese in the Spinel Structure, Phys. Rev. **116**, 561 (1959).

[Stauss 1969] G. H. Stauss, *Nuclear Magnetic Resoanance of Cd in $CdCr_2Se_4$ and $CdCr_2S_4$, and Transferred Spin Polarization in Chromium Chalcogenide Spinels*, Phys. Rev. **181**, 636 (1969).

[Sugano 1958] S. Sugano and Y. Tanabe, *Absorption Spectra of Cr^{3+} in Al_2O_3, Part A. Theoretical Studies of the Absorption Bands and Lines*, J. Phys. Soc. Japan **13**, 880 (1958).

[Taguchi 2001] Y. Taguchi, Y. Oohara, H. Yoshizawa, N. Nagaosa and Y. Tokura, *Spin Chirality, Berry Phase, and Anomalous Hall Effect in a Frustrated Ferromagnet*, Science **291**, 2573 (2001).

[Takada 2003] K. Takada, H. Sakurai, E. Takayama-Muromachi, F. Izumi, R. A. Dilanian, and T. Sasaki, *Superconductivity in Two-Dimensional CoO_2 Layers*, Nature (London) **422**, 53 (2003).

[Takatsu 2009] H. Takatsu, H. Yoshizawa, S. Yonezawa, and y. Maeno, *Critical Behavior of the Metallic Triangular-Lattice Heisenberg Antiferromagnet $PdCrO_2$*, Phys. Rev. B **79**, 104424 (2009).

[Takatsu 2010] H. Takatsu, S. Yonezawa, C. Michioka, K. Yoshimura, and Y. Maeno, *Anisotropy in the Magnetization and Resistivity of the Metallic Triangular-Lattice Magnet $PdCrO_2$* , jpconf **200**, 012198 (2010).

[Takatsu 2010] H. Takatsu, S. Yonezawa, S. Fujimoto, and Y. Maeno, *Unconventional Anomalous Hall Effect in the Metallic Triangular-Lattice Magnet $PdCrO_2$*, Phys. Rev. Lett. **105**, 137201 (2010).

[Takatsu 2010] H. Takatsu and Y. Maeno, *Single Crystal Growth of the Metallic Triangular-Lattice Antiferromagnet $PdCrO_2$*, Journal of Crystal Growth, **312**, 3461 (2010).

[Tatara 2002] G. Tatara and H. Kawamura, *Chirality-Driven Anomalous Hall Effect in Weak Coupling Regime*, J. Phys. Soc. Jpn. **71**, 2613 (2002).

[Tchernyshyov 2002] O. Tchernyshyov, R. Moessner, and S. L. Sondhi, *Order by Distortion and String Modes in Pyrochlore Antiferromagnets*, Phys. Rev. Lett. **88**, 067203 (2002).

[Terada 2006] N. Terada, S. Mitsuda, H. Ohsumi, and K. Tajima, *"Spin-Driven" Crystal Lattice Distortion in Frustrated Magnet CuFeO2: Synchrotron X-ray Diffraction Study*, J. Phys. Soc. Jpn. **75**, 023602 (2006).

[Tomita 1970] K. Tomita and T. Kawasaki, Green's Function Theory of Magnetic Relaxation. IV, Prog. Theor. Phys. **44**, 1173 (1970).

[Tomiyasua 2008] K. Tomiyasu, H. Suzuki, M. Toki, S. Itoh, M. Matsuura, N. Aso, and K. Yamada, *Molecular Spin Resonance in the Geometrically Frustrated Magnet $MgCr_2O_4$ by Inelastic Neutron Scattering*, Phys. Rev. Lett. **101**, 177401 (2008).

[Tomiyasub 2008] K. Tomiyasu, H. Hiraka, K. Ohoyama, and K. Yamada, *Resonance-Like Magnetic Excitations in Spinel Ferrimagnets $FeCr_2O_4$ and $NiCr_2O_4$ Observed by Neutron Scattering*, J. Phys. Soc. Japan **77**, 124703 (2008).

[Tsujii 2007] N. Tsujii and H. Kitazawa, *Substitution Effect on the Two-Dimensional Triangular-Lattice System $CuCrS_2$*, J. Phys.: Condens. Matter **19**, 145245 (2007).

[Van Vleck 1939] J. H. Van Vleck, *On the Magnetic Behavior of Vanadium, Titanium and Chrome Alum*, J. Chem. Phys. **7**, 61 (1939).

[Van Vleck 1948] J. H. Van Vleck, *The Dipolar Broadening of Magnetic Resopnance Lines in Crystals*, Phys. Rev. **74**, 1168 (1948).

[Voelkel 1991] A. R. Völkel, G. M. Wysin, A. R. Bishop, and F. G. Mertens, *Dynamic Correlations in The Classical Two-Dimensional Antiferromagnetic Heisenberg Model with Easy-Plane Symmetry*, Phys. Rev. B **44**, 10066 (1991).

[Weber 2006] S. Weber, P. Lunkenheimer, R. Fichtl, J. Hemberger, V. Tsurkan, and A. Loidl, *Colossal Magnetocapacitance and Colossal Magnetoresistance in $HgCr_2S_4$*, Phys. Rev. Lett. **96**, 157202 (2006).

[Winterberger 1987] M. Winterberger and Y. Allain, Structure Magnetique Helicoidale de $CuCrS_2$, Solid State Commun. **64**, 1343 (1987).

[Wu 2005] Shao-Yi Wu and Hui-Ning Dong, *Theoretical Investigations of the Spin Hamiltonian Parameters for the Two Trigonal Cr^{3+} centers in GASH*, Journal of Magnetism and Magnetic Materials **285**, 169 (2005).

[Yamada 1972] I. Yamada and M. Ikebe, *Temperature and Frequency Dependence of the ESR Line Width in Two-Dimensional Ferromagnet K_2CuF_4*, J. Phys. Soc. Jpn. **33**, 1334 (1972).

[Yamaguchi 2008] H. Yamaguchi, S. Kimura, M. Hagiwara, Y. Nambu, S. Nakatsuji, Y. Maeno, and K. Kindo, *High-field Electron Spin Resonance in the Two-Dimensional Triangular-Lattice Antiferromagnet $NiGa_2S_4$*, Phys. Rev. B **78**, 180404(R) (2008).

[Yamaguchi 2010] H. Yamaguchi, S. Kimura, M. Hagiwara, Y. Nambu, S. Nakatsuji, Y. Maeno, A. Matsuo, and K. Kindo, *High-field ESR and Magnetization of the Triangular-Lattice Antiferromagnet $NiGa_2S_4$*, J. Phys. Soc. Jpn. **79**, 054710 (2010).

[Yamaguchi 2010] H. Yamaguchi, S. Ohtomo, S. Kimura, M. Hagiwara, K. Kimura, T. Kimura, T. Okuda, and K. Kindo, *Spiral-Plane Flop probed by ESR in the Multiferroic Triangular-Lattice Antiferromagnet $CuCrO_2$*, Phys. Rev. B **81**, 033104 (2010).

[Ye 2006] F. Ye, Y. Ren, Q. Huang, J. A. Fernandez-Baca, Pengcheng Dai, J. W. Lynn, and T. Kimura, *Spontaneous Spin-Lattice Coupling in the Geometrically Frustrated Triangular Lattice Antiferromagnet $CuFeO_2$*, Phys. Rev. B **73**, 220404(R) (2006).

[Yokaichiya 2009] F. Yokaichiya, A. Krimmel, V. Tsurkan, I. Margiolaki, P. Thompson, H. N. Bordallo, A. Buchsteiner, N. Stüßer, D. N. Argyriou, and A. Loidl, *Spin-driven Phase Transitions in $ZnCr_2Se_4$ and $ZnCr_2S_4$ Probed by High-Resolution Synchrotron X-ray and Neutron Powder Diffraction*, Phys. Rev. B **79**, 064423 (2009).

[Yokota 1955] M. Yokota, *A Note on the Paramagnetic Relaxation*, J. Phys. Soc. Jpn. **10**, 762 (1955).

[Yosefin 1985] M. Yosefin and E. Domany, *Phase Transitions in Fully Frustrated Spin Systems*, Phys. Rev. B **32**, 1778 (1985).

[Yoshida 2006] M. Yoshida, T. Hirano, Y. Inagaki, S. Okubo, H. Ohta, H. Kikuchi, I. Kagomiya, M. Toki, and K. Kohn, *High Field ESR Study of Three Dimensional Spin Frustrated System $MgCr_2O_4$*, J. Phys. Soc. Japan **75**, 044709 (2006).

[Young 1979] A. P. Young, *Melting and the Vector Coulomb Gas in Two Dimensions*, Phys. Rev. B **19**, 1855 (1979).

[Zavoisky 1945] E. K. Zavoisky, *Spin Magnetic Resonance in Paramagnetics*, J. Phys. USSR **9**, 245 (1945).

[Zeiger 1973] H. J. Zeiger, and G. W. Pratt, *Magnetic Interactions in Solids*, Oxford University Press (1973).

[Zhou 1983] M. G. Zhou, J. A. Xu, G. R. Bai and H. S. Xie, *d-Orbital Theory and High-Pressure Effects upon the EPR Spectrum of Ruby*, Phys. Rev. B **27**, 1516 (1983).

List of Publications

- *Vortex Dynamics and Frustration in Two-Dimensional Triangular Chromium Lattices*

  M. Hemmida, H.-A. Krug von Nidda, N. Büttgen, A. Loidl, L. K. Alexander, R. Nath, A. V. Mahajan, R. F. Berger, R. J. Cava, Yogesh Singh, and D. C. Johnston, Phys. Rev. B **80**, 054406 (2009).

- *ESR in 2D Triangular Chromium Lattices*

  M. Hemmida, H.-A. Krug von Nidda, A. Loidl,
  Journal of Physics: Conference Series **200**, 022016 (2010).

- *Magnetic Fluctations and Superconductivity in Fe Pnictides probed by Electron Spin Resonance*

  N. Pascher, J. Deisenhofer, H.-A. Krug von Nidda, M. Hemmida, H.S. Jeevan, P. Gegenwart, and A. Loidl,
  Phys. Rev. B **82**, 054525 (2010).

- *On the Magnetism of $Ln_{2/3}Cu_3Ti_4O_{12}$ (Ln = lanthanide)*

  A. Dittl, S. Krohns, J. Sebald, F. Schrettle, M. Hemmida, H.-A. Krug von Nidda, S. Riegg, A. Reller, S. G. Ebbinghaus, and A. Loidl,
  Eur. Phys. J. B **79**, 391 (2011).

- *Traces of Z_2-vortices in $CuCrO_2$, $AgCrO_2$, and $PdCrO_2$*

  M. Hemmida, H.-A. Krug von Nidda, A. Loidl,
  J. Phys. Soc. Jpn. **80**, 053707 (2011).

- *Phase separation and frustrated square lattice magnetism of $Na_{1.5}VOPO_4F_{0.5}$*

  A. A. Tsirlin, R. Nath, A. M. Abakumov, Y. Furukawa, D. C. Johnston, M. Hemmida, H.-A. Krug von Nidda, A. Loidl, C. Geibel, and H. Rosner,
  Phys. Rev. B **84**, 014429 (2011).

Acknowledgements

First of all I would like to express my deepest gratitude to Prof. Dr. Alois Loidl, not only for giving me the opportunity to write this thesis in his group, but also for his support and offering an ideal research environment.

I would like to thank Prof. Armin Reller for his willingness to referee this thesis.

I cannot express enough thanks to my advisor Priv.-Doz. Dr. Hans-Albrecht Krug von Nidda without whom, this thesis would not have been accomplished. I acknowledge his assistance, many fruitful discussions, suggestions and above all I am deeply indebted to him for his kind character.

My special gratitude and thanks are going to the crystal growth team: Dr. Vladimir Tsurkan and Dipl.-Chem. Anna Pimenov for their providing me with several samples. Also my thanks are going to Dipl.-Ing. Dana Vieweg for x-ray and SQUID in several compounds.

I am indepted to Prof. Satoru Maegawa and Prof. Yoshiteru Maeno from University of Kyoto, Japan, as well as Dr. Christine Martin from University of Caen, France, for providing me with polycrystalline $KCr_3(OH)_6(SO_4)_2$ and single crystals $PdCrO_2$ and $CuCrO_2$, respectively.

I thank all my colleagues in the group, and especially Dr. Joachim Deisenhofer for his motivated support and fruitful discussions, as well as diploma student Dieter Ehlers for supplying me with a few structural figures. My grateful thanks also go to M.Sc. Michael Sekania for his help to use the LATEX program.

I am obliged to our administrative staff: Anny Skroblies and Birgitta Eisenschmid.

I cannot thank enough my parents, brother, sisters, relatives, and friends for their constant moral support.

This work was supported by the Deutsche Forschungsgemeinschaft (DFG) within Sonderforschungsbereich SFB 484 (Augsburg) and the Transregional Collaborative Research Center TRR 80 (Augsburg-Munich).

Curriculum Vitae

Name	Mamoun Hemmida
Date of Birth	31.05.1977
Place of Birth	Khartoum, Sudan
Nationality	Sudanese

07/1983 - 04/1989	Primary School at Khartoum North
07/1989 - 04/1992	Intermediate School at Khartoum North
07/1992 - 04/1995	Senior Secondary School at Khartoum North
05/1995	Sudanese Secondary School Certificate (Abitur)

01/1996 - 05/2001	Studies of Physics at the University of Khartoum, B.Sc. Honours, Thesis: "Gravitation"
08/2001 - 02/2003	Civilian Service, Sudanese Committee of Climatology, Khartoum
10/2004 - 01/2007	Master of Material Science at the Institute of Physics, University of Augsburg, Thesis: "Electron Spin Resonance in Two-Dimensional Magnets"
07/2007 - present	Research Assistant at Experimental Physics V, Center for Electronic Correlations and Magnetism, Institute of Physics, University of Augsburg